Numerical modeling and optimization of a regenerative Stirling refrigerating machine for moderate cooling applications

Muluken Zegeye Getie

THÈSE DE DOCTORAT DE L'ÉTABLISSEMENT UNIVERSITÉ BOURGOGNE FRANCHE-COMTÉ

PRÉPARÉE À L'UNIVERSITÉ DE FRANCHE-COMTÉ

École doctorale n°37

Sciences Pour l'Ingénieur et Microtechniques

Doctorat de Énergétique

par

MULUKEN ZEGEYE GETIE

Numerical modeling and optimization of a regenerative Stirling refrigerating machine for moderate cooling applications
Modélisation numérique et optimisation d'une machine frigorifique de type Stirling destinée à la production de froid à température modérée.

Thèse présentée et soutenue à Belfort, le 25 juin 2021

Composition du Jury :

BONJOUR JOCELYN	Professeur des universités, INSA de Lyon	Président
STOUFFS PASCAL	Professeur des universités, Université de Pau et des Pays de l'Adour	Rapporteur
GROSU LAVINIA	Maître de conférences HDR, Université Paris Nanterre	Rapporteur
ADMASU BIMREW T.	Associate Professor, Bahir Dar University, Ethiopia	Codirecteur de thèse
LANZETTA FRANÇOIS	Professeur des universités, Université de Franche-Comté	Directeur de thèse
BÉGOT SYLVIE	Maître de conférences HDR, Université de Franche-Comté	Codirectrice de thèse

N° | X | X | X |

école doctorale **sciences pour l'ingénieur et microtechniques**

Title: Numerical modeling and optimization of a regenerative Stirling refrigerating machine for moderate cooling applications
Modélisation numérique et optimisation d'une machine frigorifique de type Stirling destinée à la production de froid à température modérée.

Keywords: Stirling refrigerator, Modified simple model, Thermodynamic and mechanical losses, Moderate cooling,Beta-type, Optimization and experiment

Abstract:

The Stirling cycle machine has many successful applications as a prime mover and cooling machine. The Stirling cycle heat engine has a good potential for use in the future because of some advantages like external combustion, and fuel flexibility. The Stirling machine is used in cryogenics but applications for domestic cooling are still underdeveloped. The main goal of this study is to develop a precise thermodynamic numerical model that could predict the performances and provide means for further optimization. Hence, this dissertation presents the numerical modeling, simulation, experimental validation, and parametric optimization of an air-filled Beta type Stirling refrigerator for domestic application.
The research shows that a non-ideal second-order numerical model called the modified simple model has been developed. The model incorporates effects of shuttle heat loss and mass leakage loss to the buffer space directly to the differential equations of pressure change, rate of change of mass of gas in compression and expansion spaces, and mass flow rates across these working spaces. Moreover, other power losses and heat losses are included as independent losses to evaluate the cooling production and associated COP. The model is simulated using MATLAB code for Beta configuration FEMTO-60 Stirling engine operating as a refrigerator. The model is validated both with an experiment conducted in the FEMTO-ST laboratory in refrigerating mode and by reversing the model to work producing engine, so that the validation could be made with different theoretical models developed by other scholars so far. The validation results confirm that the proposed numerical model could be used to design a Stirling cycle refrigerating machine with reasonable accuracy. The contribution of this study also includes investigation of the effect of different working fluids (air, nitrogen, hydrogen and helium), effects of losses (shuttle heat and mass leakage) that have a direct effect on the operating condition of the cooling machine and parametric optimization. Air and nitrogen showed better cooling performance than helium and hydrogen mainly due to the higher mass flow rate. The effects of incorporating shuttle heat loss in the differential equations on the temperature and pressure of working gas and the overall performance of the Stirling refrigerator are analyzed. Parametric optimization includes the effect of operating (rotational speed, charging pressure, and temperature) and geometrical (phase angle, regenerator length, porosity, displacer height, displacer gap, piston-cylinder clearance gap, swept volume ratio, and piston diameter to stroke ratio) parameters on the cooling performance as well as on share of different power and heat losses. Finally, we propose a set of parameters to optimize a refrigerating Stirling machine achieving a COP of 1.3 for a cooling power of 625 W at a temperature of -4^oC.

Titre : Numerical modeling and optimization of a regenerative Stirling refrigerating machine for moderate cooling applications
Modélisation numérique et optimisation d'une machine frigorifique de type Stirling destinée à la production de froid à température modérée.

Mots-clés : Réfrigérateur Stirling, Modèle simple modifié, Pertes thermodynamiques et mécaniques, Refroidissement modéré, Architecture bêta, Optimisation et expérimentation

Résumé :

Les machines à cycle Stirling sont utilisées aussi bien en cycle moteur que récepteur. Le moteur à cycle Stirling possède un bon potentiel d'utilisation en raison de certains avantages comme la combustion externe et la flexibilité du carburant. La machine Stirling est utilisée en cryogénie mais les applications pour le refroidissement domestique sont encore peu développées. L'objectif principal de ce travail est de développer un modèle numérique thermodynamique permettant de déterminer et d'optimiser les performances d'une machine frigorifique pour des applications de froid domestique. Cette thèse présente donc la modélisation numérique, la simulation, la validation expérimentale et l'optimisation paramétrique d'un réfrigérateur Stirling de type Beta, conçu au laboratoire fonctionnant avec de l'air pour une application domestique.
Nous avons développé un modèle numérique non-idéal du second ordre appelé modèle simple modifié. Ce modèle incorpore des pertes thermiques et fluidiques par conduction, effet navette pompage, pertes de charge, fuites de gaz vers le volume tampon. Ces pertes sont directement intégrées dans le modèle d'équations différentielles permettant d'exprimer les variations de pression, de température, de masse de gaz dans les volumes de compression et de détente, ainsi que les débits massiques de gaz traversant les différents volumes de la machine Stirling. La prise en compte de ces pertes permet de calculer la production de froid et le coefficient de performance (COP) associé. Le modèle est simulé à l'aide du code MATLAB. Les résultats numériques sont comparés aux résultats expérimentaux et aux résultats issus de la littérature. Le modèle numérique proposé peut être utilisé pour concevoir une machine frigorifique à cycle Stirling avec une précision raisonnable. La contribution de cette étude comprend également l'investigation de l'effet des différents fluides de travail (air, azote, hydrogène et hélium) sur les performances de la machine frigorifique et son optimisation paramétrique. Dans la gamme d'utilisation de la machine, l'air et l'azote ont montré de meilleures performances de refroidissement que l'hélium et l'hydrogène, principalement en raison du débit massique plus élevé. L'optimisation paramétrique des performances de la machine frigorifique comprend également les effets des paramètres de fonctionnement (vitesse de rotation, pression de charge et température) et géométriques (angle de phase, dimensions et porosité du régénérateur, jeu entre le piston et le cylindre, rapport du volume balayé et rapport du diamètre du piston à la course). Enfin, nous proposons des jeux de paramètres permettant d'optimiser un réfrigérateur Stirling présentant un COP de 1.3, une puissance frigorifique de 625 W à une température de -4^oC.

UBFC UNIVERSITÉ BOURGOGNE FRANCHE-COMTÉ
Université Bourgogne Franche-Comté
32, avenue de l'Observatoire
25000 Besançon, France

ACKNOWLEDGMENTS

This thesis becomes a reality with the kind support of many individuals. I would like to extend my sincere thanks to all of them.

Foremost, I want to thank the almighty GOD for the wisdom he bestowed upon me, empowering and giving me internal courage and strength to accomplish this research.

I owe to express my sincere gratitude to my esteemed supervisor prof. François Lanzetta for his kind and continuous support in providing technical and scientific guidance throughout this research. Since the first day, I shook hands with him in Belfort train station, I have continuously benefited a lot from his experience. It has been a great honor and real pleasure to work under his supervision as he was not only generous with his expertise but he was also a good friend to me. I sincerely hope that he could enjoy our collaboration as much as I did.

I am highly honored, also to appreciate my esteemed thesis co-supervisors Dr. Sylvie Bégot and Dr. Bimrew Tamerate for their continuous support of my research, patience, motivation, enthusiasm, and immense knowledge. Their guidance helped me in all the time of research and writing of this thesis. It has been also a great honor and real pleasure to work under their supervision as they were generous with their expertise and friendly to work together. What I could generally say is that I was lucky enough to have them as my supervisor and Co-supervisors.

I also thank EIPHI Graduate School (contract $ANR-17-EURE-0002$), Region Bourgogne-Franche-Comte, Bahir Dar Institute of Technology, the Embassy of France to Ethiopia and the African Union, and the Ministry of Science and Higher Education of Ethiopia for sponsoring and facilitating my study.

Throughout the past three years, I have enjoyed the friendship and generous support of Steve, Martin, Fatima, Isabelle, and other members of the FEMTO-ST laboratory. It will be very hard to accomplish my task in France as I was new to the culture as well as to the language. As the research has been conducted partially in Ethiopia, the community of Bahir Dar institute of technology has also an important role in my research. Especially, the long-lasting friendship, cooperation, and unreserved motivation and support from my best friends Dessie Tarekegni and Muluken Temesgen was remarkable. I am very grateful for all your support and encouragement.

Last but not list I would like to extend my thanks to all my family for your unconditional love and motivation throughout my life. My beloved and supportive wife, Seblewongale who is always by my side since the start of my PhD. It was a great moment having you at the right time. You were with me at every moment and during this time you gave me a very important gift, Yafet who is becoming the source of fun for our life. My beloved father Mr. Zegeye Getie, my brothers Yirsaw, Abirham and...others you have a special place on my journey.

CONTENTS

LIST OF FIGURES

List of Tables

NOMENCLATURE

Abbreviations

CFC	chlorofluorocarbon
$FPSC$	Free Piston Stirling Cryocooler
GWP	Global Warming Potential
$HCFC$	hydrochlorofluorocarbon
HFC	hydrofluorocarbon
VCR	Vapor Compression Refrigerator
$VISR$	V-type integral Stirling refrigerator

General symbols

A	cross sectional area [m2]
A_{wgr0}	no matrix regenerator wetted area [m^2]
A_{wg}	wetted area of the metal [m^2]
A_{wr}	regenerator housing wall area [m^2]
$Amat$	area of regenerator matrix [m^2]
C	average molecular speed [$m.s^{-1}$]
C_p	isobaric specific heat [$J.kg^{-1}.K^{-1}$]
C_v	isochoric specific heat [$J.kg^{-1}.K^{-1}$]
COP	Coefficient of Performance [-]
$Cqwrt$	regenerator housing thermal conductance [$W.K^{-1}$]
d	hydraulic diameter [m]
d_d	diameter of displacer [m]
d_p	piston diameter [m]
D_w	diameter of wire [m]
D_{ri}	regenerator matrix internal diameter [m]
D_{ro}	regenerator matrix outer diameter [m]

f	frequency [Hz]
f_r	Reynolds friction factor
G	mass flux [kg.m^{-2}.s^{-1}]
h	convective heat transfer coefficient [W.m^{-2}.K^{-1}]
J	annular gap between cylinder and piston/displacer [m]
k	thermal conductivity [W.m^{-1}.K^{-1}]
L	length [m]
L_d	length of displacer [m]
L_p	length of piston [m]
m	mass of working fluid [kg]
n	rotational frequency [rpm]
N_{st}	Stanton number
NTU	Number of Transfer Unit
Nu	Nusselt number
P	pressure [Pa]
Pr	Prandtl number
Q	heat [J]
R	gas constant [J.kg^{-1}.K^{-1}]
Re	Reynolds number
s	stroke [m]
T	temperature [K]
U_p	linear velocity of piston [m.s^{-1}]
V	volume [m^3]
V_b	overlap volume [m^3]
W	work [J]
$\dot{m}$	mass flow rate [kg.s^{-1}]
$\dot{Q}_p$	Pumping heat loss [W]

Greek symbols

α	phase angle [rad]
Δ	difference

ϵ	regenerator effectiveness
η	clearance efficiency
γ	ratio of specific heats, (C_p/C_v)
μ	dynamic viscosity[Pa.s]
ϕ	Porosity of regenerator
τ	compression ratio
θ	crank angle [rad]
ω	angular speed [rad.s^{-1}]

Subscripts

$buffer$	buffer space
c	compression space
clc	compression clearance
cle	expansion clearance
$cond$	conduction
cr	chiller
cre	chiller-expansion spaces interface
e	expansion space
$fin.sp$	finite speed of piston
g	gas
h	hot heat exchanger
hys	gas hysteresis
iad	ideal adiabatic
$leak$	leakage
$mec.fr$	mechanical friction
mod	modified ideal adiabatic
r	regenerator
rho	regenerator housing outer
rl	regenerator imperfection loss
$shut$	shuttle
swc	compression swept

swe	expansion swept
t	total
wcr	wall of chiller
wh	wall of hot heat exchanger
wrl	regenerator wall loss
i, in	inlet of ith control space
i, o	outlet of ith control space

I

Introduction and State of the art

1

INTRODUCTION

1.1/ BACKGROUND

The rise of fuel and other energy resources price as well as global warming push scientists to set the problem of searching innovative technologies for energy transformation, to develop new technologies on the base of thermodynamic cycles with high efficiency, to use new working mediums in order to develop ecologically safe energy systems, which can satisfy residential and industrial sector utilities for a minimum amount of energy used. Refrigeration and Air-Conditioning systems are part of day to day life in the world in which they are using energy to produce cold. They are definitely belonging to one of the most important engineering achievements of the 20^{th} century.

Food preservation, medicine storage and transportation, and industry would not be what they are today without refrigeration. Refrigeration has had a large impact on industry, lifestyle, agriculture, health care, and settlement patterns. The comfort, ease, and happiness they bring to our everyday lives are endless. Air conditioning brings comfort and environmental flexibility that has impacted people more than they realize. Refrigeration is the process of removal of heat from an enclosed space to lower the temperature in the region. The term refrigeration means cooling a space, substance or system to lower and/or maintain its temperature below the ambient one and the removed heat is rejected at a higher temperature. In other words, refrigeration is artificial (human-made) cooling. Before mechanical refrigeration systems were introduced, ancient peoples, including the Greeks and Romans, cooled their food with ice transported from the mountains. Refrigeration, especially at very low temperatures, has had an incredible impact on the medical world.

The purpose of any refrigerator is to extract heat as much as possible from a cold reservoir with an expenditure of as little power as it could be. This implies that the power requirement should be minimized for a given cooling load. Most of the refrigeration demand of the world is largely dependent on the reverse-Rankine cycle particularly called the vapor-compression refrigerator (VCR). VCR was first developed in the latter part of the 19^{th} century based on the phase change process of Chlorofluorocarbon (CFC) or hydrochlorofluorocarbon (HCFC) fluids. In a single-stage, VCR produces a cold end temperature below 230 K, provided an appropriate refrigerant is used. The VCR currently exists at the saturated technological level and is suited for household applications. Although VCR is an efficient technology, especially for moderate temperature refrigeration applications, its environmental concern resulted in different scenarios.

In the year 1987, a protocol was signed in U.K. with an objective to protect the ozone layer from further depletion by CFC emission. This protocol is called Montreal protocol and it stated that CFC group of refrigerants, which is the main culprit for ozone layer depletion should be banned by the year 2010 [134]. The other related protocol signed in the year 1997 called Kyoto protocol, aimed to prevent global warming due to the use of HCFC/CFC refrigerants. Annual global direct and indirect CO2-equivalent emissions from greenhouse gas emissions for residential and commercial air conditioning (A/C) systems in 2010 is shown in Fig. 1.1.

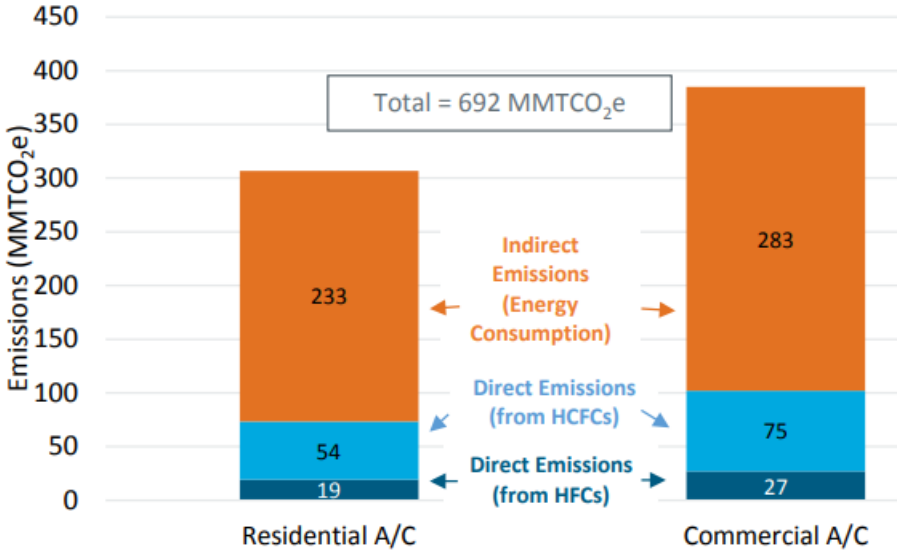

Figure 1.1: Estimated global GHG emissions from air-conditioning systems in 2010 [97].

Now days, as a result of Montreal protocol, shifting of refrigerating gases from CFC to hydrofluorocarbon (HFC) gases and increased in demand of refrigeration have raised the consumption of HFC gases. Global warming potential (GWP) of fluorinated-gases is many times greater than that of carbon dioxide (CO2) [161]. Then, emissions of fluorinated greenhouse gases mainly HFC gases, which are used as replacements for ozone-depleting substances (CFCs), have risen sharply since 1995. The rapid increase in HFC gas emissions coupled with their global warming potential (GWP) has led to increased worldwide attention to monitoring emission levels and subsequently regulating the use of fluorinated-gases [156]. Several policies and regulations are being approved to control the working fluids used in existing and future installations. The Kigali Amendment (KA) to the Montreal Protocol agreed upon in October 2016 and which entered into force on 1 January 2019 is a global agreement to phase down and almost eliminate the consumption of HFCs by 2050 [122].

The refrigeration, air conditioning and heat pump industry is a significant contributor to the climate change through its associated direct and indirect greenhouse gas (GHG) emissions [155]. The major share of fluorinated gases (about 99%) is used for refrigeration and air conditioning systems, from the total consumption for cooing approximately 75% of F-gases is used for refrigeration and stationary air conditioning and 25% is used in mobile air conditioning [156].

Recently, in addition to the effort to improve the working condition of VCR through replacement of HFC gases, two global challenges (overall global warming and continued

increase in demand for refrigeration in almost all parts of the world) have pushed the engineering community to search for alternatives to vapor-compression refrigeration. Non-vapor compression technologies, at the intersection of better energy efficiency and GWP reduction, provide potential value for both direct and indirect emissions reduction opportunities as one important piece of the long-term solution (see Fig 1.2). In consistent with this, it is emphasized that the utilization of environmentally safe fluids and improved energy efficiency leads to a number of new refrigerants that are under consideration and to the introduction of new technologies including Stirling refrigerators [21]. The Stirling cycle refrigerating machine is a member of family of closed-cycle regenerative thermal machines, including Stirling engine, heat pumps, and refrigerators and collectively known as Stirling cycle machines. Stirling refrigerator is a reversed Stirling cycle or family of gas cycle refrigerators. The working fluid is a gas that is compressed and expanded but does not change phase in this Stirling cycle refrigerator. The development of Stirling refrigerators for moderate temperature application is one of the technologies that was brought from the concern about the use of CFC refrigerants and their effect on the environment. These machines theoretically have the highest efficiency possible for any practical thermodynamic system, and thus become a potential alternative to the existing vapor-compression refrigeration system.

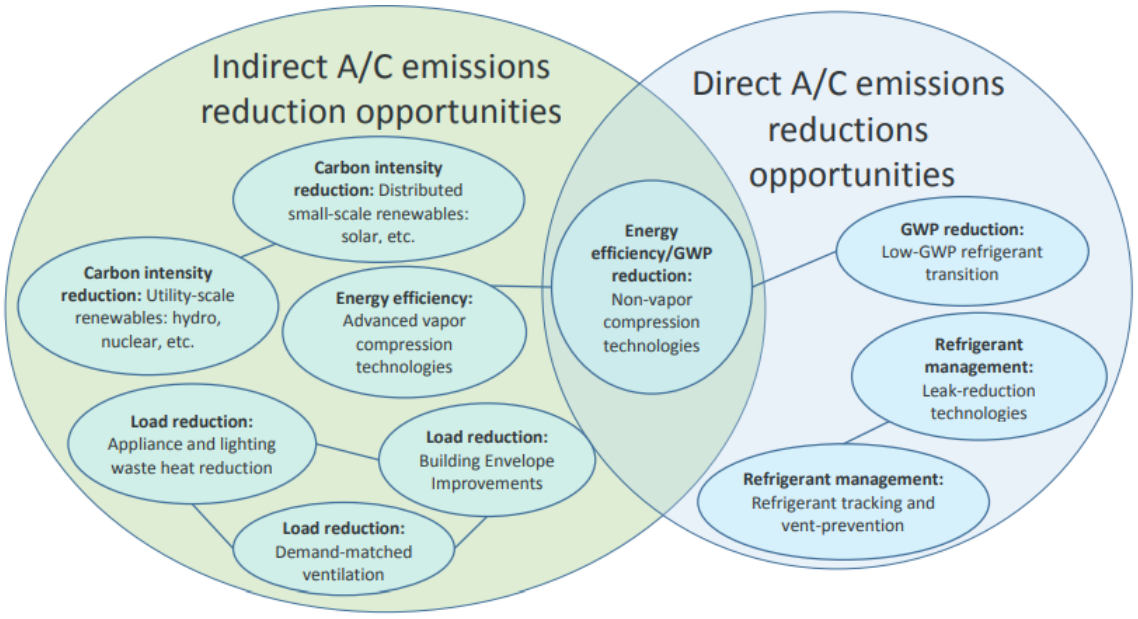

Figure 1.2: Elements of sustainable, low emissions cooling systems [118].

Refrigerators use mechanical energy to drive heat from a low-temperature source to a high-temperature sink, and the Stirling machine is one of these which can be used for this purpose. Stirling refrigerators are one type of mechanical refrigerators that have the potential of being researched. The Stirling cycle machine uses mostly working fluids (air, helium, hydrogen) contained in a closed system. Through reversing the cycle, the Stirling engine can operate as a refrigerating machine or heat pump. The first mention of the operation of the Stirling engine as a refrigerating machine dates back to J. Herschel's works in 1834, and the first refrigerating machine was built by Kirk in 1874 [1].

1.2/ MOTIVATION

In spite of great scientific strides over the last century, the most widely used refrigeration technologies used today are the same as those used for the last century. Though Stirling refrigerators were proposed since the mid-1800's [15], they still have a limited commercial use for domestic refrigeration and air-conditioning. The number of researches made on Stirling refrigeration for domestic temperature (near to ambient) applications are very few as compared to studies made about the Stirling engine and Stirling cryocooler. A major reason for the limited researches in the area of Stirling refrigerators is that vapor-compression refrigerators are already in use due to their better performance and convenience as they approach perfect design conditions, and the necessity to develop other refrigeration systems is limited if the GWP of refrigerants is not taken into account. However, currently increasing public and government concern at the impact of CFC/HCFC refrigerants on the ozone layer of the Earth has got attention to the search for alternatives to the present vapor-compression refrigerating systems. This social concern leads to unparalleled opportunities for the research and development of moderate temperature Stirling cycle refrigerating machines for the application of household and commercial purposes. Generally, the environmental concern on one side and the highest theoretical coefficient of performance of reversed Stirling cycle on the other side as well as the availability of limited researches on the area lead to the initiation of this research. On the other hand, for Stirling refrigerators with moderate temperature, where there is no need for high working temperature and pressure as that of Stirling engine, the mass production cost could be reduced significantly and could easily be applied. Nowadays, researches are conducted in this area and great promise in improvement of performance has been recorded. Still, further engineering researches are needed to make such refrigerators sufficiently reliable, less expensive, and efficient to be used regularly for many other potential application areas.

1.3/ OBJECTIVES

The general objective of this research work is to model, study and design an optimal regenerative Stirling machine for domestic refrigeration using air as working fluid.

The specific objectives are to:

- develop a mathematical model that best suits for Stirling cycle refrigerating machine with inclusion of all relevant losses,
- simulate the mathematical model using an appropriate simulation tool,
- validate the mathematical model using experiment and other previous researches in the area,
- investigate the effcet of various losses as a function of operating and design parameters,
- conduct parametric optimization for optimum cooling performance.

1.4/ THESIS STRUCTURE

The thesis is divided into 5 chapters.

The first chapter gives a brief introduction to refrigeration technologies, motivation, objectives of the thesis as well as the scope of the research.

Chapter two briefly presents the Stirling cycle refrigerating machine. In this chapter, the working principle of the Stirling refrigerating machine, its configurations, driving mechanisms, low-temperature Stirling cycle coolers, and moderate temperature Stirling refrigerating machine are reviewed. The review also tries to investigate the main thermodynamic and parametric criteria as well as the modeling techniques that were considered to design the refrigerating machine for different applications. Finally, research gaps are identified.

Chapter three describes and presents the developed numerical model (modified simple), starting the analysis from an ideal adiabatic model, and describing the method of solution, validation as well as some simulation results. The modified simple model is developed for a Beta-type Stirling refrigerator using air as working fluid.

In Chapter four, parametric optimization has been presented for some operating and geometric parameters. Furthermore, combination of optimized parameters have been proposed for optimum cooling performance.

Finally, in chapter five, general concluding remarks about the findings and proposed future works are presented.

2

Literature Review

2.1/ Introduction

Stirling cycle machine is a type of closed thermodynamic cycle machine invented in 1816 by Robert Stirling as a heat engine to convert thermal energy to mechanical energy. The air was used as a working fluid to replace the steam engine since they were prone to life-threatening explosions. The Stirling refrigerator, which is the counterpart of the Stirling engine was first recognized in 1832 [6]. The system was practically realized in 1862 when Alexander Kirk built and patented a closed cycle refrigerator based on Stirling cycle [1]. Until 1949, it was reported that very little development of Stirling refrigerators occurred, when the Philips Company in Holland ran a Stirling engine in the reverse direction by a motor and found that it liquefied air over the cold tip [2]. In the year 1971, Beale stated that Stirling cycle machines could be used for both work producing or refrigerating machines by reversing the cycle [8]. Therefore, Stirling cycle machine in this review is mostly dedicated to Stirling cycle refrigeration machine [154].

Devices using the Stirling cycle are still expensive to construct due to limited production volume and the working condition (high temperature and high pressure especially in case of Stirling engine) that demands special materials and relatively high technology. Numerous researches have been conducted on Stirling machines especially about Stirling engines and Stirling cryocoolers for almost a century. The results reveal that the efficiency and performance improvements have been recorded and are still showing great improvement for Stirling engines and cryocoolers and wider applications are considered. Cooling by using Stirling cycle machine is rarely used at moderate/ambient temperatures for domestic or commercial refrigeration. On the other hand, for Stirling refrigerators with moderate temperature, where there is no need for high working temperature and pressure, the mass production cost can be reduced significantly as compared to a Stirling engine.

A major reason for the limited application of Stirling refrigerators is that vapor compression-type refrigerators, which are already functioning in household refrigerators, approach very high performances conditions, and the necessity to develop other refrigeration systems is limited is the GWP of refrigerant is not taken into account. For this reason, the number of researches conducted on the Stirling refrigeration for moderate temperature (near to ambient) applications are very few as compared to studies made about Stirling engine and Stirling cryocooler.

2.2/ CONFIGURATION AND DRIVING MECHANISMS

2.2.1/ GENERAL

The main parts of a Stirling cycle machine are the piston, the displacer, the cylinder, the heat exchangers (heater, cooler and regenerator), and the crank mechanism as seen in Fig. 2.1.

- The heater, which must accept heat from a high temperature source and then transfer this heat to the engine working fluid .
- The regenerator, which ideally stores the heat received when the hot working fluid flows from the hottest to the coldest space of the cycle, and then releases this stored heat during the reverse flow.The regenerator is the most important component of a Stirling engine. It is the heat exchanger in which the highest heat is transferred within a cycle.
- The cooler that removes the heat in the cold side of the engine before the compression of the working gas.

The systematic understanding of component configurations, common drive systems and their possible combination for Stirling cycle refrigeration is vital to develop appropriate selection criteria to use the machine for different applications. The Stirling cycle refrigerating machine can be classified based on their piston-cylinder configurations or based on the drive systems that ensure appropriate flow of working gas. Many different combinations of configuration and driving mechanisms are proposed for different applications [144]. Therefore, in this part of the review, we try to go through the various common arrangements of the Stirling cycle refrigeration systems and the associated researches done so far.

2.2.2/ CONFIGURATION

Stirling machines have a wide range of applications by varying their configuration. The mechanical configurations of Stirling cycle refrigeration machines are exactly similar to Stirling engine. Numerous designs of Stirling cycle machine exist but the following common elements shall be identified:

- A closed system containing a fixed mass of gas.
- Compression and expansion spaces with the volume of gas, which are controlled by a piston-cylinder arrangement. The enclosed working fluid flows in alternate directions between two interconnected gas spaces, at different temperatures, which is controlled by changing the succession volume.
- A displacement arrangement to shuttle the working fluid back and forth between the hot end and cold end gas spaces.
- A regenerator connecting the heater and cooler of the machine. The processes of heating and cooling are noticeably improved by the regenerator which generally consists of a matrix of fine wires or simply annular gaps made by winding foil.

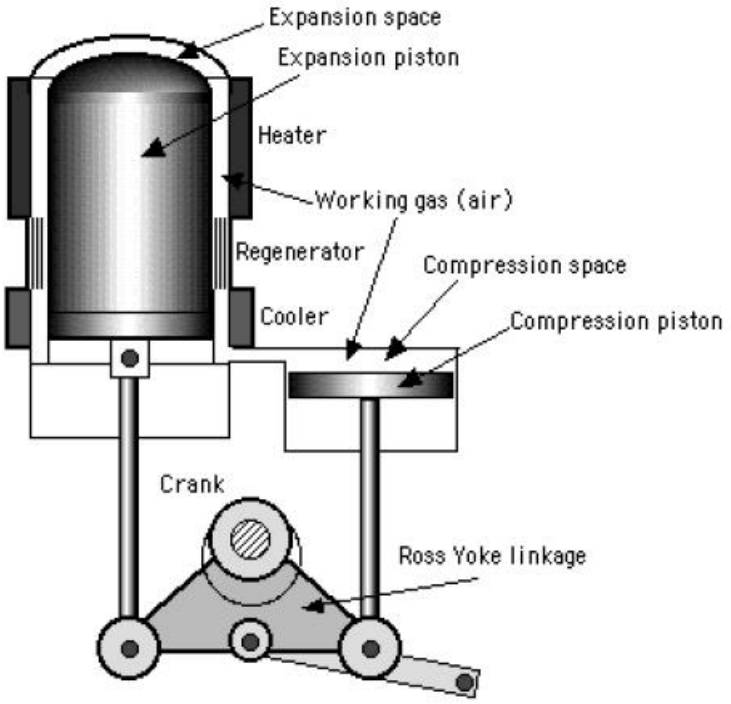

Figure 2.1: Main components of a Stirling machine [123].

- Heater and cooler for transferring heat to and from the cycle or they could act as heat reservoirs. Heater and coolers could be named as chiller and hot heat exchanger in case of refrigerating machines.

The basic parts of a Stirling cycle machine are the piston, the displacer, the cylinder volumes, the heat exchangers, and the crank mechanism [109]. The Stirling cycle machines are generally divided into three groups based on piston and piston/displacer-cylinder arrangement such as the Alpha, Beta, and Gamma configurations [4, 18, 20]. All configurations are working with the same thermodynamic cycle but with different mechanical design. The three configurations of the Stirling cycle machine could be described as:

1. *Alpha configuration:* two pistons in separate cylinders connected in series by a heater, a regenerator and a cooler [55, 70, 77, 94, 129]. The configuration of Alpha Stirling refrigerator is shown in Fig. 2.2. In this configuration, a displacer is not used. Both pistons need to transfer work and the piston-cylinder contact space is sealed to maintain the working gas at relatively higher pressure. The two pistons are arranged to move uniformly in the same direction and provide constant-volume heating or cooling processes of the working fluid. Based on different drive mechanisms, Stirling machines with Alpha configuration are found more suitable for medium and high-temperature difference applications [144]. Similarly, it is reported that Alpha type engine configurations are not suitable for low-temperature difference (LTD) applications [80]. This is because there is a direct relation between the optimum compression ratio and the temperature ratio and Alpha configuration Stirling machines have higher compression ratio.

2. *Beta configuration:* unlike the Alpha configuration, the Beta configuration Stirling

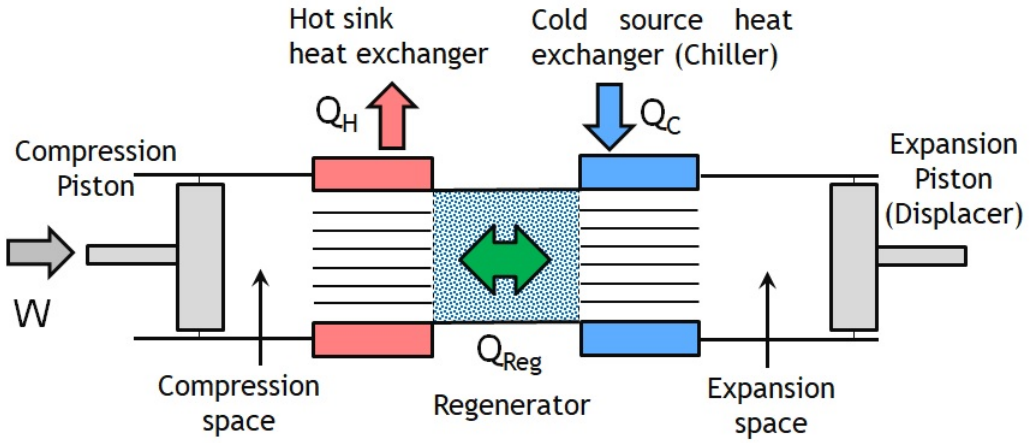

Figure 2.2: Alpha configuration for Stirling refrigerator.

machine has a single power piston and a displacer enclosed within a single cylinder [44, 105, 130]. A Beta configuration Stirling refrigerator is shown in Fig. 2.3. The main task of the displacer is to displace the working fluid and shuttle it between the compression space and the expansion space through the series of heat exchangers. From the patent drawing of 1816, it is shown that the Stirling machine first configuration was a Beta configuration. Egas and Clucas [144] reported that Beta configuration Stirling machines could be used conveniently from low to high-temperature differential applications according to different drive mechanisms with the crank drives more preferred from low to moderate temperature and rhombic drive mechanism more applicable from moderate to the high-temperature difference. This due to the fact that Beta configuration have relatively moderate compression ratio.

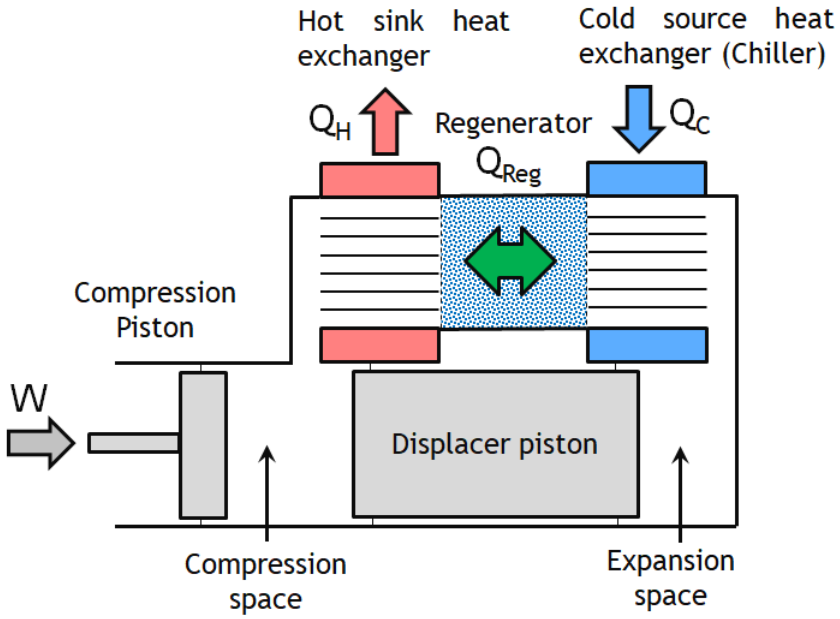

Figure 2.3: Beta configuration for Stirling refrigerator.

3. *Gamma configuration:* Gamma Stirling cycle machines have the same piston and

displacer configuration [141] as Beta type Stirling machines. Unlike the Beta configuration, the power piston and the displacer are arranged in separate cylinders. A particular arrangement of Gamma type Stirling refrigerator is shown in Fig. 2.4. It is reported that only Gamma configurations are suitably applicable for low and very low-temperature differential applications [80, 144] due to lower compression ratio driving system and which is associated to lower temperature ratio.

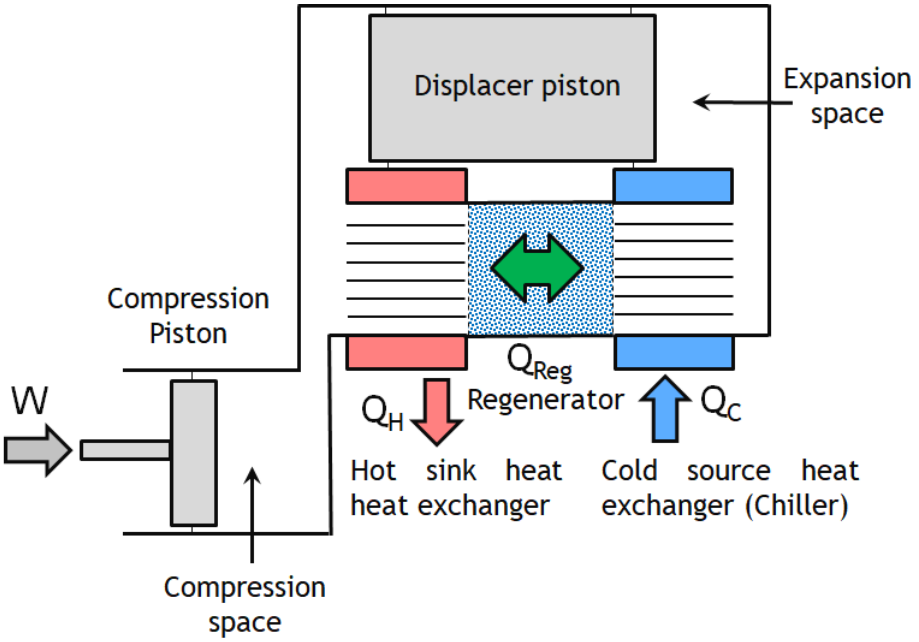

Figure 2.4: Gamma configuration for Stirling refrigerator.

2.2.3/ DRIVING MECHANISMS

To ensure the appropriate flow of working gas for the complete Stirling cycle, different types of drive systems are identified. According to the different configurations of the machine and to facilitate movement of the gas in the system, Stirling refrigerating machines are classified into kinetic, free-piston, pulse tube/thermoacoustic and liquid piston types. Among these drive systems, the first three types are the most commonly used at the different stages of the refrigeration system and discussed as follows:

- *Kinetic driven mechanism:* in kinetic drive mechanisms, the mechanical piston and piston/displacer are driven by kinetic drive mechanisms such as the simple crank-slider, Ross-yoke, rhombic drives, swash-plate and others as shown in the Fig. 2.5. The movement of the working gas in the Stirling machine is controlled by these mechanisms. The drive system is designed in such a way that the piston at the cold end should always move leading the piston in the hot end. All kinematic Stirling machines, no matter what the arrangements are, face several significant engineering design challenges which may affect the effective application to any commercial success. Mechanical friction may be one challenge. The crank driven Stirling refrigerator with a Beta configuration is shown in Fig. 2.6.
- *Free piston Stirling machine:* in response to the shortcomings of the conventional

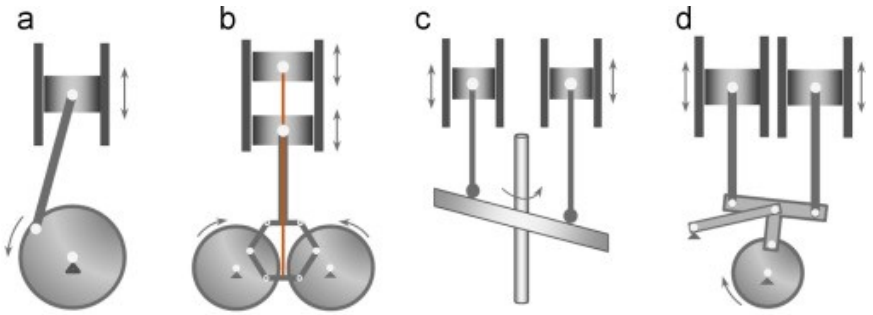

Figure 2.5: Kinetic drive mechanisms used for Stirling machines: (a) crank-slider drive; (b) rhombic drive; (c) swash-plate drive; and (d) Ross-yoke drive [126].

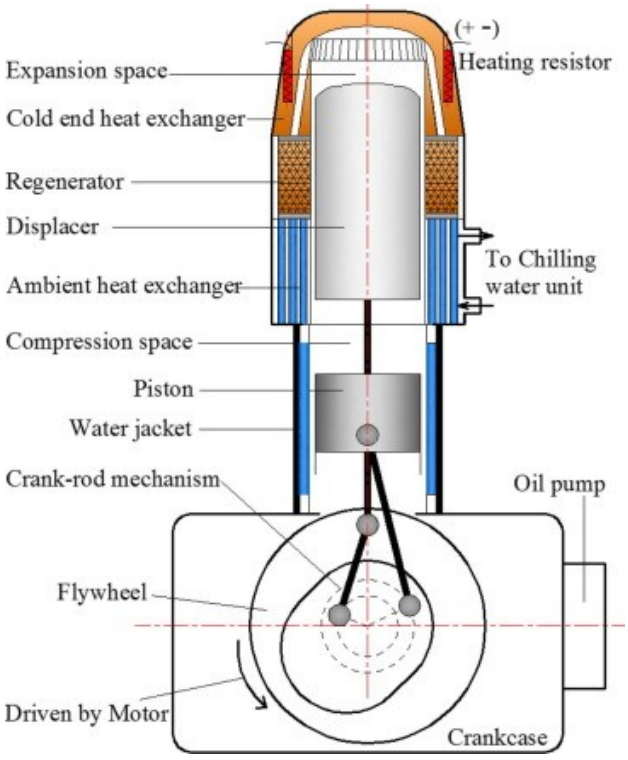

Figure 2.6: Stirling cooler with kinetic drive mechanism [140].

kinematic Stirling machine, in the year 1964 William Beale invented the free-piston Stirling engine (FPSE) [7]. The mechanical pistons do not have any mechanical linkages therefore the crank mechanism is eliminated (see Fig. 2.7, 2.8, and 2.9) and replaced by gas springs and metallic springs in the free-piston Stirling machine [10]. The movements of the pistons are self adapted to the required conditions by using appropriate piston-spring resonant mechanisms or pneumatic force. The thermodynamic process is strongly coupled to the piston-spring pneumatic force action. It is simple, compact and long life but it has some limitations such as a less predictable motion of moving parts and performance. Small free-piston Stirling refrigerators are widely used for the cooling of cryogenic infrared sensors.

- *Pulse tube refrigerators (PTR):* The moving displacer in the kinetic and free piston Stirling refrigerators has limitations.The displacer creates vibration, has a short life-

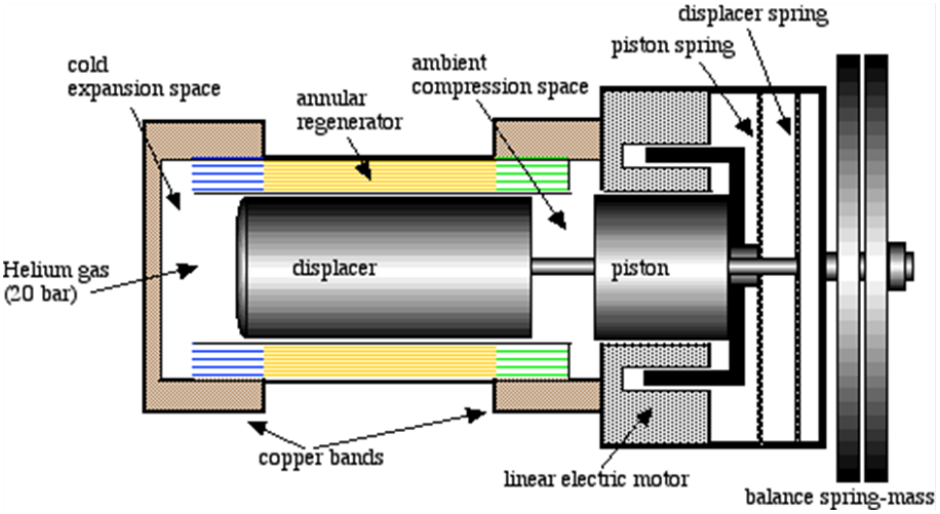

Figure 2.7: Free piston configuration.

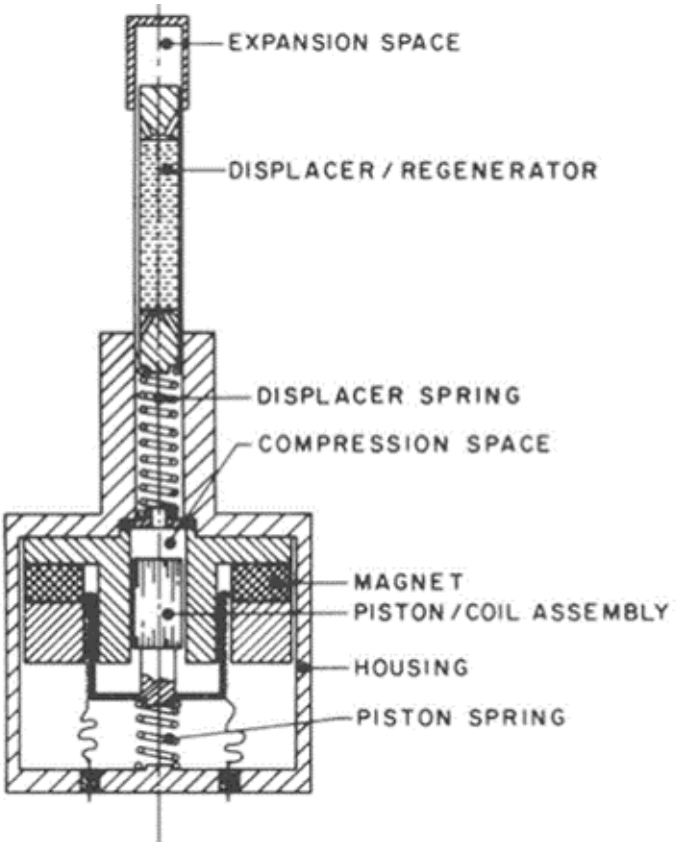

Figure 2.8: Free piston configuration [10].

time, and leads to axial heat conduction and to shuttle heat losses. In a pulse tube refrigerator, the mechanical displacer is removed and oscillating gas flow in the thin tube produces cooling. This phenomenon is called pulse tube action. In the pulse tube refrigerator, the displacer is eliminated and replaced by a pulse tube as shown in the Fig. 2.10. The proper gas motion in phase with the pressure is achieved by using phase shifters, such as orifice-reservoir, inertance tube, active displacer,

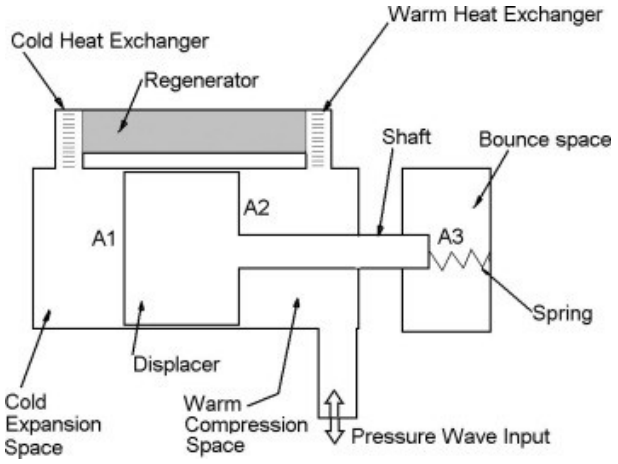

Figure 2.9: Split free piston configuration [114].

etc. The reservoir is designed to be large enough that negligible pressure oscillation occurs in it during the oscillating flow. The oscillating flow through the orifice acts as displacer in separating the heating and cooling spaces. For large industrial systems, the mechanical compressor is replaced with thermoacoustic drivers to give a refrigerator with negligible moving parts. The first pulse tube refrigerator was discovered accidentally at Syracuse University in the mid-1960s [5].

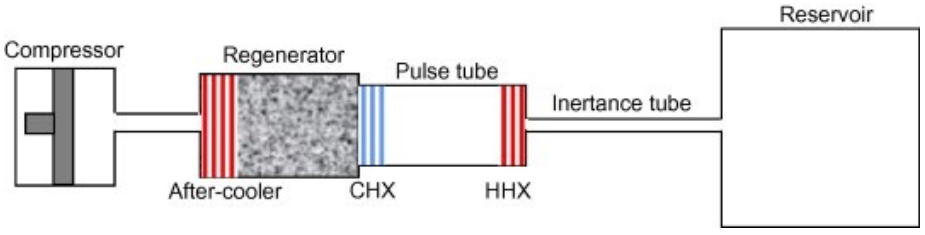

Figure 2.10: Stirling type pulse tube refrigerator [86].

2.3/ Overview of Stirling refrigerating machine

A Stirling cycle refrigerating machine consists of two variable volumes (compression and expansion) spaces at different temperatures and physically separated by the regenerator. The presence of an economizer called the regenerator grouped Stirling cycle machine as a regenerative machine. The working gas is alternatively compressed and expanded by the power piston, while the displacer shuttles the gas back and forth between the cold end, where heat is absorbed, and the warm end, where heat is rejected. When the Stirling-cycle machine operates as a refrigerating machine, heat is lifted from the cold zone during the expansion process and rejected to the hot heat exchanger duing compression process as shown in Fig. 2.11. The work of expansion is lower than the work of compression. Therefore, the net work input is needed in the refrigeration cycle to compensate for the compression work. The cooling effect is shown in the expansion space (see Fig. 2.12).

An ideal Stirling refrigeration cycle consists of four separate thermodynamics processes

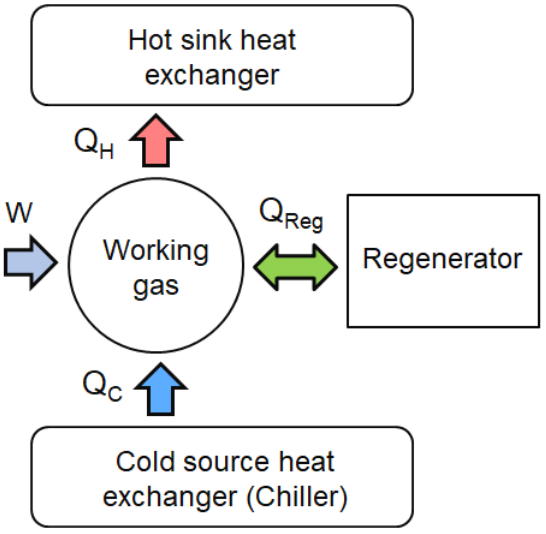

Figure 2.11: Schematic diagram of a Stirling refrigerator.

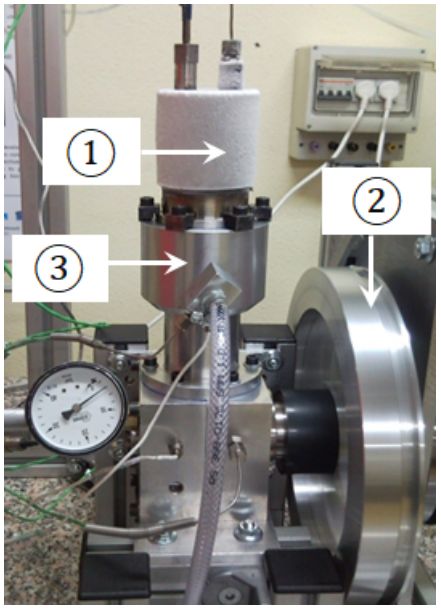

Figure 2.12: Refrigeration Stirling machine (Beta type) at cooling stage with nitrogen asworking gas (FEMTO-ST laboratory) [121].
where: 1. Cold source heat exchanger (chiller) 2. Flywheeel 3. Hot sink heat exchanger (water-cooling)

which are explained as follows (see also Fig. 2.13):

1. *Isothermal compression (process 1-2):* the working gas is compressed by the compression piston isothermally at the hot end, hence rejecting heat to the hot space called warm (hot) heat exchanger.

2. *Constant volume heat rejection (process 2-3):* both pistons or a piston and a displacer move together to transfer all the working gas to the cold end of the refrigerator(expansion space) isochorically through the Stirling regenerator. Heat is rejected from the gas to the regenerator matrix as it passes through the regenerator, thus

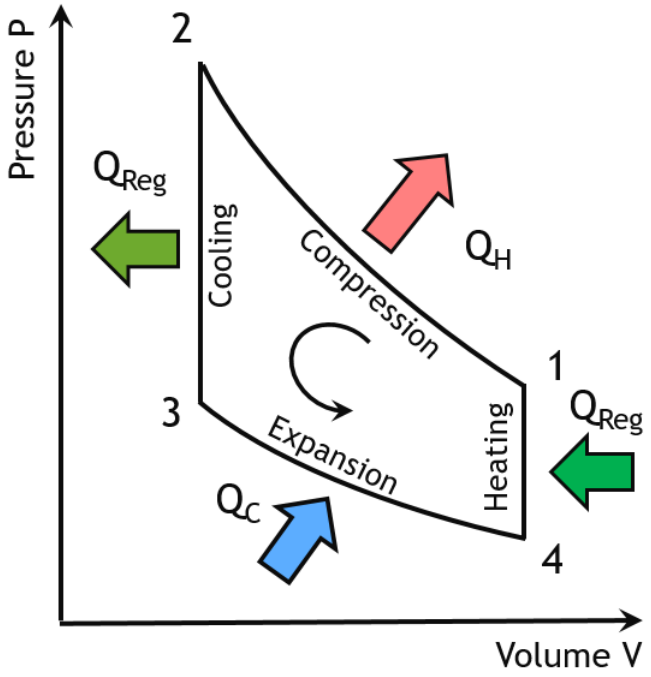

Figure 2.13: P-V diagram of the ideal Stirling refrigeration cycle.

lowering the temperature of the gas to that of the cold space. Heat is stored in the regenerator matrix.

3. *Isothermal expansion (process 3-4):* the low-pressure working gas expands isothermally at cold end temperature, hence absorbing heat from the cold space via the cold heat exchanger called chiller.

4. *Constant volume heat addition (process 4-1):* both pistons or a piston and a displacer move together to transfer all the working gas to the hot end of the Stirling refrigerator (compression space) isochorically through the regenerator. Heat is restored to the gas from the regenerator matrix as it passes through the regenerator, thus raising the temperature as well as the pressure of the gas to that of the hot space and the cycle returns again to its initial position.

The surface delimited by the cycle represents the amount of net work input which must be provided to the refrigerating machine.

The PV diagram of actual Stirling cooler is different from the ideal cycle (seen in Fig. 2.13). The working volume of most real Stirling machines follow sinusoidal variation based on the configuration and drive mechanisms. A 100 W capacity beta-type Stirling cycle cooler designed, experimentally tested and the actual PV diagram of the operation have been constructed [44]. The particular PV diagram for this Stirling cooler at a frequency of 13.3 Hz, cold head temperature of 233 K, and hot heat temperature of 303 K is shown in Fig. 2.14.

The major components of the Stirling machine are presented as shown in Fig. 2.1 and the motion of piston and piston/displacer with respect to time results in variation of the volume of the two working spaces (compression space and expansion space) as seen in the Fig. 2.15.

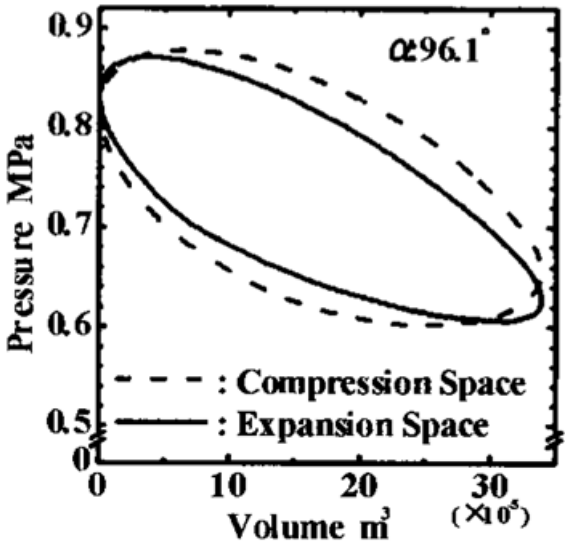

Figure 2.14: P-V diagram of a particular real Stirling refrigeration cycle [44].

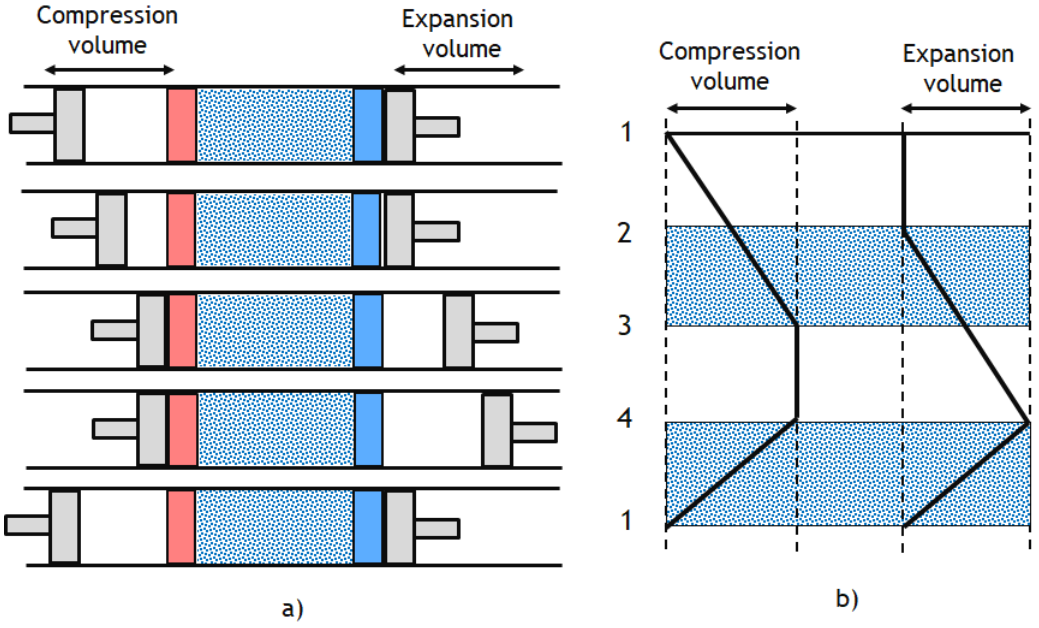

Figure 2.15: (a) Full operation Stirling refrigerating cycle and (b) Ideal time displacement diagram. 1-2 : isothermal compression process 2-3 : constant volume heat rejection (regeneration) 3-4 : isothermal expansion process 4-1 : constant volume heat addition (regeneration).

According to the classical theory of thermodynamics, the performance of a Stirling cycle machine is a function the following independent parameters [20, 18, 13]:

- Pressure of the working fluid.
- Speed of the machine.
- Phase angle between piston and displacer.

- Ratio of the temperatures (compression and expansion temperatures).
- Ratio of the swept volumes.
- Volume and efficiency of the regenerator and heat exchangers.

Hence, the effects of such parameters have to be evaluated. Practically, the parameters phase angle, ratio of temperature, ratio of swept volume and volume of the heat exchangers must be selected at the design stage of the Stirling cycle machine.

Heat is transferred in or out of the working fluid in the Stirling cycle refrigerators during all four phases of their operation, and their performance depends on the non-isothermal heat exchanges performed reversibly or irreversibly. It should also be noted that the regenerator is one of the most important components in a Stirling refrigerator. Namely, the regenerator is typically the largest source of power loss in the system, due to friction losses, imperfect solid-gas heat transfer, and axial heat conduction [103].

2.4/ THERMODYNAMIC MODELING TECHNIQUES

2.4.1/ GENERAL

The design and development of Stirling cycle refrigerators require an understanding of the processes that govern the operation of the machine. Thermodynamic models enable either to simulate the working processes within the Stirling machine or to optimize the size of components of the machine such as cylinder volumes, heat exchangers dimensions, regenerator, and piston and phase angle. This has promoted the development of different analysis methods with different modeling methods. Different modeling methods have different accuracy levels. The analysis methods for the Stirling machine can be classified with different criteria. The criteria adopted in this research include a variety of Stirling machine models and are based on the previous reviews [11, 16, 18, 49, 128, 139]. According to these criteria, the modeling techniques could be characterized into zero-order, first order, second order, third order, and fourth order.

In general, the Stirling machine modeling techniques could also be grouped into three levels of modeling based on their degree of complexity. These are:

- Ideal analysis estimates which may include zero-order and first-order models [38, 67, 128].
- The decoupled (second-order) analysis takes the outcomes of the ideal analysis and improves the result, considering a selected number of main losses [65, 87, 89, 141, 159].
- The coupled analysis includes third and four order models and is based on a fine discretization of the machine in different control volumes with all the main losses [96, 106].

2.4.2/ ZEROTH-ORDER MODELS

Empirical correlations are used to estimate the output of a machine in the zero-order models considering the overall size of the Stirling machine. These zero-order models are models based on experimentation and the empirical findings from experiments of the Stirling engine [49]. The recommended way of estimating the power output of the Stirling engine is to use the Beale number method that shows the power output is proportional to the mean working pressure, operating operating frequency and volume of the machine as described by Walker [13]. These types of models are usually used by engine designers as a way of quickly estimating the power output for a set of specified parameters of the engine [16].

The zero-order methods cannot be used for designing a new machine and calculating the work and heat of the machine. They give quick overview of the overall performance and enable to compare different technologies and machines.

2.4.3/ FIRST-ORDER OR APPROXIMATE DESIGN METHODS

First-order models also called approximate design methods are the simplest mathematical models. These models are used for a simplified and quick way of initial Stirling machine analysis and performance estimation [16]. The technique starts the calculation of the cyclic power output with the assumption of idealized loss-free isothermal analysis, and then a generalized correction factor that accounts for all the losses is applied to calculate the estimated performance output. These performance correction factors are determined from experience with a real machine. The first analysis of this kind was done by Gustav Schmidt in 1871 for the case of sinusoidal volume variations in the expansion and compression spaces [49].

Although the first-order models provide a way of estimating Stirling machine performance (power output and cycle efficiency in case of the engine and cooling power and coefficient of performance (COP) in case of cooling), they cannot be used as detailed design methods. Therefore, these methods are traditionally believed satisfactory only in evaluating the feasibility of employing a Stirling machine for a given temperature range.

2.4.4/ SECOND-ORDER MODELS OR DECOUPLED METHODS

The second-order models begin with a simplified cycle analysis for the estimation of the cyclic power and heat energy interactions. The cycle analyses are typically classified as being either ideal-isothermal or ideal-adiabatic, different in the way in which heat transfer is modelled for the expansion and compression space volumes. The modeling accuracy improved further as they include the different losses existing in the process in these models. The major improvements of these second-order models, compared to the first-order design techniques is that individual losses and their mechanisms are identified and determined. Heat energy losses include regenerator imperfection loss, shuttle heat losses, and conduction due to temperature difference. Power losses include fluid friction losses in heat exchangers, mechanical friction loss, and (hysteresis) losses. The energy losses are assumed to be decoupled from one another in all second-order models. Several authors use this analysis [20, 65, 73, 80, 87, 89, 141, 159].

Second-order modeling methods are further subdivided into three classes according to the way the expansion and compression spaces are handled in the analysis. They are modelled as either being isothermal, adiabatic, or semi-adiabatic [16]. These analysis techniques were derived according to the heat transfer rate between machine the cylinder wall and working fluids. If heat transfer rate between cylinder wall and working fluid is assumed infinite, it is called isothermal, if the rate of heat transfer is zero, it is called adiabatic and on the other hand it is called semi-adiabatic if the heat transfer rate is assumed finite. Isothermal model considers the system divided into 3 volumes: compression volume, regenerator and expansion volumes. So during compression and expansion process there are heat exchange simultaneously which lead to isothermal processes by temperature compensation. As a more realistic approximation to modeling the Stirling cycle, the ideal-adiabatic cycle analysis, that assumes the compression and expansion spaces are perfectly insulated surfaces [3]. The external heat transfer occurs only in the heater and cooler sections.

It has been suggested that the standard Stirling cycle model should be the second-order adiabatic model, as the working spaces in actual Stirling machines are adiabatic and not isothermal [20]. The second-order models present a reasonable accuracy with a fast solution and thus became appropriate for fast design stages and optimization studies.

Generally, the second-order models are numerical zero-dimensional models that have sufficient accuracy for most cases. Moreover, they can be easily applied to various Stirling engines/coolers. In other words, second-order models can be utilized to simulate every type of Stirling engines/coolers with reasonable accuracy. On the other hand, due to much lower computation time compared to third-order models, these models can be used easily for design and optimization purpose.

2.4.5/ THIRD-ORDER MODELS OR NODAL DESIGN METHODS

Third-order analysis techniques increased the level of complexity and the accuracy of prediction of outputs in the models. Third-order modeling, also known as nodal analysis, follows three basic steps. These are:

- The Stirling machine is divided into control volumes or network of nodes.
- The differential equations of energy, mass, and momentum conservation, along with the equations of state are written for each control volume.
- The differential equations are solved simultaneously using numerical methods is conducted [16]. All of the third-order model analysis methods use finite difference of the spatial derivatives to convert the partial differential equations to a system of ordinary differential equations (with only time derivatives remaining).

Using the numerical solutions in this third-order modeling, it is possible to determine instantaneous velocity, pressure and temperature of the working fluid at each working space (compression and expansion chambers and the heat exchangers). These analyses describe more precisely thermal and hydrodynamic processes that take place in the Stirling engines [58, 151].

Generally, the third-order models can also be based on the Computational Fluid Dynamics (CFD). In this case third-order models suffer from some limitations, including the high

computational cost and the lack of generality that makes it impossible to be used to simulate every type of the engine. Instead, the third-order models should be developed for a specific type of engine, and the results cannot be extended to other engines.

2.4.6/ METHOD OF CHARACTERISTICS

The method of characteristics solves systems of nonlinear partial differential equations of hyperbolic type by determining characteristic curves for the equations. The characteristics curves are used to transform the partial differential equations into a system of ordinary differential equations that are valid only along the characteristic curves. Little has been done on this level of analysis. This is because the third-order analysis is faster and for the most part has been an adequate engineering tool. However, to improve efficiency further it is capable of determining flow losses and pressure drops and it can show exactly how the gas is heated up and cooled down and helps to make heat exchangers more efficient by optimizing flow conditions, pressure drops and heat transfer [49]. This method has been used successfully in the study of compressible gas flow and has been applied to the analysis of one-dimensional, unsteady flow in the Stirling machine.

2.5/ REVIEWS ON STIRLING CRYOCOOLERS (LOW TEMPERATURE)

2.5.1/ GENERAL

In the previous years, the cryocoolers with Stirling cycle advanced rapidly because of their high efficiency, low power consumption, light weight, small size, fast cool-down, and high reliability etc. Because of the increasing demand for cryogenic temperatures below 120 K since the middle of the 20^{th} century, lots of studies were conducted and resulted in a wide variety of application areas. The major applications of cryocoolers for several years were used for the military to cool infrared sensors to about 80 K and for tactical uses in tanks, airplanes and missiles [40]. The high capacity cryocooler working below 30 K cooling temperature finds lots of applications including superconducting motors, superconducting cables, and cryopumps. The cryocooler technology is extremely applied in energy, medical, and aerospace areas [51, 60, 69, 104]. This is mainly fostered with the advancement of high-temperature superconductor (HTS) materials and technological advancement. The requirements imposed in each of the above listed applications have been difficult to meet and have been the motivation for considerable research and development in the area of cryocoolers since the past decades. Different kinds of cryocoolers are frequently experimented in laboratories and resulted in continual improvements in the performance and reliability and implementation for commercial and space applications [72].

It is reported that the gas cycle refrigeration systems, including the Stirling refrigerator, has the highest cycle efficiency at lower source temperatures [29]. This argument leads to the fact that Stirling cycle refrigeration is more effective for cryogenic applications. This is because in Stirling coolers low temperatures could be obtained rapidly, which increases its effectiveness as compared to other alternative refrigerating technologies. Stirling refrigerators are well established in the cryogenic temperature range and found to be the system of choice in the miniature closed cycle. Stirling cycle machines are used for

cryogenic applications with the cooling capacities ranging from fractions of a watt to 30 kW and in further research their performance and cooling range have been improved for the last decades. The landscape shown in Fig. 2.16 demonstrates the temperature and cooling power capabilities of available technologies with the temperature and cooling requirements of various applications that operate at cryogenic temperatures [74]. It shows the temperature and cooling power capabilities of available technologies and overlays with the temperature and cooling requirements of various applications that operate at cryogenic temperatures. The working fluid is invariably gaseous with hydrogen and helium gases as the more preferred fluids because of their favorable thermodynamic and transport properties.

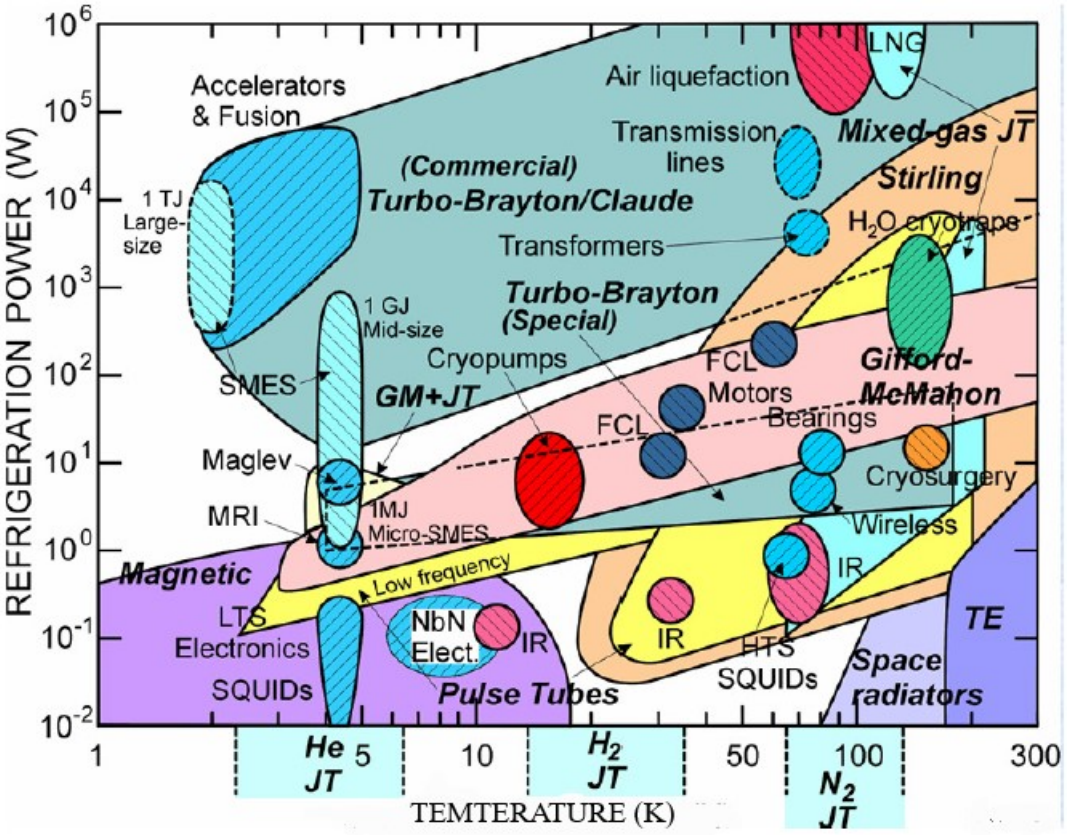

Figure 2.16: Landscape of cooler types (bold typeface) and applications [74].

2.5.2/ KINETIC DRIVEN STIRLING CRYOCOOLERS

The kinematic Stirling cryocoolers driven by crank-shaft mechanisms can generate a higher system efficiency [125]. This cooler was designed for a cooling capacity of 4 W and to operate at cryogenic temperatures of 77 K. Stirling refrigerators have been put to practical use in the fields of superconduction and space engineering for low cooling capacity cryocoolers, in order to obtain temperatures in the range of 10-15 K [44]. It is reported that mechanical cryocoolers represented a significant enabling technology for NASA's earth and space science enterprises [60].

Researchers applied different analysis techniques to design the Stirling cryocoolers and come up with different results. Microcomputer simulation for Stirling cryocoolers was de-

veloped using isothermal assumption in compression and expansion volumes [22]. The performance of Stirling cryocoolers has been analyzed by considering an adiabatic model for compression and expansion spaces [23]. It is reported that the Stirling cryocoolers are divided and studied as either fully isothermal (for constant volume process) or fully adiabatic (compression space and expansion space) and a numerical model was developed [31]. Narasaki et al. [51] developed a two-stage Stirling cryocooler and experimented it for an infrared astronomical satellite. The researchers reported the design of the cooler and the experimental results including cooler performance, vibration, thermal vacuum, and lifetime tests. The Stirling cycle cryocooler with a low-cost, high-capacity was studied to meet different cryogenic system applications [95]. In the study, a cold end temperature near to 50 K was reported.

In the year 2002, Tyagi et al. [46] applied the concept of finite-time thermodynamics to study the effect of internal and external irreversibility for Stirling and Ericsson refrigerator at different operating conditions. Further, the researchers developed a thermo-economic optimization mode in the year 2004, to maximize the cooling load per unit cost of the system using finite time thermodynamics for an irreversible Stirling cycle cryogenic refrigerator [53]. In this research, the authors considered external irreversibilities due to the finite temperature difference between the system and the external reservoirs and the internal irreversibilities caused by the regenerative heat loss. A high power Stirling cryocooler has been analyzed through a numerical simulation using the SAGE software [98] and a result showed the cold head could reach a no-load cooling temperature of 38 K and a cooling capacity of 1012 W at 77.35 K with a power supply of 7.72 kW. A mathematical model has been developed based on thermodynamic theory to evaluate the lifetime of the split Stirling refrigerator [91]. In the same year, Stirling cryogenic refrigerator cycles were analyzed including both internal and external irreversibilities by a multi-objective optimization technique [87]. The optimization work includes reduction of the input power with maximization of the cooling load and the coefficient of performance (COP). Li and Gorsu [132] developed an isothermal model for a Stirling cryocooler by considering various losses at the same time. A high cooling capacity single-stage Stirling cryocooler driven by the kinetic driving system was developed and studied systematically [140]. The researchers found a cooling capacity of 700 W at 77 K and a relative Carnot efficiency of 18.2 % as shown in Fig. 2.17. A CFD model has been developed and validated using experimental work, to investigate the effect of various parameters for the purpose of developing an efficient miniature alpha type Stirling cooler capable of cooling to a temperature lower than $-40\,^{o}C$ [129].

The effect of operational and geometrical parameters on the performance of the cooler has been studied by different researchers and the associated losses were described. Nie et al. [71] pointed out that in the micro/nano scaled Stirling refrigeration devices, the surface area of the system (boundary) has a major effect on the refrigeration heat and COP that in addition to other parameters. An optimal performance of regenerative cryocoolers have been analyzed by considering the losses due to imperfect regeneration and viscous dissipation in the year 2011 [81]. Results revealed that optimum performance could be found at large warm space to the regenerator void volumes ratio. Li and Grosu [132] investigated the effects of various parameters on cooling performance of the Stirling cryocooler and found that the biggest heat loss was due to conduction loss and the biggest work loss was due to the mechanical friction loss. The researchers also described the trend of the input power, cooling power, and COP variation with the phase shift between displacer and piston as seen in Fig. 2.18. The parametric study confirmed that a phase

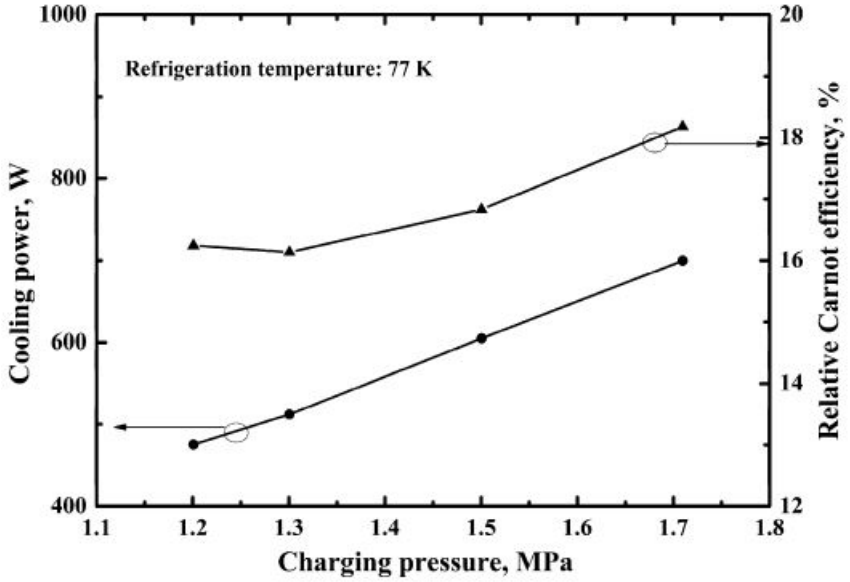

Figure 2.17: Cooling power and relative Carnot efficiency versus charging pressure [140].

angle of 90^o and a regenerator porosity of 50 % would be desirable for the optimum performance of the investigated Stirling cooler, different from the higher porosity typically applied to Stirling engines [129].

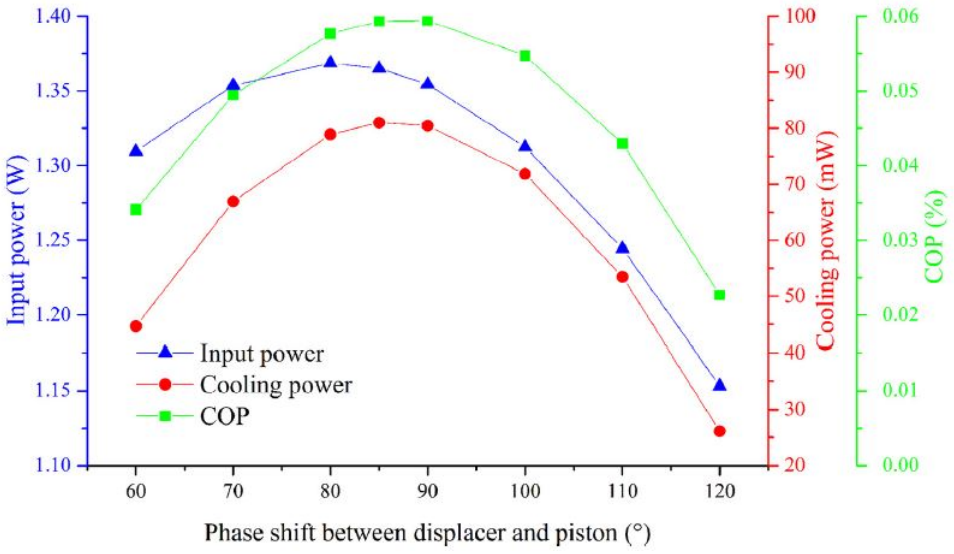

Figure 2.18: Input power, cooling power, and COP trend vs phase shift between displacer and piston [132].

2.5.3/ FREE-PISTON STIRLING CRYOCOOLER(FPSC)

The free piston configuration, which was initially designed by W. Beale in the late 1960's, is one of the most novel applications of the Stirling cycle machine [7]. Ackermann [14] described the phasor analysis to analyze and understand the operation of free-piston Stirling cryocoolers. Park et al. [45] tested the performance of free piston/free displacer type

Stirling cryocoolers and investigated the effect of operating parameters on the cooling performance. In the year 2003, the authors further evaluated the effect of the phase shift between the piston and displacer through experiments [48]. [47] conducted a dynamic analysis of small free-piston-type Stirling refrigerator to understand the characteristics of the refrigerator using an isothermal thermodynamic model. A two-dimensional axisymmetric Computational Fluid Dynamics (CFD) model was developed to characterize the thermodynamic losses for cryocooler application [62]. Theoretical and experimental studies were conducted to evaluate the phase shift characteristics including displacement, pressure and expansion phase difference for free piston and free displacer Stirling cryocooler [68]. Due to its attractive virtue of compact size and having high thermal efficiency, the free piston Stirling cryocooler (FPSC) was reported a good candidate for high cooling capacity ranging from 80 K to 120 K applications [99].

In recent years, many researches have been conducted on high-capacity single-stage free piston Stirling cryocoolers. These cryocoolers could supply several hundred watts of cooling power at around 77 K, but the lowest temperature is difficult to reach. A numerical model was developed based on the thermoacoustic principle to optimize a two-stage free piston Stirling cryocooler system which could operate below 30 K [110]. The researcher reported that a cooling power of 141 W at 77 K in the first stage and 60 W cooling power at 30 K in the second stage were achieved simultaneously using PV power of about 2.23 kW. Experimental work was conducted on a two-stage free piston Stirling cooler so as to fulfill the necessity of the high temperature superconductor (HTS) motor applications [126]. A lowest cold head temperature of 27.6 K was reported with an input electric power of 3.12 kW and a mean pressure of 2.58 MPa.

A new concept that uses a pair of metal diaphragm was proposed to seal and suspend the displacer for free-piston Stirling cryocooler using SAGE modeling tools and a prototype was constructed [114]. The researcher achieved a cryogenic temperature and reported a no-load temperature of 56 K and a cooling load of 29 W at 77 K. Caughley et al. [113] constructed CFD model as a tool to understand the underlying fluid dynamics and heat transfer mechanisms that happened inside a diaphragm Stirling Cryocooler with the aim to improve the performance. The results of CFD analysis showed good agreement with experimental values and also highlighted possible areas of improvement such as increasing the length of the warm heat exchanger to achieve relatively better cooling performance. Furthermore, the model showed that the gas was found the coldest and at the highest velocity in the center of the expansion space.

2.5.4/ STIRLING TYPE PULSE TUBE CRYOCOOLER (SPTC)

The basic Pulse tube refrigerator was first described with experimental models in the year 1964 [5]. After it was first perceived in the mid-1960s, pulse tube refrigerator has been an academic interest until the middle of 1980s as the demand for cryogenic temperature steadily increases [40]. Since then, improvements in its efficiency have been increased rapidly. Mikulin et al. [19] included an orifice tube inside the pulse tube close to the warm end and obtained a cooling temperature of 105 K. Shaowei et al. [24] introduced the concept of double Inlet Pulse tube refrigerator. Mathematical investigation and experimental findings have confirmed that the double inlet pulse tube cooler has higher performance as compared with the orifice pulse tube refrigerator. It was reported that on the heels of basic research, commercial developers are harnessing acoustic processes in gases to make

reliable, inexpensive engines and cooling devices with no moving parts and a significant fraction of Carnot's efficiency [32]. Since there is no or only one moving part in pulse tube refrigerators, the different arrangements of these refrigerators such as an orifice, double inlet, and inertance tube, pulse tube refrigerators were considered as superior to most other Stirling refrigerators [19, 24, 27, 54].

The performance of a pulse tube expander was experimentally investigated [43]. Tward et al. [52] developed a high capacity miniature pulse tube cryocooler which could provide large cooling power for space application over a range of temperatures. Based on efficiency, maintainability, operational flexibility, the feasibility of integration and performance/cost ratio criterion, pulse tube refrigerator was found to be applicable for HTS from 20 K to 77 K temperature ranges [50]. Zia [57] described the rapid evolution of pulse tube cryocooler from a laboratory-based prototype to a commercial offering that produces cooling of 200 W at 80 K.

Yuan et al. [56] developed a thermodynamic model for single stage Stirling type pulse tube cooler and constructed a prototype for experimentation. The researchers' test result showed the cooler reached a lowest no-load temperature of 37 K within 30 minutes and a cooling capacity of 50 W at 55 K with an input power of 3.4 kW. The researchers further reported that at 80 K of cooling temperature, 11% Carnot efficiency has been obtained. The design and fabrication of large capacity, single stage, Stirling type, Pulse tube refrigerator(PTR) was developed followed by a sequence of design modifications which have been focused on the optimization of the flow transition [59].

An experimental investigation was conducted and a numerical model was developed using the SAGE software to understand the origin of parasitic streaming in the regenerator of Stirling-type pulse tube cryocooler [61]. Zhu et al. [79] introduced a nodal numerical model for the simulation of the pulse tube Stirling machine. It has been reported that two single-stage high-frequency coaxial PTCs, with each of them reaching a cooling temperature lower than 30 K and input power of less than 250 W have been designed and tested [78]. It has been further explained that for single stage PTC, optimization with both double-inlet and inertance tube is of crucial to achieving temperature below 30 K. A single-stage high-frequency multi-bypass pulse tube cryocooler(PTC) was designed and experimentally tested [84]. The researchers reported that a single-stage multi-bypass PTC achieved the lowest temperature of 18.6 K with an input power of 268 W, and it was the lowest temperature reported so far with single stage PTC. In the same year, the author designed and tested a single stage Stirling type pulse-tube cryocooler by optimizing the regenerator and a new lower temperature of 15.5 K has been recorded [85]. The new optimized design was reported as it could deliver a cooling power of 386 mW at 20 K for an input power of 246 W which was found to be comparable to the two-stage Stirling pulse tube cryocooler with the same input power.

A three stages high frequency pulse tube cryocooler (HPTC) has been developed, and a no-load temperature of 3.6 K has been reported using helium-4 as working gas [142]. The temperature found from the research has been reported as the lowest temperature found for high frequency pulse tube cryocooler. The researcher has made four improvements (on compressor, regenerator material, intertance tube and on cold inlet structure) to optimize the design. [119] designed a pulse tube cryocooler to suit the demands of small liquid natural gas (LNG) distribution stations which could work at a temperature of 120 K, cooling power of 1.2 KW and a relative Carnot efficiency greater than 20 %. The researchers pointed out that one-third of the acoustic work is dissipated in the inertance

tube and resulted in efficiency deterioration.

Zhou et al. [111] developed a high frequency coaxial single stage like structure and multi-bypass PTR which could achieve a no-load temperature of 13.9 K at an input power of 250 W. [127] established a two-dimensional axis-symmetric CFD model of a miniature coaxial Stirling pulse tube cooler. A numerical simulation was conducted for an inertance tube PTR by removing the dissipative inertance tube and reservoir and replacing a mass-spring displacer directly coupled to a compression space with an objective of recovering power dissipated [124]. From the simulation result, researchers concluded that the COP could be significantly improved due to the extra power recovered by the mass-spring displacer. Theoretical analyses and modeling were conducted to evaluate the dynamic and thermodynamic characteristics of moving-coil linear compressor in the inertance tube Stirling pulse tube cryocooler [116]. The researchers deduced the characteristics governing equations. To verify the theoretical analyses and modeling conducted [116], experimental investigations were carried out in the same year [117]. A better efficient cascade cryocooler was analyzed and experimentally tested, that is capable of recovering most of the expansion work wasted as heat in a pulse-tube cryocooler [140]. A modified type pulse tube refrigerator was proposed numerically to reduce the direct current gas losses that could have an impact on cooling power in the orifice type pulse tube refrigerator by introducing an additional compressor [135].

The effect of the regenerator and pulse tube length on the efficiency of a pulse tube cryocooler was analyzed [92]. The effects of geometrical parameters of the linear compressor on the performances of Stirling-type pulse tube cryocooler were mathematically investigated and some experimental work was performed [117]. Tang et al. [138] analyzed a double-inlet pulse tube refrigerator focusing on the interaction between Gedeon streaming and the local temperature. Experimental work was conducted and a 32 % cooling efficiency improvement was found for a cascade cryocooler as compared with a traditional single-stage pulse-tube cryocooler [140]. In the report on these cascade pulse tube cryocoolers, the second stage cooler covered around 18.1 % of the overall cooling power. A cold end temperature of 98 K was achieved by a modified pulse tube refrigerator based on the CFD simulation [135], whereas a simple orifice type pulse tube refrigerator with the same dimension reached a cold end temperature of 130 K.

Hu et al. [92] reported that the pulse tube cryocooler could offer 520 W of cooling power at a cooling temperature of 80 K with a relative Carnot efficiency of 18.2%. Zhou et al. [111] developed a pulse tube refrigerator that could be a potential choice especially for small cooling loads at a low temperature such as 31.3 K and 20 K for 50 W and 100 W power inputs respectively. Zhao et al. [127] analyzed and calculated the different types of regenerator losses, and reported that the pressure drop is dominant for most regenerator's length and decrease monotonously from warm space to cold space. Double-inlet pulse tube refrigerator was simulated to analyze the impact of Gedeon streaming on the efficiency of the machine [138]. The short summary of research findings about Stirling cycle cryocooler is shown in Table 2.1.

Review summary of Stirling cooler performances.			
Author	*Method*	*Main Findings*	*Remark*
[98]	Numerical simulation	A no-load temperature of 38 K & 1012 W at 77.35 K with a PV power of 7.72 kW	Kinetic drive
[140]	Experimental test	A cooling power of 700 W at 77 K & a relative Carnot efficiency of 18.2% has been achieved	Kinetic drive
[132]	Isothermal model	The biggest heat loss is conduction loss & biggest work loss is the mechanical friction loss	Kinetic drive
[129]	CFD modeling & testing	The optimum performance found at phase angle of 90^o and a regenerator porosity of 50%	Alpha kinetic drive
[110]	Numerical optimization	141 W at 77 K in the first stage & 60 W at 30 K in the second stage at input power of 2.23 kW	FPSC
[124]	Numerical & experimental	A lowest temperature of 27.6 K with an input power of 3.12 kW & a mean pressure of 2.58 MPa	FPSC
[85]	Design & testing	Lowest temperature of 15.5 K & 386 mW/20 K cooling power at 246 W input power	Single stage SPTC
[142]	Design & testing	Lowest temperature of 3.6 K & 6 mW/4.2 K cooling power at 250 W input power	Three-stage SPTC

Table 2.1: Review summary of Stirling cooler performances.

2.6/ Reviews on moderate temperature Stirling refrigerating machine

Due to its adiabatic behavior, Stirling machine was generally considered as less efficient for small temperature differences between the compression and expansion side. However, STM has discovered ways to improve the efficiency considerably [30]. A prototype free-piston Stirling refrigerator intended for domestic cooling was experimentally tested and results were reported [25]. Gauger [29] reported that the gas cycle refrigeration systems including the Stirling refrigerator have the highest cycle efficiency at lower source temperatures. Berchowitz [26] discussed the impact of irreversibilities for moderate temperature Stirling refrigerating machine with reference to the machine design. The researcher reported the configuration of free-piston Stirling cycle refrigerating machine resulted in better performance than the crank driven Stirling refrigerating machine.

The free piston Stirling refrigeration machines were found superior to the vapor compression refrigeration machine for domestic purpose [28, 115]. The researchers further described that the FPSCs are far more superior than the VCR in their respective COP. Berchowitz [28] explained the development of free-piston Stirling refrigeration machine would continue with noticeable achievements and they are expected to meet or exceed the life time and reliability expectations of ordinary refrigerators while being cost competitive. Based on the optimization work conducted in the year 1996, it was found that the free-piston Stirling coolers together with super insulated cabinets and cold stores offer an ideal combination for practical photovoltaic powered refrigerators [33].

The impact of finite-rate heat transfer and regenerative losses on Stirling refrigerators cooling performance was investigated [34]. A finite time heat transfer analysis was also conducted in the year 1998 for an air refrigeration cycle with non-isentropic compression and expansion [37]. The researcher derived the relation between COP and cooling load with pressure ratio. Chen [36] developed an irreversible cycle model to predict the performance and the input power required for the Stirling refrigerator optimized on a specified cooling capacity. Some dimensionless parameters have been proposed to link the entropy variation rate and the temperature differences at the heat exchangers for an irreversible refrigerator [90].

Researches were conducted on an optimal relation between the cooling rate and the coefficient of performance of the refrigerating machine [34, 36, 75]. Haywood et al. [42] reported that there are conditions for Stirling refrigerating machines to provide higher performance than vapor compression machines. The finding of the researchers can be seen in Fig. 2.19. The maximum cooling capacity was obtained when the volume ratio was almost equal to the temperature ratio for the developed Beta type prototype refrigerator [44]. The researchers also found that nitrogen had a better cooling capacity than helium. Nie et al. [71] pointed out the refrigeration heat capacity and COP of large-scaled Stirling refrigeration are independent with the surface area. The COP of V-type Stirling-cycle refrigerator near-ambient cooling conditions has been reported to be comparable with the vapor compression refrigerating systems and applicable for domestic refrigeration [55, 70] and it is confirmed as seen in Fig. 2.19. The impact of three different fluids (air, hydrogen, and helium) on the performance of a Stirling refrigerator was investigated and the result showed that almost all the three working gases behave in a similar way but hydrogen slightly outperforms most of the time [77].

A Beta-type Stirling cycle machine of 100 W refrigeration capacity for household refrigeration application was mathematically designed and experimentally tested [44]. The researchers studied the effect of parameters such as dead volume ratio, the ratio of the compression volume to the expansion volume, types of working fluids, and the piston and displacer phase difference on the refrigerating performance. Ataer and Karabulut [55] conducted a thermodynamic control volume analysis on a V-type Stirling-cycle refrigerator subjected to periodic mass flow and evaluated the work done, instantaneous pressure, and coefficient of performance of the Stirling refrigerator. The V-type integral Stirling refrigerator (VISR) for domestic application was investigated based on simulation and experimentations and the parameters such as the power intake and the coefficient of performance were analyzed under different rotating frequencies and charged pressures [70]. Furthermore,Tekin and Ataer [77] investigated the thermodynamic performance of a V-type Stirling refrigerating machine in a view for higher cooling capacity and COP as an alternative to vapor compression type refrigerator. In this research, the effect of porosity of regenerator, the phase angle between the pistons, pressure and frequency on

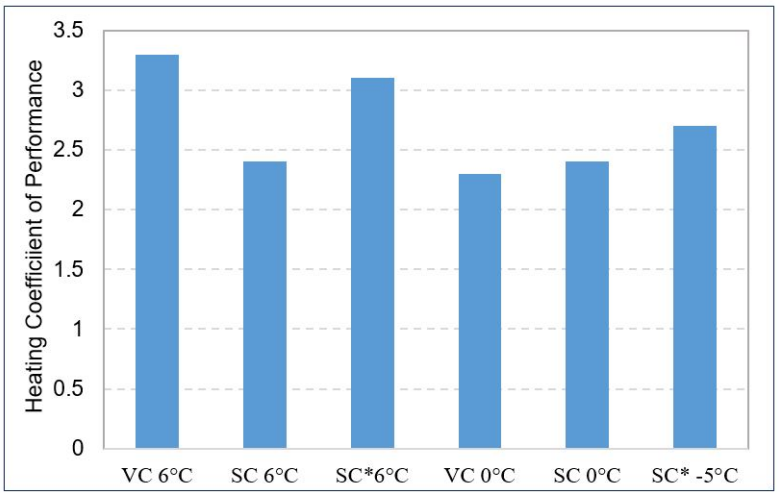

Figure 2.19: Results from the Stirling-cycle heat-pump development program [42]. (VC is typical vapour compression machine, SC is Stirling machine prior to seal development program, SC* is Stirling machine after seal development program. The indoor temperature in all cases is 20^oC)

COP and cooling capacity for the three working fluids had been investigated. Razani et al. [75] developed a thermodynamic model for an exergy flow analysis for Stirling refrigerator. Sauer et al. [136] pointed out that one-dimensional differential models are important tools for the design and optimization of regenerative machines since they require far less computing time than multi-dimensional computational fluid dynamics models and are still capable of describing the various losses.

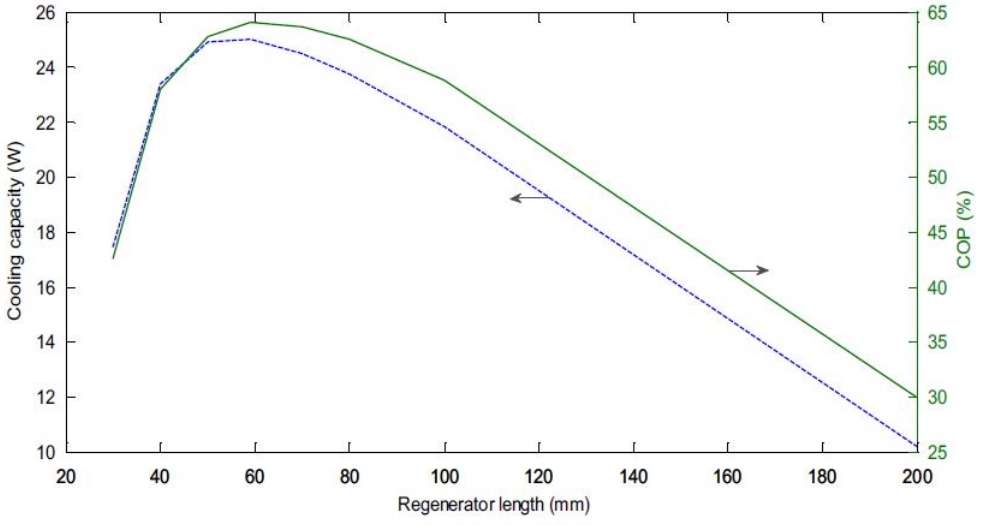

Figure 2.20: Cooling capacity and COP evolution versus regenerator length [130]

Stirling heat pump was investigated as a realistic alternative to vapor compression machine [42, 87, 100]. A non-linear mathematical model was developed for an air-filled Alpha Stirling refrigerator by incorporating air thermodynamics, heat transfer from the walls, as well as heat transfer and fluid resistance in the regenerator and different variables were determined for both working spaces [94]. Furthermore, the researchers tested the

machine experimentally by replacing the piston-cylinder assembly with a flexible chamber and investigated the performance of the refrigerator. Ahmadi et al. [88] optimized a Stirling heat pump using multi-objective criteria in finite time. The researchers simultaneously considered the three objective functions such as the maximization of heating load and coefficient of performance, and the minimization of input power of the Stirling heat pump. The researcher analyzed both external and internal irreversibilities. External irreversibility is due to a finite temperature difference between the gas and the heat exchangers while the internal irreversibility is due to the regenerative heat loss and entropy generation. In the year 2015, the author used the finite time thermodynamics approach for thermo-economic multi optimization of Stirling heat pumps [100]. Hachem et al. [105] evaluated the performances of a Beta type Stirling refrigerating machine having a regenerative displacer by considering complex phenomena which are related to compressible fluid mechanics, thermodynamics and heat transfer for the energy analysis.

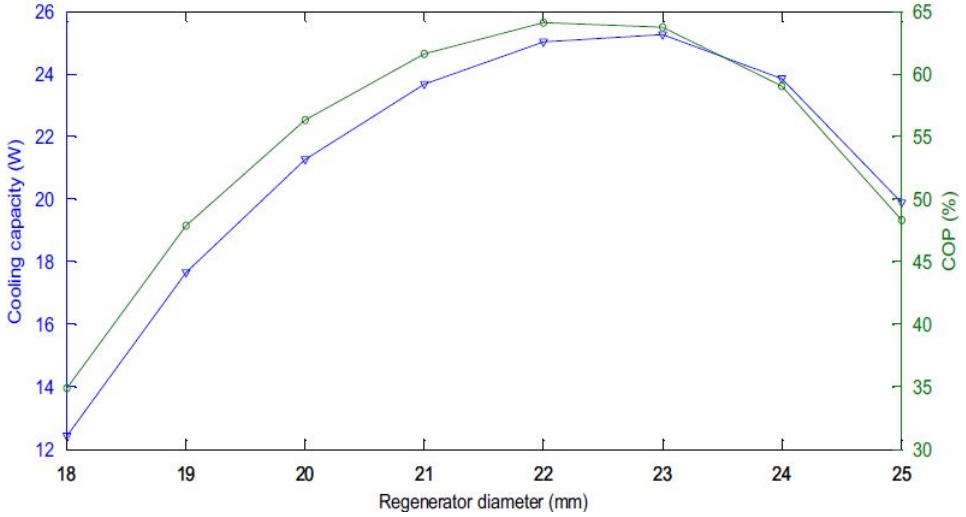

Figure 2.21: Stirling refrigerator performances versus regenerator diameter [130].

To design an experimental Stirling cycle refrigeration unit, an adiabatic numerical model was developed [120]. The research presented a simple time discretization model considering the cylinders as adiabatic spaces and the results were verified by another modeling technic called the full three dimensional CFD. The result of the analysis showed the compliance of the adiabatic model with the full 3D CFD model. Various Stirling refrigerators were analyzed with and without a regenerator and the coefficient of performance of the machine was evaluated [133]. Hachem et al. [130] developed a thermodynamic model and conducted an experimental validation to optimize an air-filled Beta-type Stirling refrigeration machine with special attention to evaluate the effect of geometrical parameters such as dead space volume and swept volume of the compression and expansion space. The regenerator parameters on the performance of refrigerator were also analyzed and optimized by the researchers(see Fig. 2.20 and 2.21). Chaudhari et al. [115] developed a mathematical formulation using loss factor to free piston Stirling cooler for domestic refrigeration application. Multi-objective optimization has been performed using non-ideal adiabatic analysis to optimize Gamma type Stirling refrigerator [141]. The researchers indicated that the cooling capacity increased with the increase of operating frequency based on analysis and experimental results where the COP has attained a maximum value. Furthermore, they described that the optimum COP value for the air occurred at a

lower operating frequency than that of helium(see in Fig. 2.22).

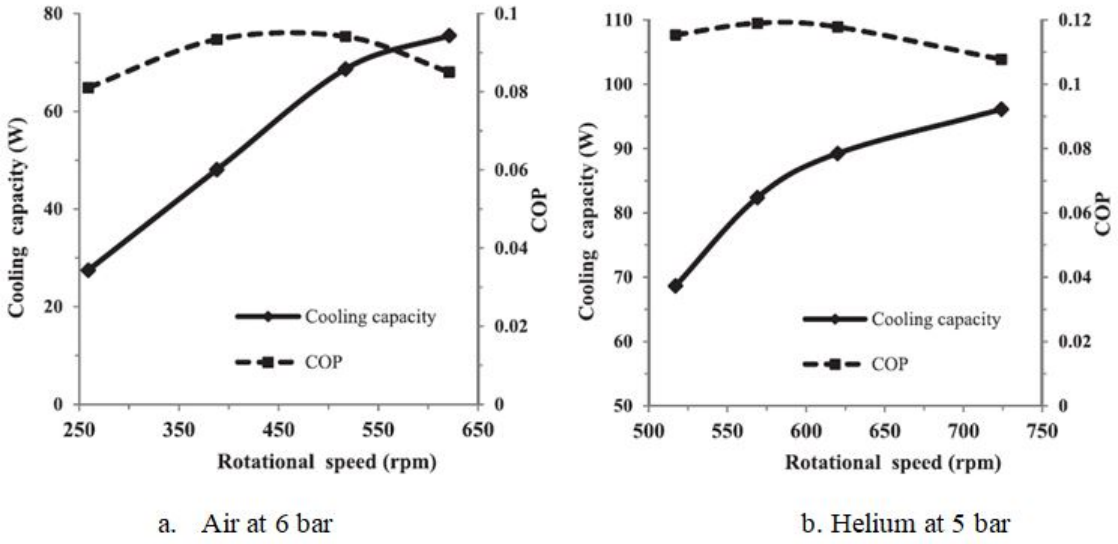

Figure 2.22: The variation of the cooling capacity and COP with operating frequency for air and helium gases [141].

Guo et al.[150] introduced a general model to various types of Stirling refrigerators with analytical solutions. A Beta-type Stirling cooler was developed with a rhombic drive system [148]. In the same year, a similar Beta-type of Stirling refrigerator was designed and fabricated to achieve a rapid transfer of heat from the system [152]. Helium and carbon dioxide have been used as a working fluid and the more efficient fluid was determined.

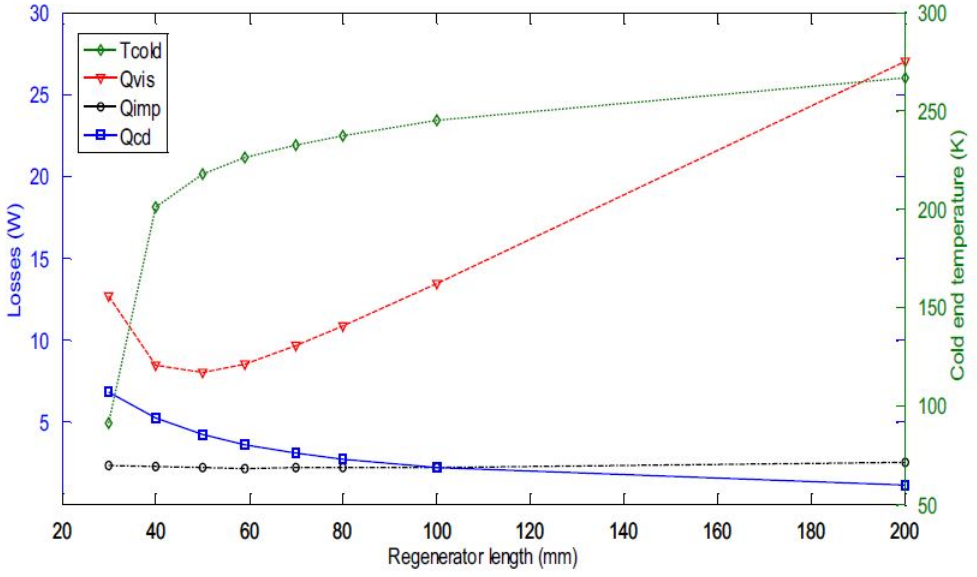

Figure 2.23: Cold end temperature and losses evolution versus regenerator length [130].

An experimental result of COP for free piston Stirling refrigerator has been reported to be 0.217 for a cold end temperature of $-33\,^oC$ and hot end temperature of $18\,^oC$ [25]. The efficiencies of free-piston Stirling refrigeration machine working at domestic refrigerating temperature were reported to exceed 32% of Carnot efficiency and are expected to

achieve very high efficiencies and replace the domestic refrigerators while achieving cost competitiveness [28]. Oguz et al. [39] conducted an experimental work and reported the COP values for FPSCs operating with warm head temperatures close to $30\,^oC$ were typically found between 2 and 3 for cold head temperatures around $0\,^oC$, falling to around 1 for temperatures approaching $-40\,^oC$. Hachem et al. [105] predicted that the drop-in heat exchanger efficiency would influence the pressure ratio and so the refrigeration capacity would be reduced substantially. In the year 2017, Hachem et al. [130] evaluated different losses associated with Stirling refrigerator that directly affect cooling performance of the refrigerator and they described these losses are functions of regenerator diameter and length as seen in Fig. 2.23. The researchers pointed out that the optimal values of diameter and length for the prototype Beta-type Stirling refrigerator are about 22 mm and 60 mm respectively. A short summary of research findings about Stirling cycle refrigerator for moderate temperature application is shown in Table 2.2.

2.7/ CONCLUSION

Currently, the Vapor Compression Refrigeration (VCR) technologically exists at the saturated level and is suited for household cooling applications. Although, VCR is an efficient technology especially for moderate temperature refrigeration applications, because of HFC refrigerants the environmental concern is increasing due to global warming. Stirling refrigerators for moderate temperature application is one of the technologies that is brought from the concern about the use of HFC refrigerants and their effect on global warming potential. A detailed review of literature has been conducted about the research and development made on the Stirling cycle refrigerators. This Stirling cycle refrigerators are the counterpart of work producing Stirling cycle engines and generally have the same configurations and driving mechanisms as their counterparts. The review covers configurations and drive mechanisms, thermodynamic modeling techniques as well as detailed review on the development status of Stirling coolers for low temperature and moderate temperature applications. The main conclusions are summarized:

- Lots of researches have been done on low-temperature coolers with different drive mechanisms. As a result of this, Stirling coolers have reached comparable performance with other technologies and are widely applied at cryogenic temperature applications.

- The number of researches are limited on Stirling cycle refrigerators for moderate temperature applications. This is mainly because of the current most commonly used vapor compression refrigerating technology is found at the optimal technological level and cost.

- For Stirling cryocoolers, the pulse-tube drive mechanism with multi-stage has achieved the lowest temperature with a three-stage high-frequency pulse tube cryocooler (HPTC) a no-load temperature of 3.6 K reported.

- Recently the demand for alternative refrigerating technology is increasing due to environmental concern resulted mostly from the existing technology HFC gas emissions.

- Even though the choice of heat exchangers design and working volumes for Stirling machine depends on the application area, most researches that have done so far particularly on moderate temperature Stirling cycle refrigerator are directly experimented by reversing the existing Stirling engine. For instance, the heater and cooler of the engine are acting as chiller and hot heat exchanger respectively for refrigerating machine. Furthermore, the regenerator parameters including the porosity and the relative size of working volumes have a greater effect on the performance of the machine. In the Stirling engine, all the components are designed and manufactured to produce the maximum power output or efficiency. Hence, such reversing a machine configuration may not produce the optimum cooling or COP.
- Second-order numerical models can be utilized to simulate every type of Stirling engines/coolers with reasonable accuracy. On the other hand, due to much lower computation time compared to third-order models, second-order models can be used easily for design and optimization purpose.
- Results from the researches done so far on the Stirling cycle refrigerating machines for moderate temperature household application shows that Stirling cycle machines are promising alternatives to the current technology in use for the same application.
- It has been recognized that one of the challenges of Stirling machines is the cost of production as it demands higher accuracy manufacturing to minimize gas leakage as well as to create smooth motion between parts, and the material has to be selected to withstand the high temperature and pressure. The operating temperature and pressure ranges of moderate temperature cooling machine are by far lower than that of its counterpart. Therefore, it could be possible to reduce the cost of cooling machine through designing and selecting a reasonable material.
- The other development problems of all Stirling machines including coolers is its difficulty to avoid gas leakage and different thermal losses. In addition, for moderate temperature cooling application, developing Stirling refrigeration machines that could outperform the conventional VCR is still challenging. However, global warming potential (GWP) concern has to be taken in to account for the comparison of different technologies.
- The researches done so far on moderate temperature Stirling refrigerator did not show clearly the configurations that have better performance for a different range of cooling temperatures.

The global concern to create clean environment and the increased demand in refrigeration; on the other hand, the high global warming potential of refrigerants used in conventional VCR technology lead to the increased interest in alternative technologies. Stirling cycle refrigerator for moderate cooling application is found to be a potential candidate. However, the Stirling cycle machines as a general have several limitations, the efforts done so far on the design of Stirling refrigerating machine is very limited and does not consider fully the design and developmental requirements of the cooling machine for particular applications. Therefore, future researches on Stirling cycle moderate temperature cooling machines have to be designed considering the operating condition as well as suitable configuration, all components must be produced, and tested based on the cooling temperature requirement.

Review summary of Stirling refrigerator for moderate cooling.			
Author	*Method*	*Main Findings*	*Remark*
[25]	Experimental	For a cold temperature of -33^oC and hot end temperature of 18^0C, the COP was found to be 0.217	FPSR
[28]	Assessment & testing	Reported 60% of Carnot efficiency achievable for domestic refrigeration	FPSR
[36]; [75]	Investigation	The optimal relation ship between the cooling rate and COP identified	
[44]	Simulation & testing	Hydrogen has better cooling capacity than helium and dead volume has major impact on cooling capacity	Beta
[55]	Thermodynamic analysis	COP of the Alpha machine is comparable with the VCR	Alpha
[70]	Simulation and experiment	Helium and nitrogen -20 to -60^oC cold end temperature ,100 W	Alpha
[77]	Thermodynamic analysis	Hydrogen relatively performs better 230-360 K ,450 W	Alpha
[42] [100]	Experiment & multi-objective	Stirling heat pump is a good alternative to vapor compression heat pump and even have better performance	Heat pump
[120]	Adiabatic model & experiment	The developed model could find applications for design and optimization due to its simplicity	Alpha
[130]	Thermodynamic & experiment	The optimal value of diameter and length for beta type Stirling refrigerator prototype is about 22mm and 60 mm	Beta
[141]	Experiment & Analytical inv.	Minimum achievable temperature are -94.2^oC and -42.6^oC for helium and air when the operating frequency and working pressure varied between 260 and 775 rpm and 4 and 7 bar, respectively	Gamma

Table 2.2: Review summary of Stirling refrigerator for moderate cooling.

II

CONTRIBUTION

3

NUMERICAL MODELING

It is noted that Stirling refrigerator have been found as potential alternative technology for domestic applications. The design of a Stirling machine requires the understanding of the processes that govern their operation. The first attempt to describe this process was through the ideal Stirling thermodynamic cycle. However, the ideal thermodynamic cycle could not show the actual process in the Stirling cycle refrigerator. Hence, in this chapter, a second-order numerical model has been adopted and suggested based on the review findings presented in section 2.4 for the design of an air-filled Beta-type Stirling refrigerator. The developed model is a non-ideal second-order numerical model called the modified simple considers the effects of various losses for domestic cooling [160]. The study categorizes and investigates losses based on their effect. Then, the simulation of the model has been performed using MATLAB code. Then, the model has been validated with the reversed model (as engine and using GPU-3 machine) and direct experimentation using Femto 60 machine as a refrigerator.

3.1/ IDEAL ADIABATIC MODELING

The dead volumes occupied inside the hot heat exchanger, regenerator, and chiller remain constant during the refrigeration cycle. On the other hand, the volume in the compression and expansion spaces changes continuously and thus determine the pressure variation over the cycle. The volume variations in compression and expansion spaces are controlled by the dynamics of the crank mechanism, which determines the position of the pistons at different crank angles of the cycle.

In real Stirling cycle machines, the compression and expansion spaces are considered as adiabatic, in which there is no heat transfer to the surroundings. The overall Stirling cycle refrigeration machine is configured into five control volumes (two working spaces and three perfectly effective heat exchangers) serially connected in the same way as described by [20]. In this respect, the model is similar to the ideal isothermal model with the gas temperature in the hot heat exchanger and the chiller is assumed as an isothermal condition with respective temperature value. The control volumes for the analysis include compression space(c), hot heat exchanger(h), regenerator(r), chiller(cr), and expansion space(e) as shown in Fig. 3.1. The assumptions taken for such ideal adiabatic analysis are as follows:

- The compression and expansion spaces are adiabatic.

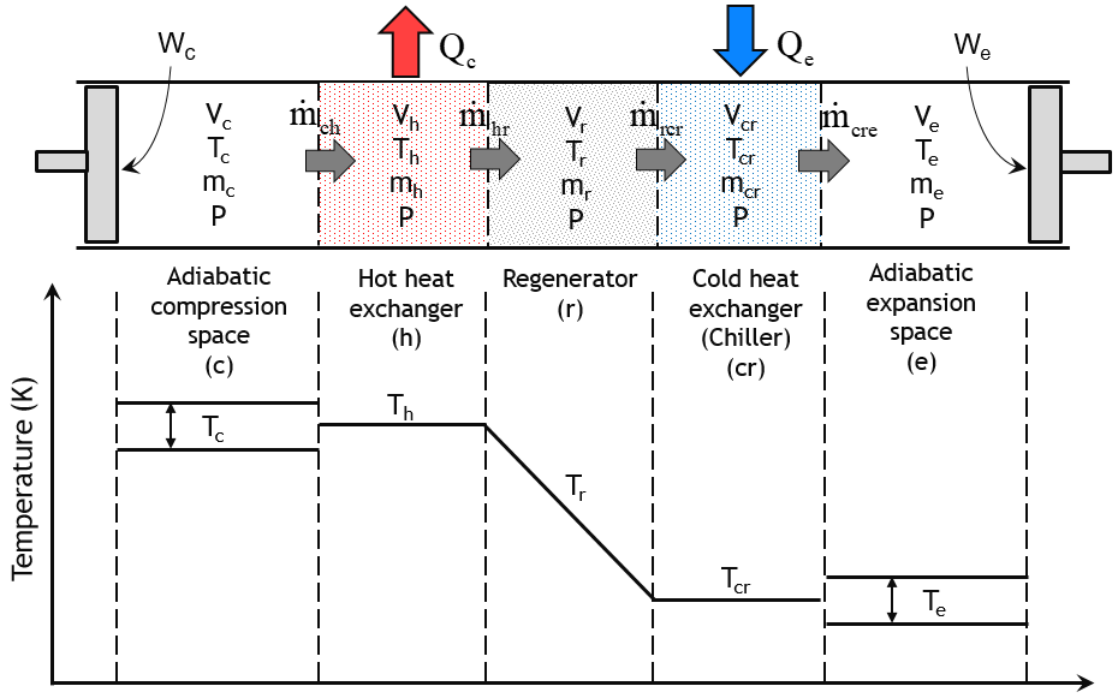

Figure 3.1: Ideal adiabatic schematic model for Stirling cycle refrigerator with five cells and four interfaces.

- The working gas is ideal.
- The temperature in the hot heat exchanger and chiller are constant.
- No gas leakage and pressure drop.
- The regenerator is perfect.
- All processes are performed in a steady-state condition.
- The temperature of the working fluid in the regenerator is linearly changed.
- The kinetic and potential energies of gas streams are negligible.
- Heat is transferred to the working fluid only in the hot heat exchanger and chiller
- Heat transfer to the environment is negligible.
- The machine is working at constant angular velocity.

Although the Stirling machine does not operate with ideal cycles, the ideal Stirling cycle demonstrates the principles behind the Stirling machine. Hence, ideal cycle would be the starting point of our analysis. In this section, the Stirling cycle refrigerating machine is numerically modelled by ideal adiabatic model in which, first, conservation laws are applied across the overall machine and then various equations are applied for each control spaces. The starting point of the analysis is the conservation of mass that is the total mass of working gas in the Stirling refrigeration machine remains constant. In ideal conditions, there is no mass leakage and therefore the total mass is the summation of masses in the five control volumes and it is given as:

$$m_c + m_h + m_r + m_{cr} + m_e = m_t \tag{3.1}$$

In the case of cooling machine, the displacer forces the working fluid between expansion and compression space whereas the power piston converts the mechanical power into pressure of the gas. The working fluid used in this analysis is air and it is an ideal gas, which is valid for the regenerative Stirling cycle refrigerators as the process is far from the critical point of the gas. Thus, the equation of state is valid for this investigation.

$$PV = mRT \tag{3.2}$$

Differentiating on both sides of Eq. (3.2) and rearranging gives;

$$\frac{dP}{P} + \frac{dV}{V} = \frac{dm}{m} + \frac{dT}{T} \tag{3.3}$$

Then, introducing the derivative operator D based on [20] with respect to time where $DX = \frac{dX}{dt}$ and X is a thermodynamic parameter ($P,\ V,\ T,\ W,\ Q,\ m$).

$$\frac{DP}{P} + \frac{DV}{V} = \frac{Dm}{m} + \frac{DT}{T} \tag{3.4}$$

Enthalpy is transported across the interface of control volumes with mass flow rate and upstream temperature, T. There are four interfaces between the five cells of Stirling cycle machine through which enthalpy is transported by virtue of mass flow $\dot{m}$ or Dm shown in Fig. 3.1. The interfaces are:

- Compression space/hot heat exchanger
- Hot heat exchanger/regenerator
- Regenerator/chiller
- Chiller/expansion space

The temperature in working spaces varies based on the degree of expansion and compression as shown in Fig. 3.1. Temperature of the gas in the compression space is either greater or less than temperature of the hot heat exchanger. Similarly, temperature of the air in expansion space may be greater or less than temperature of the chiller. So, the direction of the flow of fluid depends on temperature gradient. By convention, we arbitrarily assume that the arrows (from compression space to expansion space) as shown in Fig. 3.1 represent the positive direction of the flow of fluid and the reverse is negative.

The working gas temperatures across compression space and hot heat exchanger (T_{ch}) as well as across chiller and expansion space (T_{cre}) are conditional temperatures based on the flow direction and are evaluated as:

$$If\ \dot{m}_{ch} > 0, T_{ch} = T_c,\quad if\ not\ \ T_{ch} = T_h \tag{3.5}$$

$$If\ \dot{m}_{cre} > 0, T_{cre} = T_{cr},\quad if\ not\ \ T_{cre} = T_e \tag{3.6}$$

Generally, temperature of the gas at the interface takes the temperature of the upstream control space. Fig. 3.1 shows that the hot heat exchanger and chiller temperatures are assumed to be constant and the regenerator temperature is assumed to vary linearly from chiller to hot heat exchanger temperature. The linear variation permits the evaluation of mean effective temperature for the regenerator space and it is given as:

$$T_r = \frac{T_h - T_{cr}}{ln(\frac{T_h}{T_{cr}})} \tag{3.7}$$

The energy balance equation based on the first law of thermodynamics for a control volume in an open system is given by:

$$\frac{\delta Q_i}{dt} + \frac{\delta W_i}{dt} = C_p(T_{i,o}\dot{m}_{i,o} - T_{i,in}\dot{m}_{i,in}) + C_v\frac{\delta(m_i T_i)}{dt} \tag{3.8}$$

with

$$\delta W_i = -PdV_i \tag{3.9}$$

Using the above operator D, equation(Eq. 3.8) becomes:

$$DQ_i + DW_i = C_p(T_{i,o}\dot{m}_{i,o} - T_{i,in}\dot{m}_{i,in}) + C_v D(m_i T_i) \tag{3.10}$$

Where,

$$DW_i = -PDV_i \tag{3.11}$$

For the three heat exchangers including regenerator ($DW_i = 0$ and $C_v D(m_i T_i) = C_v T_i D m_i$), owing to constant volume and constant temperature. The energy balance equation(Eq. 3.10) for heat exchangers will be reduced to:

$$DQi = C_p(T_{i,o}\dot{m}_{i,o} - T_{i,in}\dot{m}_{i,in}) + C_v T_i D m_i \tag{3.12}$$

The change in mass in three heat exchangers (hot heat exhanger, regenerator, and chiller) due to pressure change could be found from (Eq. 3.4) as:

$$Dm_i = \frac{m_i DP}{P} = \frac{V_i}{T_i}\frac{DP}{R}(where\ i = h, r, cr) \tag{3.13}$$

Then, the ideal heat transfer in the hot heat exchanger, regenerator and chiller respectively are reduced to:

$$DQ_{h,iad} = \frac{V_h DPC_v}{R} - C_p(T_{ch}\dot{m}_{ch} - T_h\dot{m}_{hr}) \tag{3.14}$$

$$DQ_{r,iad} = \frac{V_r DPC_v}{R} - C_p(T_h\dot{m}_{hr} - T_{cr}\dot{m}_{rcr}) \tag{3.15}$$

$$DQ_{cr,iad} = \frac{V_{cr} DPC_v}{R} - C_p(T_{cr}\dot{m}_{rcr} - T_{cre}\dot{m}_{cre}) \tag{3.16}$$

In idealized modeling conditions, as there is no pressure drop, pressure shall not be suffixed for different control volumes and hence pressure P represents the instantaneous

pressure throughout the system. Since the pressure is assumed uniform throughout the interior surfaces of the Stirling cycle refrigerator, from (Eqs. 3.1 and 3.2), we obtain the equation of pressure:

$$P = \frac{m_t R}{\frac{V_c}{T_c} + \frac{V_h}{T_h} + \frac{V_r}{T_r} + \frac{V_{cr}}{T_{cr}} + \frac{V_e}{T_e}} \tag{3.17}$$

Based on the reciprocating movement of piston and displacer, the expansion and compression volumes for Beta configuration Stirling cycle refrigerating machine are given as:

$$V_e = V_{cle} + \frac{1}{2} V_{swe}(1 + cos\theta) \tag{3.18}$$

$$V_c = V_{clc} + \frac{1}{2} V_{swc}(1 + cos(\theta - \alpha)) + \frac{1}{2} V_{swe}(1 - cos\theta) - V_b \tag{3.19}$$

where V_b is the overlap volume in compression space.

$$V_b = \frac{(V_{swc} + V_{swe})}{2} - \sqrt{\frac{(V_{swc})^2 + (V_{swe})^2}{4} - \frac{V_{swe} V_{swc} cos\alpha}{2}} \tag{3.20}$$

Overlap volume is the volume shared by both the displacer and piston movements. It is a unique characteristic of a Beta-type Stirling machine and needs consideration while estimating the actual performance of the machine.

Differentiating the mass conservation (Eq. 3.1)

$$Dm_c + Dm_h + Dm_r + Dm_{cr} + Dm_e = 0 \tag{3.21}$$

Substituting (Eq. 3.13) in (Eq. 3.21) gives:

$$Dm_c + Dm_e + \frac{DP}{R}\left(\frac{V_h}{T_h} + \frac{V_r}{T_r} + \frac{V_{cr}}{T_{cr}}\right) = 0 \tag{3.22}$$

Considering adiabatic compression and expansion, the change in mass in compression and expansion chambers is found as:

$$Dm_c = \frac{PDV_c + \frac{V_c DP}{\gamma}}{RT_{ch}} \tag{3.23}$$

$$Dm_e = \frac{PDV_e + \frac{V_e DP}{\gamma}}{RT_{cre}} \tag{3.24}$$

Substituting for Dm_c and Dm_e in Eq. (3.22) and simplifying,the change in pressure is found as:

$$DP = -\frac{P\gamma\left(\frac{DV_c}{T_{ch}} + \frac{DV_e}{T_{cre}}\right)}{\frac{V_c}{T_{ch}} + \gamma\left(\frac{V_h}{T_h} + \frac{V_r}{T_r} + \frac{V_{cr}}{T_{cr}}\right) + \frac{V_e}{T_{cre}}} \tag{3.25}$$

Summary of ideal adiabatic model.	
Parameters	*Equations*
Pressure	$P = \frac{mR}{\frac{V_c}{T_c}+\frac{V_h}{T_h}+\frac{V_r}{T_r}+\frac{V_{cr}}{T_{cr}}+\frac{V_e}{T_e}}$ $DP = \frac{-P\gamma(\frac{DV_c}{T_{ch}}+\frac{DV_e}{T_{cre}})}{\frac{V_c}{T_{ch}}+\gamma(\frac{V_h}{T_h}+\frac{V_r}{T_r}+\frac{V_{cr}}{T_{cr}})+\frac{V_e}{T_{cre}}}$
Mass	$m_i = \frac{PV_i}{RT_i}(where\ i = c,h,r,cr,e)$
Change of mass	$Dm_i = \frac{m_i DP}{P} = \frac{DP}{R}\frac{V_i}{T_i}(where\ i = h,r,cr)$ $Dm_c = \frac{PDV_c+\frac{V_c DP}{\gamma}}{RT_{ch}}$ $Dm_e = \frac{PDV_e+\frac{V_e DP}{\gamma}}{RT_{cre}}$
Mass flow	$\dot{m}_{ch} = -Dm_c\ ,\quad \dot{m}_{hr} = \dot{m}_{ch} - Dm_h$ $\dot{m}_{rcr} = \dot{m}_{cre} + Dm_{cr}\ ,\quad \dot{m}_{cre} = Dm_e$
Conditional temperature	If $\dot{m}_{ch} > 0, T_{ch} = T_c$ if not $T_{ch} = T_h$ If $\dot{m}_{cre} > 0, T_{cre} = T_{cr}$ if not $T_{cre} = T_e$
Temperature variation	$DT_e = T_e(\frac{DP}{P} + \frac{DV_e}{V_e} - \frac{Dm_e}{m_e})$ $DT_c = T_c(\frac{DP}{P} + \frac{DV_c}{V_c} - \frac{Dm_c}{m_c})$
Energy and power	$DQ_{h,iad} = \frac{V_h DPC_v}{R} - C_p(T_{ch}\dot{m}_{ch} - T_h\dot{m}_{hr})$ $DQ_{r,iad} = \frac{V_r DPC_v}{R} - C_p(T_h\dot{m}_{hr} - T_{cr}\dot{m}_{rcr})$ $DQ_{cr,iad} = \frac{V_{cr} DPC_v}{R} - C_p(T_{cr}\dot{m}_{rcr} - T_{cre}\dot{m}_{cre})$ $W_{iad} = W_c + W_e$ $DW_{iad} = DW_c + DW_e$ where $DW_c = -PDV_c$ and $DW_e = -PDV_e$

Table 3.1: Summary of ideal adiabatic model.

The change in temperature in the expansion and compression spaces could be found from differential Eq. (3.4) as:

$$DT_e = T_e(\frac{DP}{P} + \frac{DV_e}{V_e} - \frac{Dm_e}{m_e}) \tag{3.26}$$

$$DT_c = T_c(\frac{DP}{P} + \frac{DV_c}{V_c} - \frac{Dm_c}{m_c}) \tag{3.27}$$

Then the overall work done on refrigeration machine is the algebraic sum of compression work and expansion work.

$$DW_{iad} = DW_c + DW_e \tag{3.28}$$

where,

$$DW_c = -PDV_c \; and \; DW_e = -PDV_e \tag{3.29}$$

A summary of ideal adiabatic equations have been shown in table 3.1.

3.2/ MODIFIED IDEAL ADIABATIC ANALYSIS

The performance of Stirling machine is strongly dependent on geometrical and operating parameters such as physical dimensions, heat transfer coefficients, heat source temperatures and regenerator characteristics. Predicting the performance of Stirling machine is important for the design of the machine. In the past decade of years, many researchers and scientists have studied the Stirling machine numerically or experimentally.

The system of the above ideal adiabatic differential equations was modified by including the effects of gas leakage from working space to buffer space (crankcase) and shuttle heat losses by displacer from compression to expansion spaces. This is by adapting and modifying the engine models (simple model by [20] and Simple-II model by [89]) to the refrigeration machine through reversing the process. The main reasons for the inclusion of mass leakage and shuttle heat losses to the differential equation are because these losses can affect the overall working of the machine by changing the pressure and temperature of the working fluid. So, the conservation equations of mass (Eq. 3.1) and energy (Eq. 3.10) of the original ideal adiabatic equations of the Stirling cycle refrigeration machine presented before have been modified by including the mass leakage loss and shuttle heat losses respectively. Due to analytical complexity, other losses are not included directly in the modified ideal adiabatic simulation and are treated separately.

The energy losses in a Stirling cycle machine are due to the thermodynamic and mechanical processes of the cycle. To accurately predict a Stirling cycle refrigeration machine performance and to design an optimal machine for a specific application, a detailed investigation of various losses has to be considered in the modified simple analysis part as discussed in section 3.3. Different types of heat and power losses are shown in Fig. 3.2.

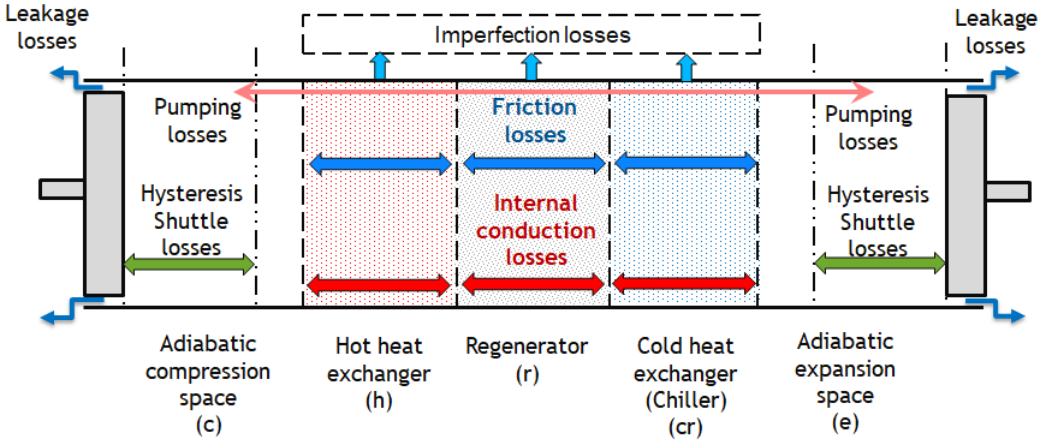

Figure 3.2: Mapping of various heat and power losses (adapted from [145]).

3.2.1/ MASS LEAKAGE LOSS

The design of seals in the Stirling machines is somewhat complicated by the fact that the running of the machine in the working space should be dry, that is without oil. Furthermore, the bearing pressure of the seals should be limited to avoid local heating and decrease mechanical friction losses. Therefore, clearance seals are usually used to avoid excessive wear and hence to extend the service life of the Stirling machine. The clearance seals cause gas leakage between the compression space and the expansion space through the displacer's clearance and between the compression space and the bounce space through the power piston's clearance [108]. Stirling cycle machine seal design therefore involves some compromise, which may result to gas leakage to some degree. The leakage loss is more critical especially at higher frequency and higher pressure Stirling machines [147]. This is because at higher pressure and higher frequency the rate of mass leakage is higher. Hence, studying the thermodynamic effect of mass leakage is one aspect of this design. Then, the original mass balance (Eq. 3.1) of ideal adiabatic model is modified by incorporating mass leakage from the compression space to the bounce space through the clearance gap between power piston and cylinder as:

$$m_c + m_h + m_r + m_{cr} + m_e - m_{leak} = m_t \tag{3.30}$$

where m_{leak} is the amount of the working fluid being lost from the compression space into the crankcase.

The amount of working gas lost per unit time from working space to the crank case is determined as [20]:

$$Dm_{leak} = d_p \pi \frac{P + P_{buffer}}{4RT_g}(U_p J - \frac{J^3}{6\mu}(\frac{P - P_{buffer}}{L_p})) \tag{3.31}$$

where $d_p, J, T_g, L_p, u_p, \mu, P$ and P_{buffer} are piston diameter, annular gap between piston and cylinder, gas temperature, piston length, piston linear velocity, viscosity of working fluid, pressure of working space and pressure of buffer space respectively.

Differentiating (Eq. 3.30), gives:

$$Dm_c + Dm_h + Dm_r + Dm_{cr} + Dm_e - Dm_{leak} = 0 \tag{3.32}$$

3.2.2/ SHUTTLE HEAT LOSSES

The main function of displacer is to displace the working fluid between compression and expansion volume. However, it also acts as a separator to maintain temperature difference between the two working spaces. During its reciprocating movement, the displacer is frequently contacting with two temperature layers (compression and expansion space) of the working fluid. This effect leads the displacer motion to shuttle heat from hot end to cold end. Shuttle heat losses resulted when the displacer oscillates across a temperature gradient. In a Stirling cycle refrigerating machine, the displacer absorbs heat at the hot end (compression side) of its stroke and gives off this heat at the cold end (expansion side) of the stroke. This loss is mainly depends on the nature of motion and the difference in temperature between the two sides.

The ideal adiabatic energy conservation (Eq. 3.10) is modified by including the shuttle heat losses as:

$$DQ_i - DQ_{shut} + DW_i = C_p(T_{i,o}\dot{m}_{i,o} - T_{i,in}\dot{m}_{i,in}) + C_v D(m_i T_i) \tag{3.33}$$

The shuttle heat losses (DQ_{shut}) as given in [128, 147, 65] is calculated by using equation:

$$DQ_{shut} = \frac{\pi s^2 k_g d_d}{8JL_d}(T_c - T_e) \tag{3.34}$$

where$s, k_g, d_d, J,\ and\ L_d$ are stroke, thermal conductivity of gas, diameter of displacer, gap between displacer and cylinder, and displacer length. T_c and T_e are gas temperature in compression and expansion spaces, respectively.

As other differential equations, the change in mass in the compression and expansion space could be found from Eqs. 3.23 and 3.24 by including the shuttle heat and gas leakage effects as:

$$Dm_c = \frac{PDV_c + \frac{V_c DP}{\gamma}}{RT_{ch}} + \frac{DQ_{shut}}{C_p T_{ch}} + Dm_{leak} \tag{3.35}$$

$$Dm_e = \frac{PDV_e + \frac{V_e DP}{\gamma}}{RT_{cre}} - \frac{DQ_{shut}}{C_p T_{cre}} \tag{3.36}$$

Substituting Eqs. 3.35 and 3.36 in Eq. 3.22 and rearranging, the change in pressure is modified as:

$$DP = \frac{-P\gamma(\frac{DV_c}{T_{ch}} + \frac{DV_e}{T_{cre}}) + \gamma R\frac{DQ_{shut}}{C_p}(\frac{T_{ch}-T_{cre}}{T_{ch}T_{cre}}) - 2\gamma R Dm_{leak}}{\frac{V_c}{T_{ch}} + \gamma(\frac{V_h}{T_h} + \frac{V_r}{T_r} + \frac{V_{cr}}{T_{cr}}) + \frac{V_e}{T_{ere}}} \tag{3.37}$$

Furthermore, particularly for the Beta-type configuration machine, shuttle heat and mass leakage effects could also affect the mass flow rate across the heat exchanger and working space interfaces. Hence the mass flow rate across the compression space and hot heat exchanger interface is given as:

$$\dot{m}_{ch} = -Dm_c - \frac{DQ_{shut}}{C_p T_{ch}} - Dm_{leak} \tag{3.38}$$

And the mass flow rate across the expansion space and chiller interface is:

$$\dot{m}_{cre} = Dm_e - \frac{DQ_{shut}}{C_p T_{cre}} \tag{3.39}$$

The other equations are the same as those of the ideal adiabatic model. So, the summary of the modified ideal adiabatic model is shown in Table 3.2.

After evaluating the modified ideal adiabatic model (to find ideal input power requirement and ideal cooling power), heat transfer losses, and power losses based on Fig. 3.3, the actual performance of a refrigerator is determined. The heat and power losses other than shuttle heat losses are presented in section 3.3. The power losses directly affect the

Summary of modified ideal adiabatic model.	
Parameters	*Equations*
Pressure	$P = R\frac{M-m_{leak}}{\frac{V_c}{T_c}+\frac{V_h}{T_h}+\frac{V_r}{T_r}+\frac{V_{cr}}{T_{cr}}+\frac{V_e}{T_e}}$ $DP = \frac{-P\gamma(\frac{DV_c}{T_{ch}}+\frac{DV_e}{T_{cre}})+\gamma R\frac{DQ_{shut}}{C_p}(\frac{T_{ch}-T_{cre}}{T_{ch}T_{cre}})-2\gamma RDm_{leak}}{\frac{V_c}{T_{ch}}+\gamma(\frac{V_h}{T_h}+\frac{V_r}{T_r}+\frac{V_{cr}}{T_{cr}})+\frac{V_e}{T_{ere}}}$
Mass	$m_i = \frac{PV_i}{RT_i}(where\ i = c,h,r,cr,e)$
Change of mass	$Dm_i = m_i\frac{DP}{P} = \frac{DP}{R}\frac{V_i}{T_i}(where\ i = h,r,cr)$ $Dm_c = \frac{PDV_c+\frac{V_cDP}{\gamma}}{RT_{ch}} + \frac{DQ_{shut}}{C_pT_{ch}} + Dm_{leak}$ $Dm_e = \frac{PDV_e+\frac{V_eDP}{\gamma}}{RT_{cre}} - \frac{DQ_{shut}}{C_pT_{cre}}$ Where, $DQ_{shut} = \frac{\pi s^2k_gd_d}{8JL_d}(T_c - T_e)$
Mass flow	$\dot{m}_{ch} = -Dm_c - \frac{DQ_{shut}}{C_pT_{ch}} - Dm_{leak}$ $\dot{m}_{hr} = \dot{m}_{ch} - Dm_h\ ,\quad \dot{m}_{rcr} = \dot{m}_{cre} + Dm_{cr}$ $\dot{m}_{cre} = Dm_e - \frac{DQ_{shut}}{C_pT_{cre}}$ Where, $Dm_{leak} = d_p\pi\frac{P+P_{buffer}}{4RT_g}(U_pJ - \frac{J^3}{6\mu}(\frac{P-P_{buffer}}{L_p}))$
Conditional temperature	If $\dot{m}_{ch} > 0, T_{ch} = T_c$ if not $T_{ch} = T_h$ If $\dot{m}_{cre} > 0, T_{cre} = T_{cr}$ if not $T_{cre} = T_e$
Temperature variation	$DT_e = T_e(\frac{DP}{P} + \frac{DV_e}{V_e} - \frac{Dm_e}{m_e})$ $DT_c = T_c(\frac{DP}{P} + \frac{DV_c}{V_c} - \frac{Dm_c}{m_c})$
Energy and Power	$DQ_{h,mod} = \frac{V_hDPC_v}{R} - C_p(T_{ch}\dot{m}_{ch} - T_h\dot{m}_{hr})$ $DQ_{r,mod} = \frac{V_rDPC_v}{R} - C_p(T_h\dot{m}_{hr} - T_{cr}\dot{m}_{rcr})$ $DQ_{cr,mod} = \frac{V_{cr}DPC_v}{R} - C_p(T_{cr}\dot{m}_{rcr} - T_{cre}\dot{m}_{cre})$ $W_{mod} = W_c + W_e$ $DW_{mod} = DW_c + DW_e$ where $DW_c = -PDV_c$ and $DW_e = -PDV_e$

Table 3.2: Summary of modified ideal adiabatic model.

actual input power and increase power requirement. Therefore, the actual input power requirement ($\dot{W}_a$) of the refrigeration model considered is evaluated as the sum of modified ideal adiabatic power and all the power losses and found as:

$$\dot{W}_a = DW_{mad} + f(W_{fr} + W_{mec.fr} + dW_{fin.sp}) + \dot{W}_{hys} \tag{3.40}$$

where W_{fr}, $W_{mec.fr}$, $dW_{fin.sp}$ and $\dot{W}_{hys}$ are pressure drop work loss in heat exchangers, work loss due to mechanical friction, work loss due to finite speed of piston, and gas hysteresis power loss.

The heat losses cause the chiller to reject less heat that means the actual cooling power decreases as a result of heat power losses. Then, the actual cooling power produced from the refrigeration system ($Q_{cr,a}$) is computed as the difference between modified ideal adiabatic cooling power and the heat power losses from the system.

The actual cooling power is given as:

$$\dot{Q}_{cr,a} = DQ_{cr,mad} - DQ_{shut} - fQ_{wrl} - \dot{Q}_{rl} - \dot{Q}_{cond} - \dot{Q}_p \tag{3.41}$$

where $f, Q_{wrl}, \dot{Q}_{rl}, \dot{Q}_{cond}, and\ \dot{Q}_p$ are frequency,heat loss due to internal conduction in the regenerator, heat power loss due to regenerator imperfection, conduction heat power loss, and pumping heat power loss, respectively.

The heat losses as well as the power losses reduce the actual COP of a refrigerator. Therefore, COP could be found as:

$$COP = \frac{\dot{Q}_{cr,a}}{\dot{W}_a} \tag{3.42}$$

3.3/ MODIFIED SIMPLE ANALYSIS

The system of analysis of losses for the Stirling cycle refrigerator is adapted from the engine model [20, 89]. Based on their effect on the working condition of the machine, the losses considered in the modified simple analysis were classified into two. The effects of first category of losses including regenerator imperfection and fluid friction losses in the heat exchangers are are used to correct the temperature and pressure of working fluid found from differential simulation in section 3.2. Then, losses such as power loss due to mechanical friction, conduction heat loss in the regenerator wall, power loss due to finite speed of piston, gas spring hysteresis loss, and pumping loss are evaluated as independent losses. Hence, the effects of these losses are considered only to correct the refrigerating performance (input power demand, cooling power, and COP).

All thermal and power losses associated with the machine are assumed to be independent one from another and the total losses are the summation of the losses with the respective category.

3.3.1/ Loss due to internal heat conduction in the regenerator

In the Stirling cycle machines, regenerators are physically located between the hot heat exchanger and cold heat exchanger/chiller. The two heat exchangers operate at different temperatures in which the difference of the temperature depends on the application of the machine. Even though the temperature difference for domestic Stirling cycle refrigerators is not as large as that of Stirling engines or cryocoolers, the internal conduction heat loss is not negligible due to heat flow from hot heat exchanger to chiller through regenerator wall. This heat loss by internal conduction through the walls of the regenerator has been expressed as [93, 137, 76, 64]:

$$Q_{wrl} = k\frac{A_{wg}}{Lf}(T_{wh} - T_{wcr}) \tag{3.43}$$

3.3.2/ Regenerator imperfection (Non-ideal heat tranfer) loss

The regenerator is designed to absorb part of the heat contained in the working fluid during constant volume heat rejection process as hotter gas passes through the regenerator and to release ideally the same amount of heat when colder gas passes back in the reverse process. Nevertheless, because of thermal imperfections of the regenerator, it is impossible to recover all of the heat absorbed. Hence, the performance of the regenerator is usually evaluated by its effectiveness, which simply expresses the fraction of the heat absorbed from the regenerator that could be recovered for a given regenerator design and operating conditions. For a Stirling cycle refrigerating system having a non-ideal regenerator, when the working gas flows from the chiller to the hot heat exchanger, the gas will have the temperature somewhat lower than the hot heat exchanger and then heat will be transferred from regenerator to the working gas.

Due to the imperfection of the regenerator, the thermal energy loss is given by:

$$\dot{Q}_{rl} = Dm_r c_p(1 - \epsilon)(T_c - T_e) \tag{3.44}$$

Where, based on [20], the effect of the non-ideal regenerator is defined by using the number of the transfer units (NTU) as:

$$\epsilon = \frac{NTU}{NTU + 1} \tag{3.45}$$

$$NTU = N_{st}\frac{A_{wg}}{A} \tag{3.46}$$

$$N_{st} = 0.023Pr^{-0.6}Re^{-0.2} \tag{3.47}$$

$$A_{wg} = 4\frac{V_r}{d_r} + \pi(D_{ri} + D_{ro})L_r \tag{3.48}$$

and

$$d_r = d_w \frac{\phi}{(1-\phi)} \tag{3.49}$$

where $\epsilon, NTU, N_{st}, A_{wg}, Re,\ andPr$ are regenerator effectiveness, Number of Transfer Units, Stanton number, wetted area of metal, Reynolds number, and Prandtl number.

Thus, the net heat per unit time absorbed from the chiller and released to the hot heat exchanger by the working fluid at respective wall temperatures are given by:

$$Q_{cr} = Q_{cr,i} - Q_{rl} = \frac{h_{cr}A_{cr}(T_{wcr} - T_{cr})}{f} \tag{3.50}$$

$$Q_h = Q_{h,i} + Q_{rl} = \frac{h_h A_h (T_{wh} - T_h)}{f} \tag{3.51}$$

The working fluid temperature in a hot heat exchanger is higher and in chiller is lower than their respective wall temperatures as the heat exchangers are considered non-ideal. Therefore, the heat exchanger temperatures are corrected using the wall temperature and the actual heat transfer as:

$$T_{cr} = T_{wcr} - \frac{fQ_{cr}}{h_{cr}A_{cr}} \tag{3.52}$$

$$T_h = T_{wh} - \frac{fQ_h}{h_h A_h} \tag{3.53}$$

Where, $h = \frac{Nuk}{d}$, is the convective heat transfer coefficient for both chiller and hot heat exchanger. Nu, k and d are Nusselt number,thermal conductivity of working gas, and hydraulic diameter, respectively.

$Nu = 0.023Pr^nRe^{0.8}$ (n=0.3 for hot heat exchanger and 0.4 for chiller)based on Urieli et al.'s works [20].

3.3.3/ LOSSES DUE TO PRESSURE DROP IN HEAT EXCHANGERS

The flowing of internal gas through the hot heat exchanger, regenerator and chiller of the Stirling cycle refrigerator is in direct contact with the walls of these heat exchangers. The flow of working fluid is forced convection heat transfer with large surface contact to enhance heat transfer. These resulted in fluid friction. The friction losses in the heat exchangers results in pressure drops and it leads to a reduction of performance of the machine. The pressure losses in heat exchangers are calculated to evaluate the amount of power losses due to the drops in pressure. The amount of energy dissipated (W_{fr}) in regenerative Stirling cycle refrigerating machine due to pressure drops at the hot heat exchanger, regenerator and chiller is evaluated as:

$$W_{fr} = \int_0^{2\pi} (\Delta P \frac{dV_e}{d\theta}) d\theta \tag{3.54}$$

Where, $\Delta P = \Delta P_h + \Delta P_r + \Delta P_{cr}$ and

$$\Delta P_i = \frac{2 f_r \mu V_i G_i l_i}{m_i {d_i}^2} \tag{3.55}$$

$$G_i = \frac{(G_{i,in} + G_{i,o})\omega}{2A_i} \tag{3.56}$$

(Where $i = h, r, cr$)

f_r, V, G, l, and m are the Reynolds friction factor, volume, mass flux, length, and mass of gas for each respective heat exchanger, respectively. f_r is a product of Fanning friction factor and Reynolds number, Re.

The Reynolds friction factor for the regenerator (woven screen) has been evaluated from the correlations given by Gedeon and Wood [35] as:

$$f_r = 129 + 2.91 Re^{0.897} \tag{3.57}$$

Then, the Reynolds friction factor for chiller and hot heat exchangers is defined based on [20, 143] as:

$$f_r = 0.0791 Re^{0.75} \tag{3.58}$$

The frictional factor used in this analysis has been obtained from empirical correlations, based on the the heat transfer coefficient correlation valid for stationary flows.

3.3.4/ MECHANICAL FRICTION LOSSES

Because of the relative motion between parts of the refrigeration machine, losses due to mechanical friction increases the amount of power input required for the process. The relative motions in such refrigerating machines include the joints in the displacer and the crank, between the piston and the crank, and between the crank and the axle of the prime mover. In addition, there is mechanical friction between the piston/displacer and the cylinder wall due to the fact that the piston/displacer does not move perfectly in its axial direction.

Therefore, the power losses due to mechanical friction in one cycle is calculated by the following equation:

$$W_{mec.fr} = 2\Delta P_{mec.fr} V_{swc} \tag{3.59}$$

Where, the pressure loss caused by mechanical friction of the components per cycle is given in [38] as:

$$\Delta P_{mec.fr} = \frac{(0.94 + 0.045 sn)10^5}{3(1 - 1/3\tau)}(1 - 1/\tau) \tag{3.60}$$

where $s, n,$ and τ are stroke, operating frequency and compression ratio, respectively.

3.3.5/ HEAT CONDUCTION LOSSES

Due to a considerable temperature difference between compression and expansion spaces in Stirling cycle machines, which are separated by displacer, the heat conduction cannot be neglected. The heat conduction losses across the displacer, regenerator and cylinder walls are an additional load for heat exchangers. This loss is independent of the machine frequency and pressure. The losses due to the heat of conduction across the displacer during the refrigerating cycle is written based on Fourier law as described by [137]:

$$\dot{Q}_{cond} = k\frac{A}{L}\Delta T \tag{3.61}$$

Where K and L are the heat conductivity and the length of the displacer or the cylinder wall, A is the corresponding cross-sectional area, ΔT is the difference in temperature between compression and expansion spaces.

3.3.6/ LOSSES DUE TO FINITE SPEED OF PISTON

In a regenerative Stirling cycle refrigerating machine, the working spaces are periodically compressed and expanded by the pistons or piston and piston/displacer. Based on the finite speed thermodynamic principle, the instantaneous pressure of compression and expansion spaces differs from the pressure in the respective piston surfaces. The work losses due to finite speed of the piston in one cycle is evaluated by the product of pressure drop and the piston swept volume [38, 106, 132].

$$dW_{fin.sp} = 2\Delta p_{fin.sp} V_{swc} \tag{3.62}$$

and,where;

$$\Delta p_{fin.sp} = \frac{1}{2}(P\frac{aU_{p,c}}{C_c} + P\frac{aU_{p,e}}{C_e})$$

P represents the instantaneous pressure, U_p is the piston speed, C is the average molecular speed.

$a = \sqrt{3\gamma}$ and $C = \sqrt{3RT}$

3.3.7/ GAS SPRING HYSTERESIS LOSSES

As the internal gas of the Stirling machine compressed and expanded periodically by the piston, it is likely that this internal gas could begin to act as a spring. This thermodynamic process is not recoverable and may introduce additional losses in the Stirling machine that could be in the form of the dissipation of the internal energy of the working fluid. The working gas acts actually as a gas spring which stores energy when it is compressed and releases energy when it is expanded. This type of dissipation loss due to non-ideal character of working gas is modelled using the following expression [20, 82]:

$$\dot{W}_{hys} = \sqrt{\frac{1}{32}\omega\gamma^3(\gamma-1)T_w P_{mean} k_g}(\frac{V_d}{2V_t})^2 A_{wg} \tag{3.63}$$

where, $\dot{W}_{hys}$,ω,V_d, are gas spring hysteresis power loss, angular speed of displacer and swept volume of displacer.

3.3.8/ PUMPING LOSSES

Because of the periodic variation of pressure throughout the working space of a Stirling cycle machine, the gap between the displacer and the cylinder wall can absorb and transfer gas from or to the expansion volume. The pumping losses are due to the fixed clearance volume existing between the displacer and the cylinder wall so that the displacer can move without rubbing. This leads to cooling loss in the refrigerating machine, named as pumping loss. Based on [41, 132] the pumping loss is given as;

$$\dot{Q}_p = (1-\eta)\dot{m}C_p(T_c - T_e) \tag{3.64}$$

where:

$$\dot{m} = \frac{2fD_dL_dJ}{R(T_c+T_e)}P_a$$

and

$$\eta = 1 - \frac{4\dot{m}^{0.6}C_p^{0.6}J}{3\pi {k_g}^{0.6}{L_d}^{0.6}D_d}$$

η is the clearance efficiency, $\dot{m}$ is mass flow rate of gas through the clearance, f is frequency, P_a is the pressure amplitude.

But, for a moderate temperature refrigeration machine, the temperature difference is very small compared to Stirling cryocoolers and heat engines, the pumping loss will be very small.

3.4/ SOLUTION METHOD

The mathematical model described in section 3.2 and 3.3 shows a set of algebraic differential equations. An algorithm was developed to describe the method for implementing the solutions of the set of formulated differential equations. The method of solving of these numerical differential equations begin with taking the geometrical parameters and initial operating conditions of the machine as input parameters. The solution algorithm of the present numerical model is illustrated by the flow chart in Fig. 3.3. Schmidt analysis is used for the initial estimation of the mass of working gas and modified ideal adiabatic analysis to determine the working pressure and temperature. As shown, the first part of the analysis is to numerically solve the set of ordinary differential equations. The step is quite similar to the original ideal adiabatic analysis developed by Urieli and Berchowitz [20], except the differential equations have been adapted to reverse cycle and corrected to include losses (shuttle heat and mass leakage) that have a direct impact on working fluid pressure and temperature of the Stirling refrigerating machine. 24 variables and 16 ordinary differential equations are solved for a full cycle after the geometries of the machine are specified. Because of the cyclic nature of the system, the adiabatic model could be formulated as an initial value problem by assigning consistent arbitrary initial conditions and classical fourth-order Runge Kutta method is applied to solve the system of the differential equations of the numerical model with MATLAB.

In the model, void/dead volume parameters of the hot heat exchanger, regenerator and chiller (V_h, V_r, and V_{cr}) are determined based on the geometrical specifications of these heat exchangers. The active volume variables including V_c, V_e, dV_c, and dV_e are obtained

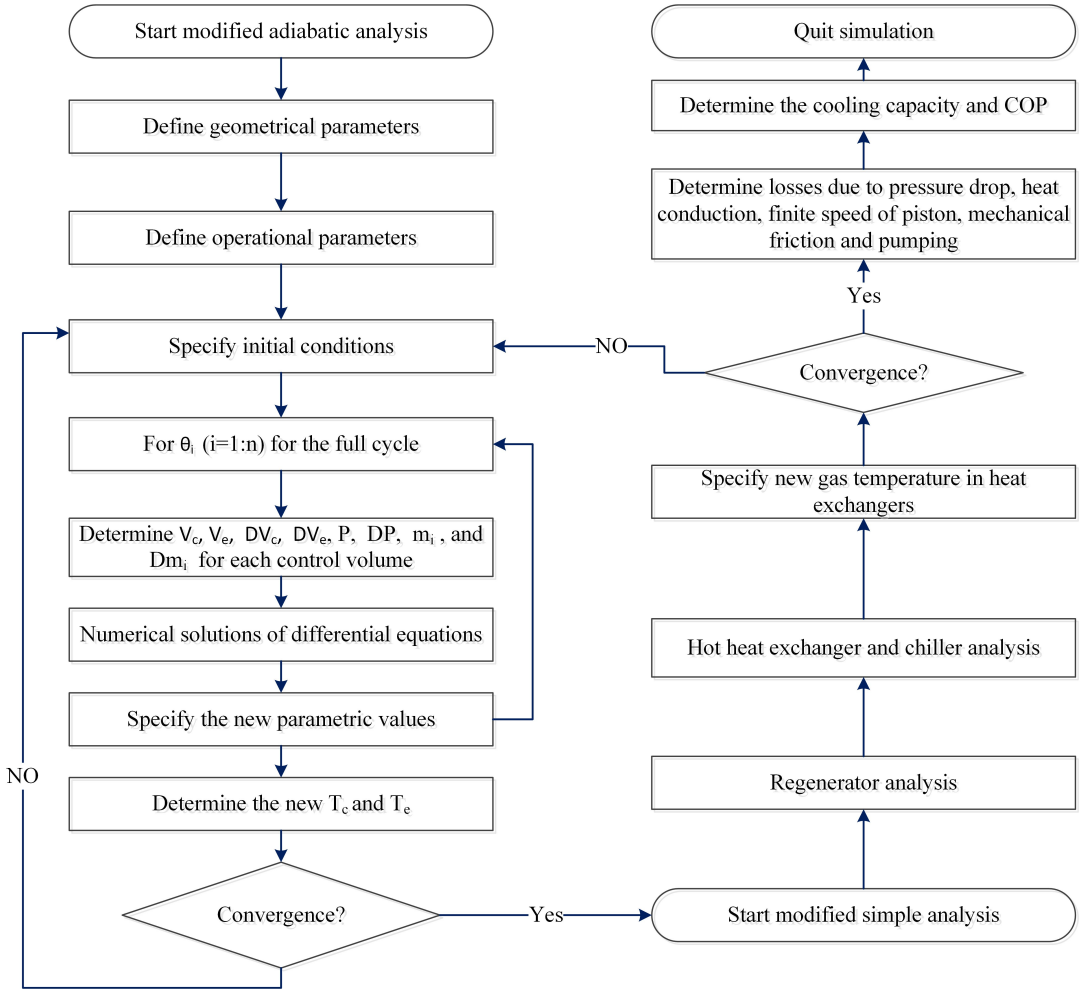

Figure 3.3: Algorithm of the model.

based on the configuration of the refrigerating machine as analytic functions of the crank angle θ (or time of operation of the engine) in one cycle of operation, which is expected to span from $= 0^o$ to $= 360^o$. Among the twenty four variables, eleven variables and derivatives including $Q_{shut}, m_{leak}, V_c, V_e, p, m_c, m_h, m_r, m_{cr}, m_e$, and W are analytically determined and seven derivatives (DT_c, DT_e, DQ_h, DQ_r, DQ_{cr}, DW_c and DW_e) are numerically integrated using the fourth-order Runge-Kutta method. The other six mass flow rate equations and boundary conditions are initial value problems. Initial gas temperatures in compression and expansion spaces have been estimated and are equal to the hot heat exchanger and chiller temperatures, respectively. Then, the numerical solution of differential equations is executed repeatedly until the steady-state condition obtained. The solution for the algebraic differential equations considered that cyclic steady state conditions are reached at boundary conditions. At the end of the steady-state cycle ($\theta = 2\pi$) the magnitude of temperature converges to the respective temperature at the beginning of the cycle ($\theta = 0$). The iterative process assumed that the initial values are known, and then the system is solved until cyclic steady state conditions, which was numerically reached when the difference between the assumed initial values and the values calculated at the end of the cycle are lower than a defined error.

As shown in Fig. 3.3, after completing analysis of the modified ideal adiabatic model, the

algorithm enters the second part of the analysis called modified simple analysis. The purpose of this analysis is to evaluate the overall performance of the machine by incorporating all expected losses. In the modified simple analysis, the effect of regenerator imperfection is considered to correct the hot heat exchanger and the chiller temperatures based on Eqs. (3.52 and 3.53). The feedback is given to the modified ideal adiabatic solution section by correcting the heat exchangers temperature until the temperatures converges. Finally, the amount of the cooling production and the magnitude of input power requirement are corrected including the effect of all considered respective losses as well as COP is evaluated.

3.5/ MODEL VALIDATION

In the previous sections, a numerical model is introduced to predict the performance of a regenerative Stirling cycle refrigerator. In this section, the model validation is presented. The developed numerical model (modified simple model) is validated by two ways. The first, validation method is by reversing the refrigeration model to the engine model and simulate the model to validate with other previous works. This is because there are no enough researches in the Stirling refrigeration area for validation. The second way of model validation is through direct experimental investigation using FEMTO 60 engine prototype.

3.5.1/ MODEL VALIDATION USING ENGINE MODEL

The modified simple numerical model for the Stirling refrigerator is validated by reversing the model to the engine model. Primarily the developed modified simple model for refrigerators is reversed to the engine model. However, it is worth mentioning here that it was difficult to find previously published numerical model results of Stirling engine of the same type and configuration (FEMTO 60) as the one considered in the present work for the purpose of validation. Hence, the parameters of 3 kW GPU-3 Stirling engine are used for validation as there are enough published papers using such type of engine. To verify the reliability of this model (modified simple), the simulation results are compared with other theoretical models' simulation results and with the experimental results. The experimental results which were tested in the NASA Lewis Research Center using 3kW GPU-3 Stirling engine were presented [12, 17]. The machine specification (GPU-3) for the validation of the model with the engine model is presented in Table 3.3.

The reversed modified simple model was simulated and engine performances (power output and efficiency) have been compared with the results of other models and experimental results as shown in Table 3.4. The comparison considers the validation of simulation result of existing modified simple model (reversed) with the results of the different models from original adiabatic models [20, 64] to the recent models [89, 101, 106, 107, 112, 147, 159] and with experimental results [12, 17]. The analysis result using the modified simple model (this study) showed a very high accuracy level with a relative error of +4% for brake power output and by +0.9% for efficiency as compared with experimental result for (GPU-3) engine. The overall result from the table shows that the present model matches better as compared with all other theoretical models.

A more detailed validation of the present model (modified simple) with other numerical

Specifications of GPU-3 Stirling engine [17].			
Parameter	*Value*	*Parameter*	*Value*
General		**Heater**	
Internal diameter of cylinder (mm)	69.90	Mean tube length (mm)	245.30
Number of cylinders	1	Tube outside diameter (mm)	4.83
Piston stroke (mm)	31.2	Tube inside diameter (mm)	3.02
Working fluid	Helium	Number of tubes per cylinder	40
Frequency (Hz)	41.7	Dead volume of heater (mm^3)	70.88
Mean pressure (Mpa)	4.13	**cooler**	
Phase angle	90	Mean tube length (mm)	46.1
Heater temperature (K)	977	Tube outside diameter (mm)	1.59
Cooler temperature (K)	288	Tube internal diameter (mm)	1.09
Regenerator		Number of tubes per cylinder	312
Regenerator lenth (mm)	22.6	Dead volume of cooler (mm^3)	13.80
Reg. external diameter (mm)	80	**Others**	
reg. internal diameter (mm)	22.6	Clearance volume of displacer (mm^3)	30.52
Number of regenerators	8	Clearance volume of piston (mm^3)	28.68
Dead volume of regenerator (mm^3)	50.55	Diameter of displacer (mm)	69.9
Material	stainless steel	Diameter of displacer rod (mm)	9.52
No. of wires per cm	79	Eccentricity (mm)	20.80
Wire diameter (mm)	0.04	Displacer clearance (mm)	0.028
Porosity of regenerator matrix	0.69	Piston clearance (mm)	0.15

Table 3.3: Specifications of GPU-3 Stirling engine [17].

models (simple [20], simple II [89], PSLV [102]) and with experimental results (reported in [17]) at different operating frequencies have been conducted and presented in Fig. 3.4 for the prediction of brake power and corresponding errors as well as in Fig. 3.5 for the prediction of engine efficiency and associated errors for two different pressures.

Fig. 3.4a and b presented the comparison of the output brake power for the present model with results of other theoretical models (simple [20], simple II [89], PSLV [102]) and with experimental results reported by [17] for a 3 kW Beta type Stirling machine called the GPU-3 Stirling engine at charging pressures of 27.6 bar and 41.4 bar respectively. The

Validation of the model with engine models using (GPU-3).				
Models	Power out put		Efficiency	
	in kW	error in %	in %	error in %
Adiabatic model [20]	8.3	+213.1	62.5	+167.9
Simple model [20]	6.7	+152.9	52.5	+ 124.4
Dynamic bestModel [64]	4.27	+61.3	38.49	+64.5
Simple II model [89]	4.57	+72.5	36.8	+57.3
CAFS model [106]	4.17	+57.4	36.1	+54.3
PFST model [107]	3.61	+36.3	23.3	-0.4
Modified PSVL [102]	2.87	+8.3	24.72	+5.6
CPMS model [112]	2.68	+1.2	21.75	-7.1
[147]	4.51	+70.1	36.56	+56.2
[159]	2.66	+0.4	20.4	-12.8
Present model (modified simple)	2.754	+4.0	23.6	+0.9
Experimental result [12]	2.649	-	23.4	-

Table 3.4: Validation of the model with engine models using (GPU-3).

result from Fig.3.4a and b demonstrate the effect of operating frequency for the experiment and theoretical models including the present modified simple model at 27.6 bar and 41.4 bar, respectively. At a mean pressure of 27.6 bar, it could be seen in Fig.3.4a, that the predicted brake power by the current model is very close to the experimental result within all operating ranges. From Fig. 3.4a, it could be seen that the accuracy of the current model (modified simple) in predicting the brake power is by far better than other models considered as it is closer to experimental results at each frequency. The optimum brake power for both present theoretical model and experimental work are found near to an operating frequency of 41.67 Hz. Similarly, Fig. 3.4b demonstrates the comparison of brake power prediction between previous researches (simple [20], simple II [89], PSLV [102]), present model, and experimental work at a mean pressure of 41.4 bar.

Generally, from both Fig. 3.4a and b, it could be verified that the present modified simple model predicts the brake power more accurately. The present model and experimental results confirmed that brake power has optimum value with respect to the operating frequency. The decrease in brake power with operating frequency after the optimum value could be due to an increase of losses in the engine (mechanical friction, losses due to the finite speed of piston, and the increase in fluid friction in heat exchangers).

The evaluation of power prediction error for different models including simple [20], simple II [89], PSLV [102], and the present modified simple model against the experimental result [17] is illustrated in Fig. 3.4c and d at charging pressures of 27.6 bar and 41.4 bar respectively. As shown in the figure, the deviations of errors decrease from the original simple model, simple II, PSLV, and the present modified simple model. The graphs generally show the more recent models have a lower deviation from experimental result. The more recent models PSVL and present modified simple models have more reasonable errors. The modified simple model (this study) has the most reasonable accuracy and even the errors at different frequencies seem uniform for this model except at very high operating frequency. The power prediction errors for this model are by far lower than all considered models (simple [20], simple II [89], PSLV [102]) at each frequency. As seen

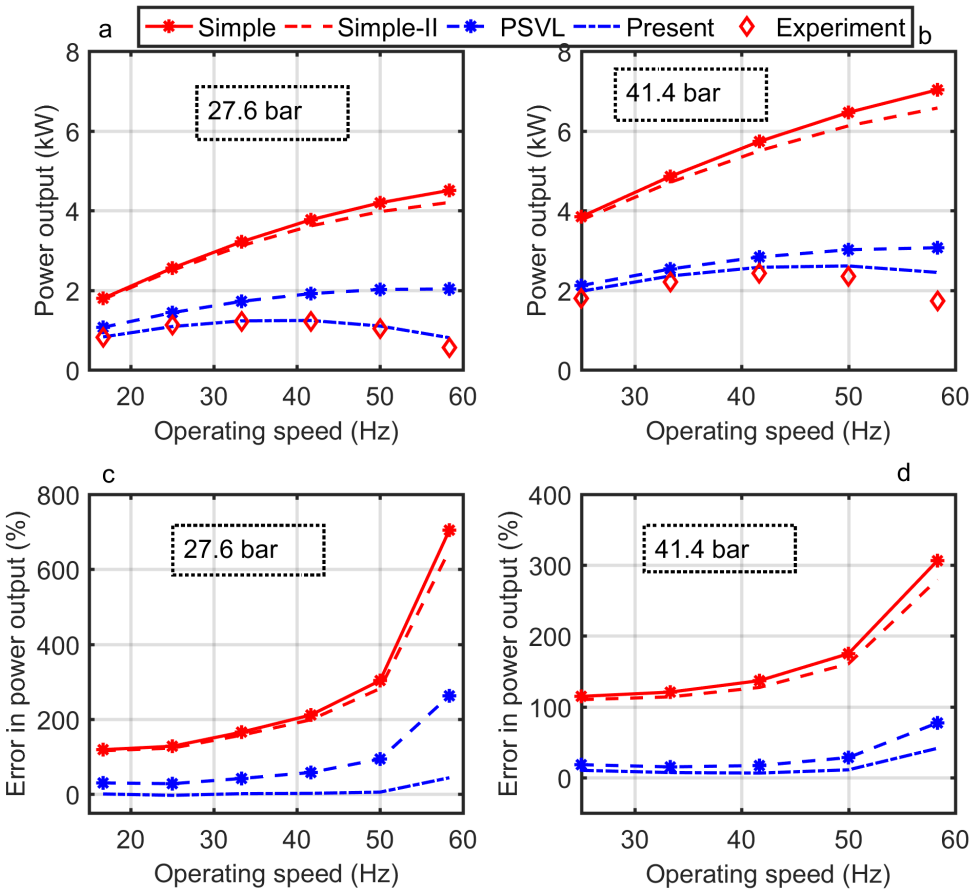

Figure 3.4: Comparison of brake power of Present Model (modified simple), other theoretical models and experimental results using GPU-3 engine.

(a, Brake power at 27.6 bar; b, Brake power at 41.4 bar: c, Power prediction error at 27.6 bar: d, Power prediction error at 41.4 bar)

in Fig. 3.4c, at a mean pressure of 27.6 bar, the prediction error of power is relatively very constant in the case of a modified simple model (this study) and the maximum error is 5.77% except at very high operating frequency (58.33 Hz). On the other hand, as the mean pressure increases to 41.4 bar as shown in Fig. 3.4d, the power prediction error for PSLV [102] model also shows a very closer trend with the modified simple model (this study) and both show the relative constant error except at very high operating frequency.

Fig. 3.5a and b presented the comparison of the brake efficiency for the present model with other theoretical models (simple [20], simple II [89], PSLV [102]) and with experimental results (reported in [17]) for the GPU-3 Stirling engine against operating frequency and at charging pressures of 27.6 bar and 41.4 bar respectively. Based on Fig. 3.5a at a mean pressure of 27.6 bar, even though, all models have different deviations from the experimental result, the predicted brake efficiency by this model (modified simple) is very close with the experimental result at all operating frequency ranges. As could be seen from Fig. 3.5a the accuracy of the current model (modified simple) in predicting the efficiency is by far better than other models considered. Similarly, Fig. 3.5b shows the com-

parison of efficiency prediction between previous researches simple [20], simple II [89], PSLV [102], present model (modified simple), and experimental work at a mean pressure of 41.4 bar. The same trend is observed that the accuracy of efficiency prediction is better in case of the current model.

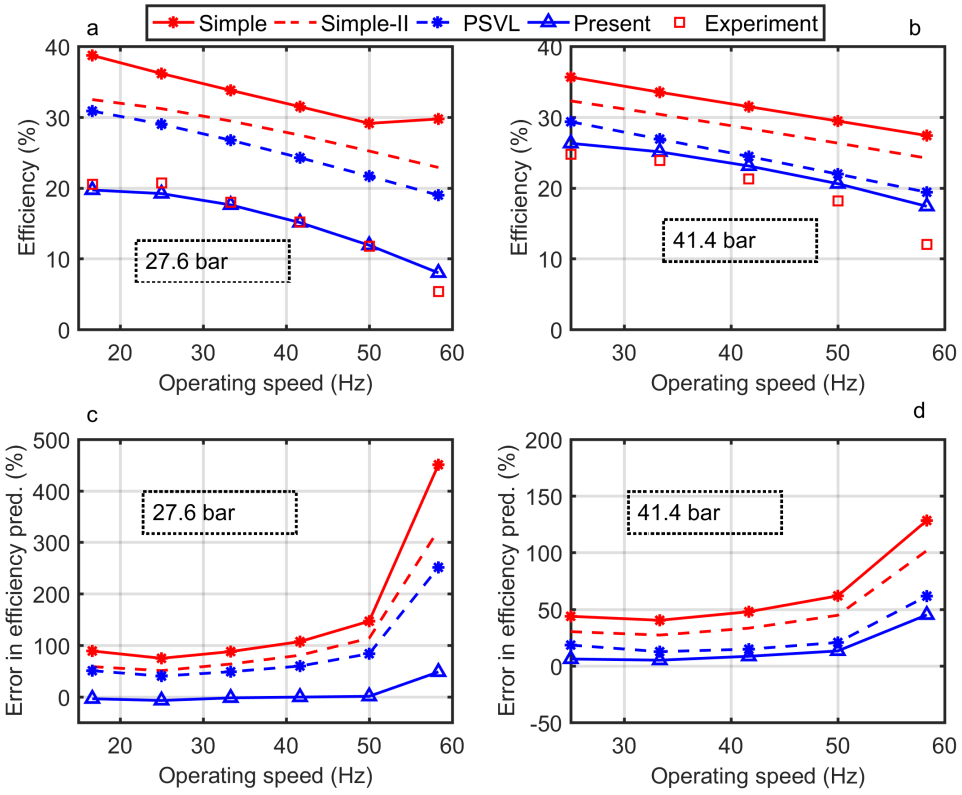

Figure 3.5: Comparison of thermal efficiency of present model (modified simple), other theoretical models and experimental results using GPU-3 engine.

(a, Brake efficiency at 27.6 bar; b, Brake efficiency at 41.4 bar: c, Efficiency prediction error at 27.6 bar: d, Efficiency prediction error at 41.4 bar).

From Fig. 3.5a and b, the efficiency for all models and experiments showed a decreasing trend with increasing operating frequency at both mean pressures (27.66 and 41.4 bar). The decrease in brake power with operating frequency could be due to an increase of losses in the engine (mechanical friction, losses due to the finite speed of piston, the pressure drop in heat exchangers).

The comparison of efficiency prediction error for different models including simple [20], simple II [89], PSLV [102], and the present modified simple model at a heater and cooler temperatures of 922 K and 286 K is demonstrated in Fig. 3.5c and d at charging pressures of 27.6 bar and 41.4 bar respectively. As shown in the figure, the deviation of errors decrease from the original simple [20], simple II [89], PSLV [102], and the present modified simple model, respectively. The graph generally shows the more recent models have a lower deviation from experimental results. The more recent models PSVL and this study (modified simple model) have more reasonable errors. The efficiency prediction errors for the current modified simple model are by far lower than all other

considered models (simple [20], simple II [89], PSLV [102]) at each frequency and the errors at different frequencies seem uniform for this model except at very high operating frequency. As clearly seen in Fig. 3.5c, at a mean pressure of 27.6 bar, the prediction error of efficiency is relatively very constant in the case of the modified simple model (this study) and the maximum error is 7.25% except at very high operating frequency (58.33 Hz). On the other hand, as the mean pressure increases to 41.4 bar as shown in Fig. 3.5d, the power prediction error increases with operating frequency in the case of the modified simple model.

Finally, from Table 3.4, Fig 3.4 and Fig. 3.5, it could be seen that the results of the present model (modified simple model) are more closer to the results of experiment as compared with the results of other models developed so far. Hence, it could be concluded that the present model predicts power and effciency of Stirling engine more accurately. The main reason for such better model results is the inclussion of appropriate losses directly in the differential equation and as independent losses based on their effect. The same trends are observed for the results of the present model as compared with experimental values for both power Fig 3.4 and efficiency Fig. 3.5 pridiction. Hence, the numerical model developed for refrigeration could be used to design a cooling machine at a reasonable accuracy.

3.5.2/ MODEL VALIDATION WITH EXPERIMENT

To validate the numerical model presented above, there are no enough published results of numerical models and experimental works for Stirling cycle refrigeration machine of the same type and configuration (FEMTO 60) as the one considered in the present work.

The numerical model presented in sections 3.2 and 3.3, was evaluated by considering the FEMTO-60 Stirling engine operating as a refrigerating machine as a case study. The photo of the cooling machine at cooling stage is shown in Fig. 3.6.

The considered experimental machine is a reversible thermal machine (motor and/or receiver) with Beta configuration and operates between two constant temperatures. This machine consists of expansion space, heater (acts as a chiller in case of the cooling machine), regenerator, cooler (acts as a hot heat exchanger in case of the cooling machine), compression space, piston, buffer space, and driving mechanisms. The power piston and displacer are arranged within a single cylinder. The displacer piston controls the variations of the expansion volume (cold room) and the power piston controls the compression space (hot room) for such Stirling refrigerating machine. The setup includes a regenerative Stirling refrigerator, cooling water system, the electric supplier, and a data acquisition system. The refrigerator is arranged with six thermometers and one pressure sensor for measuring the working conditions.

The setup, the arrangement, and testing procedures of the experimental device was the same as described by Djetel-Gothe et al. [153] and is shown in Fig. 3.7. The characteristics of the Stirling refrigerator such as cold temperature, cooling capacity, and coefficient of performance were investigated experimentally. The thermal load was applied by two resistance heaters to the cold head of the Stirling cycle refrigerator, and steady-state characteristics of the refrigerator were measured. For a varied input voltage, different tests were carried out to determine the variation of the cooling performance with the cold head temperature of the coolers varied from -40^oC to 0^oC.

Figure 3.6: Photo of refrigerating Stirling machine (Beta type) at cooling stage (FEMTO-ST laboratory).

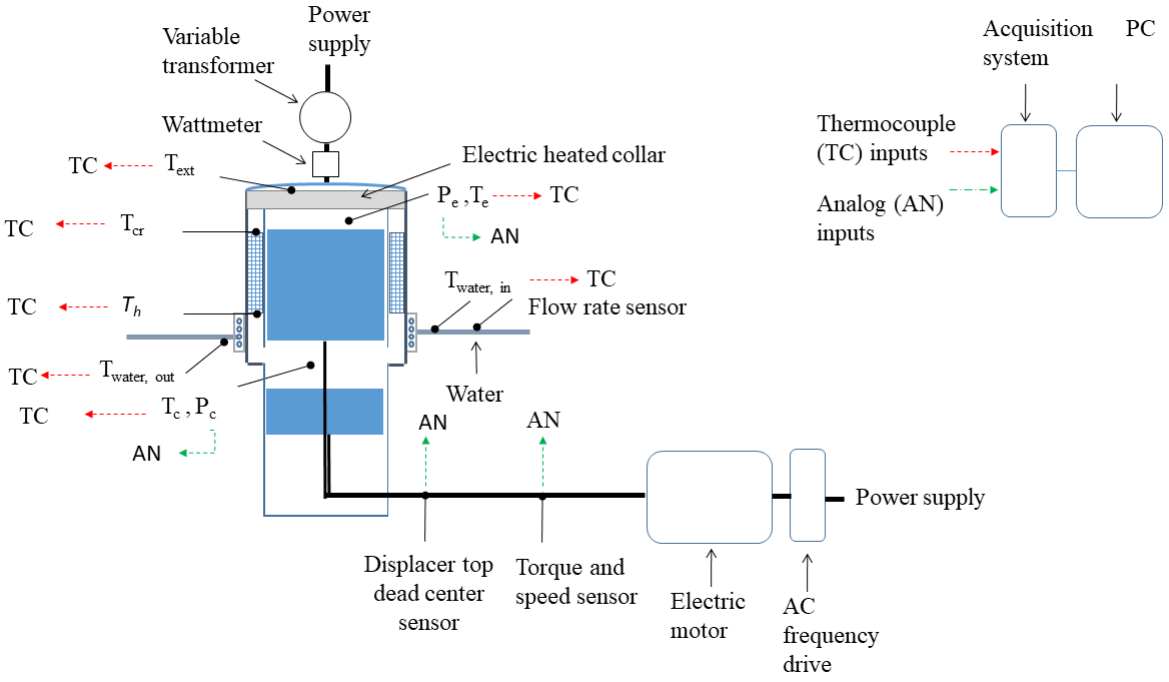

Figure 3.7: Experimental setup for the measurement of the Stirling prototype.

The considered working gas for the experimental validation was nitrogen, which is assumed to behave like a perfect gas. The hot heat exchanger and the chiller both have slot geometric arrangement and the configuration of the regenerator is an annular configuration with a stainless steel woven screens matrix. The main parameters and dimensions of the experimental device are tabulated in Table 3.5.

Specifications of Stirling machine for this study.		
No	*Parameters*	*Value*
1	Hot heat temperature (K)	305
2	Cooling temperature (K)	270
3	Piston diameter (mm)	60
4	Displacer diameter (mm)	59
5	Piston stroke (mm)	40
6	Regenerator length (mm)	50
7	Diameter of regenerator (mm)	82
8	Regenerator wire made of	stainless steel
9	Wire diameter (μm)	112
10	Porosity (%)	64
11	Compression space swept volume (cm^3)	103
12	Expansion space swept volume (cm^3)	113
13	Compression dead volume (cm^3)	4.24
14	Expansion dead volume (cm^3)	4.24
15	Working gas	Nitrogen
16	Frequency (Hz)	5-13
17	Charging pressure (bar)	15-20

Table 3.5: Specifications of Stirling machine for this study.

The thermal model was validated with an experiment conducted at 7.3 Hz and 9.7 Hz for a series of cooling temperatures and a charging pressure of 17.5 bar using FEMTO-60 engine model.

The comparison of cooling load of developed numerical model (modified simple) with experimental results and the associated percentage of relative error is demonstrated in Fig. 3.8. Fig. 3.8a, illustrates the comparison of the cooling load of the numerical model (modified simple model) with experimental values for operating frequencies of 7.3 Hz and 9.7 Hz. Fig. 3.8, shows the relative error evaluated in predicting the cooling load of the cooling machine for operating frequencies of 7.3 Hz and 9.7 Hz. The maximum relative prediction error of -7.71 % was found for an operating frequency of 9.7 Hz.

Fig. 3.9 depicted the comparison of COP and the associated percentage of relative error of developed non-ideal second-order thermal model (modified simple) with experimental values. Fig. 3.9a, demonstrates the comparison of the COP of the numerical model (modified simple model) with experimental values for operating frequencies of 7.3 Hz and 9.7 Hz. From the figure, we could see that the COP for simulation result shows more closer values to the experimental results at all temperature ranges in the case of 7.3 Hz than at 9.7 Hz. Fig. 3.9b, illustrates the relative error evaluated in predicting the COP of the prototype Stirling machine for an operating frequencies of 7.3 Hz and 9.7 Hz. It has seen that the maximum relative prediction error of 23.9 % was found for operating frequency of 9.7 Hz (as shown in Fig. 3.9b).

Generally, from Fig. 3.9 and Fig. 3.8, it could be confirmed that the present modified simple model predicts the cooling power and COP of the Stirling refrigerating machine for moderate cooling application with reasonable accuracy.

At a cold end temperature of 4^oC, operating frequency of 7.3 Hz,and charging pressure

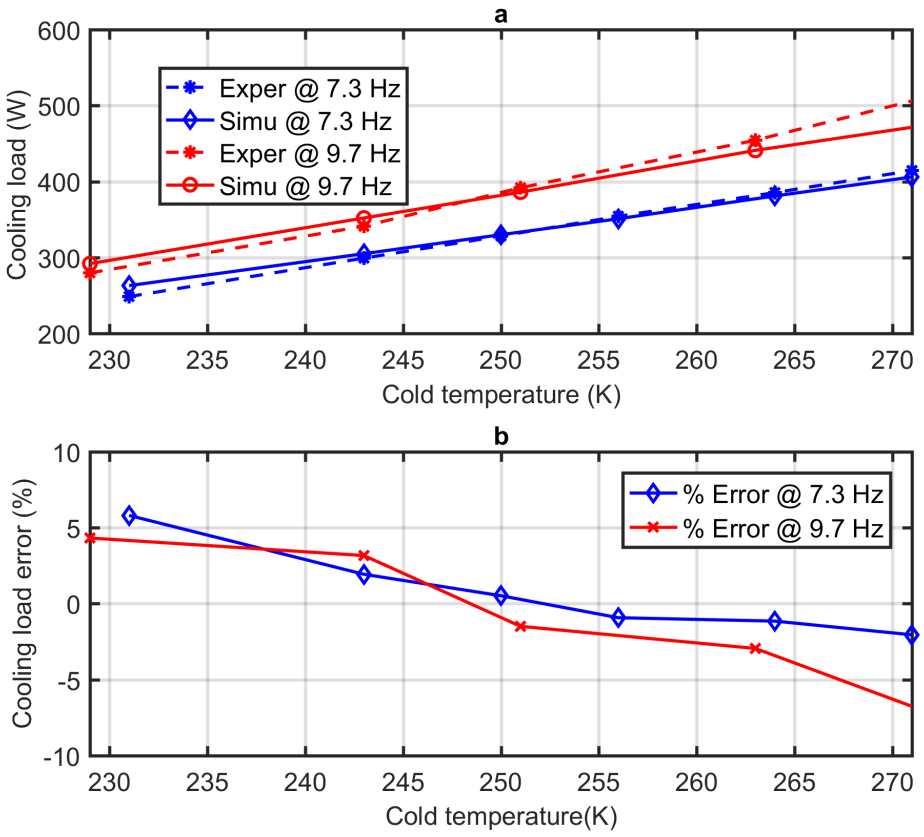

Figure 3.8: Evaluating cooling load prediction accuracy of thermal model with experimental data.

of 17.5 bar:

- The cold production from numerical analysis and experimental were found as 439 W and 450 W, respectively. This result shows that the numerical model is in close agreement with the experiments result with a particular error of -2.4%.
- The COP of refrigerating machine from numerical analysis and experimental were found as 0.92 and 0.9 respectively. This shows that the numerical model has a particular error of +2.2% as compared with the experimental value.

3.6/ RESULTS AND DISCUSSION

The discussion concerns simulation of a numerical model for the Stirling cycle refrigerator with Beta configuration (FEMTO 60 Stirling engine working in reversed mode) conducted at($T_{cr} = 270$ K, $T_h = 300$ K, P = 17.5 bar and $f = 7.5$ Hz) . As described in section 3.5.2, the working fluid used for experimental validation purpose was nitrogen. However, the overall analysis and the optimization work have been conducted using air as a working fluid except in comparison to the effects of the working fluids on cooling performance. In this analysis, simulation results, particularly the mass flow rate of the working fluid, the

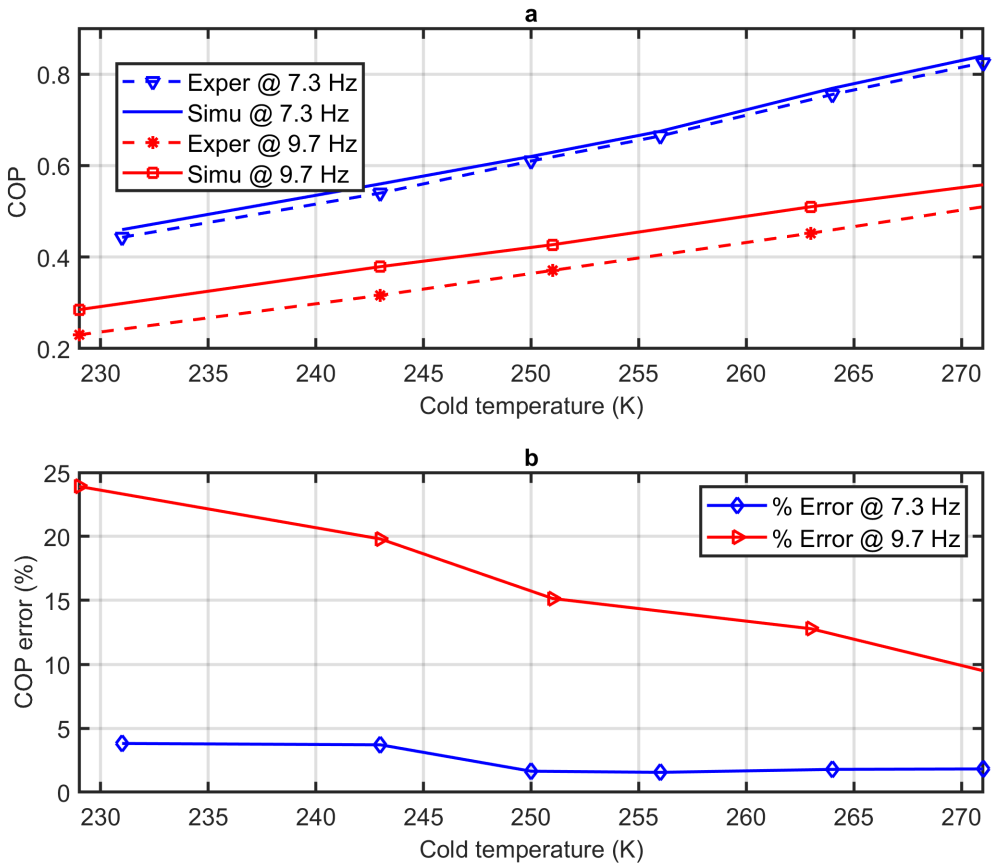

Figure 3.9: Evaluating COP prediction accuracy of thermal model with experimental data.

temperature of working fluid at a different section of the machine the pressure trend in working volumes as well as the pressure drop in heat exchangers have been presented. The solution of the numerical model is solved using MaATLAB code and the results are presented after the steady-state condition is reached.

Fig. 3.10 demonstrates a plot of mass versus crank angle in five control volumes of the refrigerating machine. As it is shown in Fig. 3.10, when the mass in compression space is minimum, the mass in expansion space is maximum and vice versa. This is basically related to the degree of compression and expansion. The amount of working fluid in the regenerator and heat exchangers also varies with the crank angle. The mass of working fluid in the regenerator is greater than the mass in the chiller and hot heat exchanger at each rotational stages. The mass in the hot heat exchanger is the smallest of all. Generally, as the void volume of heat exchangers increases, the amount of working fluid also increases. Furthermore, the mass variation in the regenerator is higher than other heat exchangers, and hence the volume of regenerator affects the performance of cooling machine more than others.

Fig. 3.11 is a plot of temperature distribution in different control volumes (working spaces, regenerator, and heat exchangers) with crank angle at hot heat exchanger temperature of $T_h = 300$ K, chiller temperature of $T_{cr} = 270$ K, and an operating frequency of 7.5 Hz. From Fig. 3.11, it is understood that the mean chiller gas temperature is 11 K less than the chiller wall temperature and, the mean gas temperature in hot heat exchangers is 15 K greater than the hot heat exchanger wall temperature. The average gas temperature in

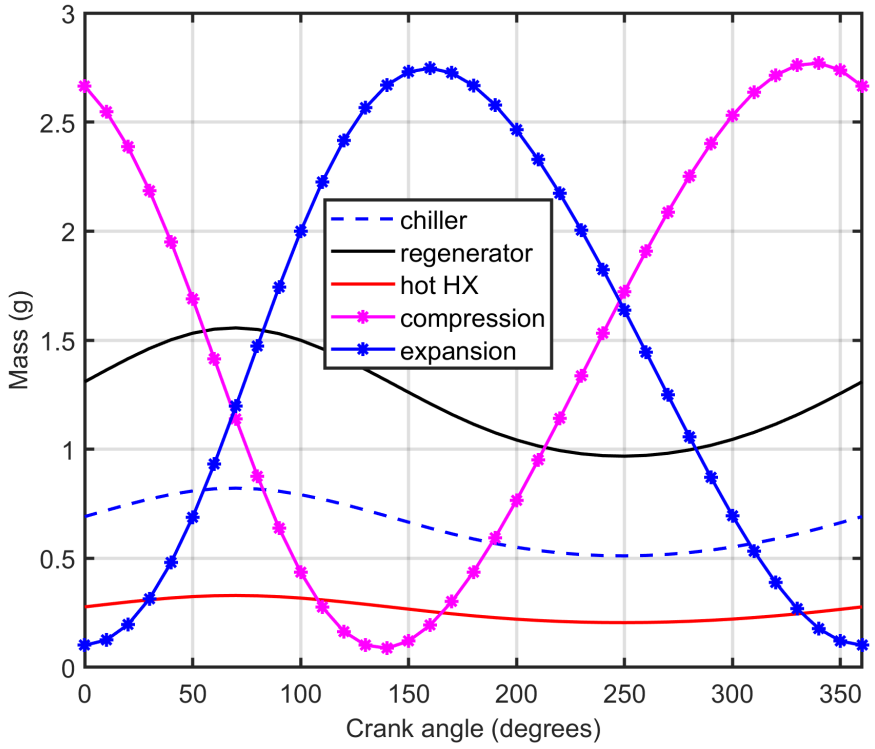

Figure 3.10: Mass variation with crank angle ($T_{cr} = 270$ K, $T_h = 300$ K, P = 17.5 bar and $f = 7.5$ Hz).

the expansion chamber at this particular situation is 259 K.

Fig. 3.12 shows the plot of the P-V diagram for the three analysis methods (Schmidt, modified ideal adiabatic and modified simple analysis). The area limited by the P-V curve represents the amount of net input power required to run the refrigerating machine. The area for the modified simple analysis diagram is greater than the other two areas. This area is the actual input power required and is greater than the ideal input power requirement as there are irreversibilities. Furthermore, Fig. 3.12 shows that the Schmidt analysis is the most ideal as the area is very small.

Fig. 3.13 demonstrates the actual P-V diagrams of compression, expansion and total spaces from the modified simple analysis. It is clear that the compression space is greater than the expansion space area which shows the net input power requirement. Furthermore, the figure demonstrates that the maximum pressure in expansion spaces is lower than the maximum pressure in compression space.

Fig. 3.14 is a diagram of energy transferred versus crank angle from modified simple analysis that shows the net input work done required, heat transfer across two heat exchangers, and heat transfer in the regenerator at a charging pressure of 17.5 bar, frequency of 7.5 Hz, hot heat exchanger temperature $T_h = 300$ K, and chiller temperature $T_{cr} = 270$ K. As it could be seen, the net input work done increases during the compression phase and decrease during the expansion phase. The input power requirement was found as 22.56 J and the cooling power was 53 J from this particular simulation of modified simple model.

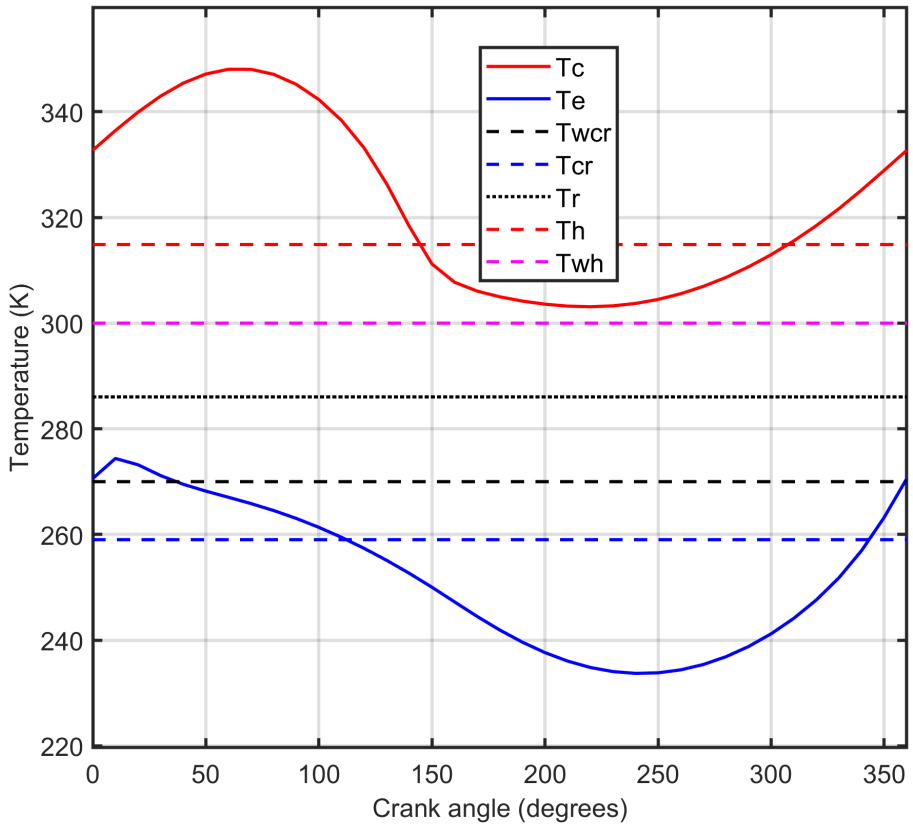

Figure 3.11: Temperature with crank angle at ($T_{cr} = 270$ K, $T_h = 300$ K, P = 17.5 bar and $f = 7.5$ Hz).

Fig. 3.15 demonstrates the actual working space (compression and expansion space) pressure variation versus crank angle at a hot heat exchanger temperature of $T_h = 300$ K, chiller temperature of $T_{cr} = 270$ K, charging pressure of 17.5 bar, and frequency of 7.5 Hz. It can be seen that the pressure in expansion space is smaller than the pressure of the compression space. This pressure difference between two working spaces results from the pressure drop due to friction of fluid flow in three heat exchangers.

Fig. 3.16 shows the pressure drop due to fluid friction across the hot heat exchanger, the regenerator, the chiller, and the total pressure drop in all these heat exchangers versus the crank angle. As could be seen from the figure the pressure drop variation in the regenerator was much higher than the pressure drop in the other two heat exchangers. The maximum pressure drops for the regenerator and the total pressure drops were found respectively as 1.23 bar and 1.30 bar (at a charging pressure of 17.5 bar, frequency of 7.5 Hz, hot heat exchanger temperature $T_h = 300$ K and chiller temperature $T_{cr} = 270$ K). This result confirms that the major pressure drop existes in the regenerator and is almost equal to the total pressure drop.

An elaborated view of pressure drop due to fluid friction in two heat exchangers (hot heat exchanger and chiller) versus crank angle (degrees) is presented in Figure 3.17. The pressure drop in the hot heat exchanger is much higher than that of the pressure drop in the chiller and there is a phase lag too. One of the reasons may be in hot heat exchanger

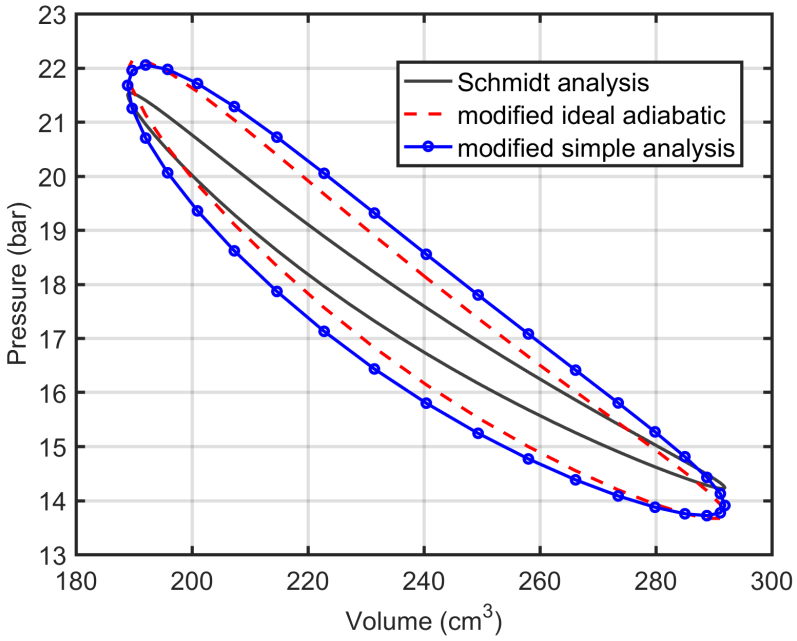

Figure 3.12: P-V diagram of three methods analysis at (T_{cr} = 270 K, T_h = 300 K, P = 17.5 bar and f = 7.5 Hz).

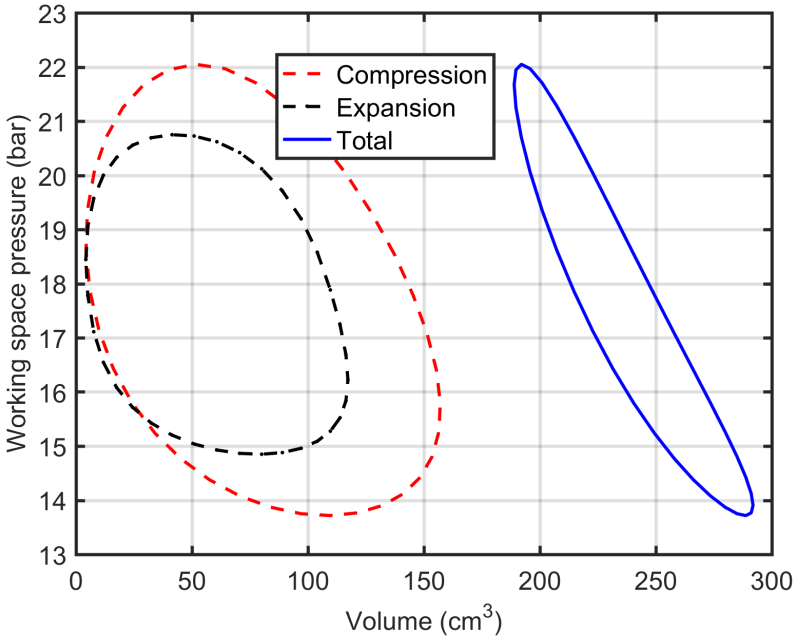

Figure 3.13: P-V diagram for modified simple analysis at (T_{cr} = 270 K, T_h = 300 K, P = 17.5 bar and f = 7.5 Hz).

the gas is hotter and it will try to move faster.

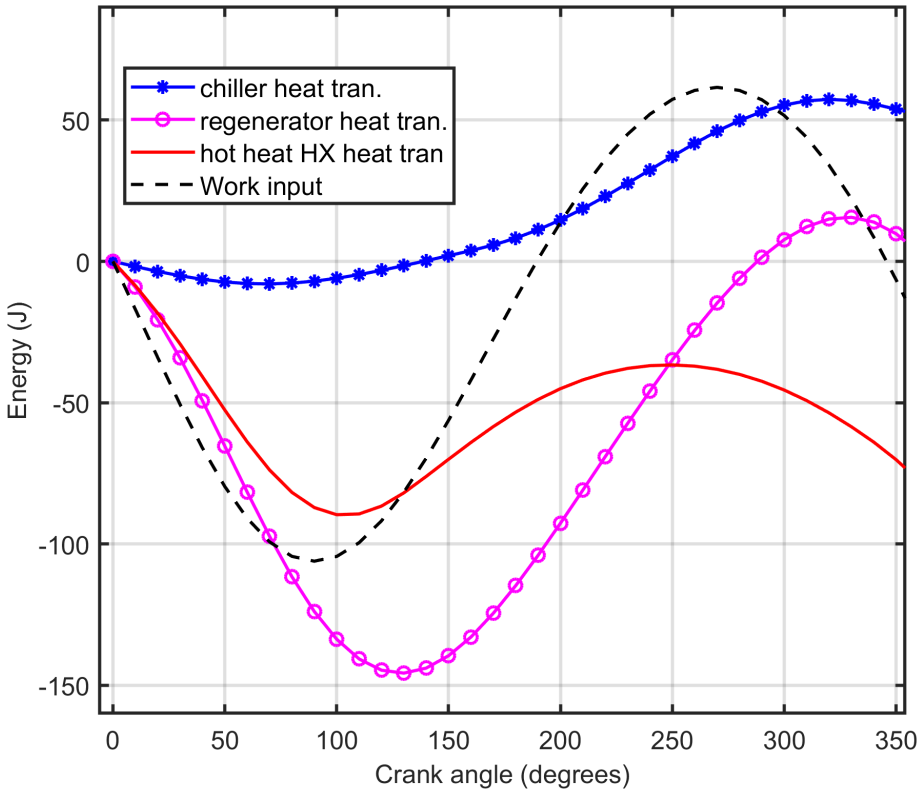

Figure 3.14: Energy flow diagram with respect to crank angle at ($T_{cr} = 270$ K, $T_h = 300$ K, P = 17.5 bar and $f = 7.5$ Hz).

3.7/ CONCLUSION

The main contribution presented in this chapter is the development of a non-ideal second order numerical model called the modified simple model considering the effects of various losses for the moderate temperature Stirling refrigerator. The purpose of this model was to design a Beta type Stirling cycle domestic refrigerator with a crank driven mechanism and using air as a working fluid. The numerical modeling of the refrigerating machine is constructed in three consecutive sections. In the first section, the ideal adiabatic model of Stirling engine is adapted for refrigeration machine. In the second section, the modeling is done through modifiying ideal adiabatic model to include the shuttle heat losses by displacer movement and mass leakage to the crank case directly in the differential equation. Lastly, the modified simple modeling is constructed by incorporating other losses (imperfect regeneration loss, internal heat conduction loss in the regenerator, losses due to pressure drop in heat exchangers, heat conduction losses, gas spring hysteresis loss, loss due to piston finite speed, and pumping loss) as independent losses.

These numerical differential equations have been solved by taking the geometrical parameters and initial operating conditions of the machine as input parameters. Classical fourth-order Runge Kutta method is applied to solve the system of the differential equations. Then, MATLAB code is developed to solve the system of these differential equations over the consecutive cycles.

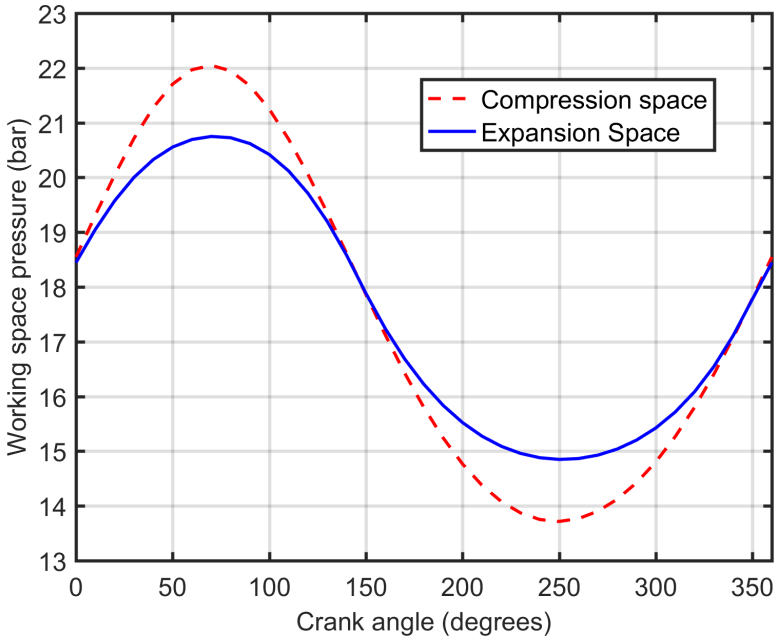

Figure 3.15: Working space pressure versus crank angle over the cycle at (T_{cr} = 270 K, T_h = 300 K, P = 17.5 bar and f = 7.5 Hz).

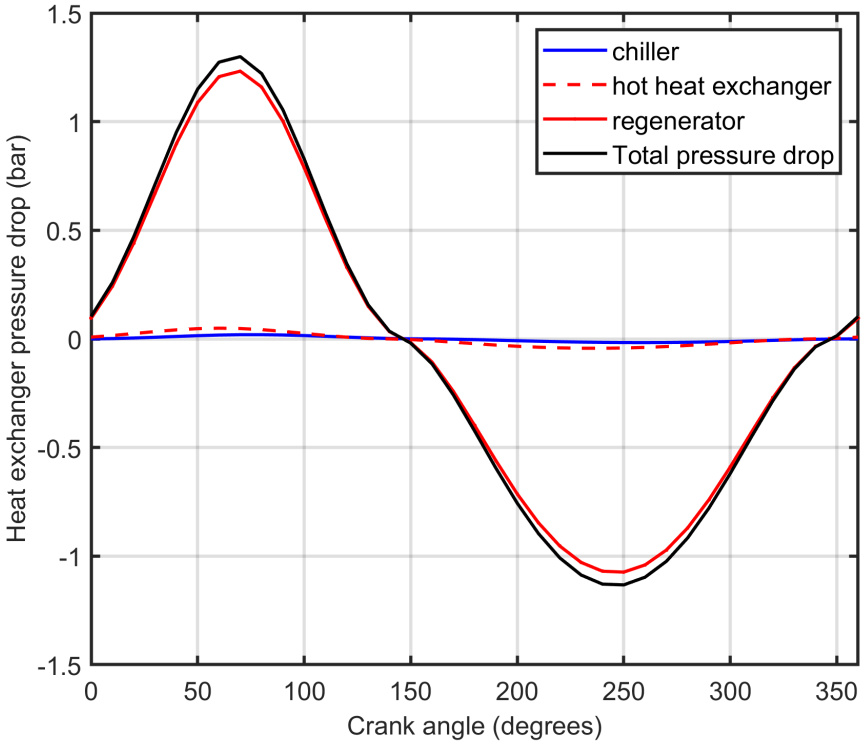

Figure 3.16: Heat exchanger pressure drop versus crank angle at (T_{cr} = 270 K, T_h = 300 K, P = 17.5 bar and f = 7.5 Hz).

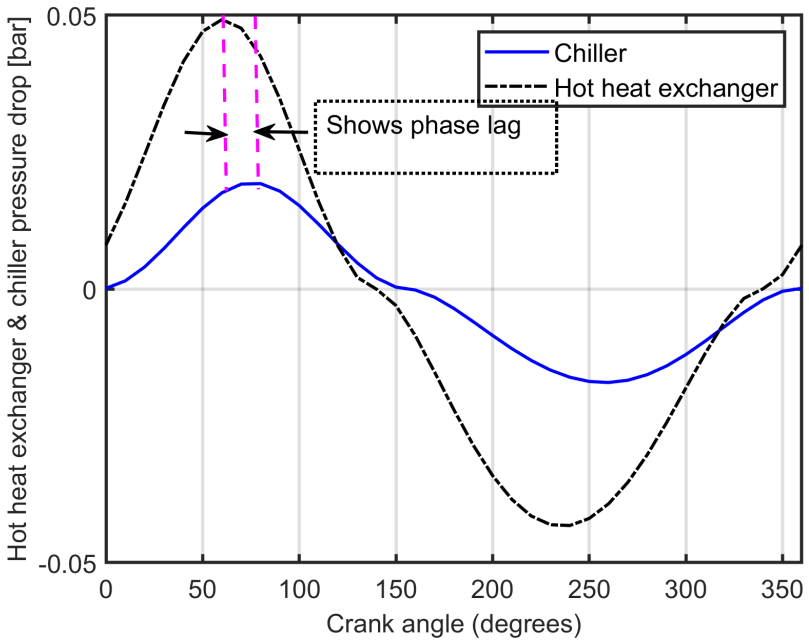

Figure 3.17: Heat exchanger pressure drop versus crank angle at (T_{cr} = 270 K, T_h = 300 K, P = 17.5 bar and f = 7.5 Hz).

The numerical model was first validated with engine models by reversing the numerical model. The developed modified simple model for refrigerators is reversed to the engine model, then the parameters of 3 kW GPU-3 Stirling engine are used for validation. To verify the reliability of this model (modified simple), the simulation results are compared with other theoretical models' simulation results and with the experimental results. Second, the numerical model is revalidated against experimental work conducted using FEMTOST engine model as a cooling machine. The cold production from the numerical analysis and experimental work are found as 439 W and 450 W, respectively at a chiller temperature of 4^oC with a relative error of -2.4%. The COP from numerical analysis and experimental work are found as 0.92 and 0.9 respectively with a relative error of +2.2%. These results confirm that the developed numerical model for domestic Stirling refrigerator have reasonable accuracy to predict the performance of the machine.

4

PARAMETRIC ANALYSIS (OPTIMIZATION)

The developed numrical model in chapter 3, can predict the performance of domestic Stirling refrigerator with very good accuracy. However, a higher performance Stirling refrigerator could be designed using the developed model if parametric optimization is conducted further. This chapter aims to analyze the effects that the different operational variables, design (geometric) variables, different working fluids, shuttle heat losses, and mass leakage losses to the buffer space might have on the cooling performance of the Stirling refrigerator. The other objective of this chapter is to analyze the effects of operating and design variables on different types of losses and to propose better operating and design variables. For this purpose, the developed numerical model was used for the simulation of the FEMTO 60 engine model working in reverse cycle under different operational and design conditions. Finally, through combining different optimized design parameters, new combinations of parameters have been proposed which could produce enhanced cooling performances of the Stirling refrigerator.

4.1/ EFFECT OF SHUTTLE AND MASS LEAKAGE LOSSES

The developed numerical model as shown in Chapter 3, incorporates the shuttle heat transfer (heat loss from compression space to expansion space) and gas leakage from the working space to the buffer space (crankcase) into the ideal adiabatic analysis. These losses have a direct impact on the temperature and the working pressure of the fluid in the working spaces. To evaluate the effect of mass leakage and shuttle heat losses on the temperature, pressure, and overall performance of the refrigerating machine, the model was run consequently without mass leakage and shuttle heat losses, only with mass leakage, only with shuttle heat losses, and with mass leakage and shuttle heat losses included in the differential equation.

The effect of shuttle heat losses on the temperature of the working fluid is illustrated in Fig. 4.1. From Fig. 4.1, it could be seen that shuttle heat losses have a major effect on the temperature of the gas. The shuttle heat losses have the effect of decreasing hot gas temperature and increasing cold side gas temperature. At a charging pressure of 17.5 bar, hot heat exchanger temperature of 300 K, chiller temperature of 270 K, and an operating frequency of 7.5 Hz, the average hot gas temperature decreases by 13 K, and the average cold gas temperature increases by 9.2 K when incorporating the shuttle

effect in the differential equation. The shuttle heat losses have effect of decreasing hot gas temperature and increasing cold gas temperature. This is because part of heat is transported from hot space to cold space. On the other hand, since the mass of working gas decreases in the compression space, the gas temperature in the compression space increases when mass leakage is incorporated in the differential equation. The summary of effect of incorporating shuttle heat losses and mass leakage losses are presented in Table 4.1.

Summary of effect of shuttle heat and mass leakage losses.			
Case	*Effect on T & P*	*Cooling [W]*	*COP*
Without including shuttle heat and mass leakage losses in the differential equations	—	450.6	0.8
When only shuttle heat losses included in the differential equations	• Average T_c decrease by 13 K • Average T_e increase by 9.2 K • ΔT decrease by 22.2 K • Have a recognized effect on PV diagram	347	0.65
When only mass leakage is included in the differential equation	• Average T_c increase by 6 K • Average T_e remains almost unchanged • ΔT increase by 6 K • The effect is not too much on PV diagram	446.2	0.78
When both shuttle heat and mass leakage losses included in the differential equation	• Average T_c decrease by 7 K • Average T_e increase by 9.6 K • Total ΔT decrease 16.6 K • Have a recognized effect on PV diagram	343	0.64

Table 4.1: Summary of effect of shuttle heat and mass leakage losses.

Furthermore, the effects of shuttle heat losses on the overall performance of the refrigerating machine have been evaluated. The cooling power and COP of the refrigerating machine are found respectively as 450.6 W and 0.8 when shuttle losses are evaluated separately and subtracted from cooling power. On the other hand, the cooling power and COP are found as 347 W and 0.65 when shuttle heat losses are incorporated in the differential equation. Furthermore, when we incorporate the mass leakage loss in the differential equation the cooling power and COP have been reduced to 343 W and 0.64.

The effect of shuttle heat losses on the P-V diagram is also investigated. Fig. 4.2 shows

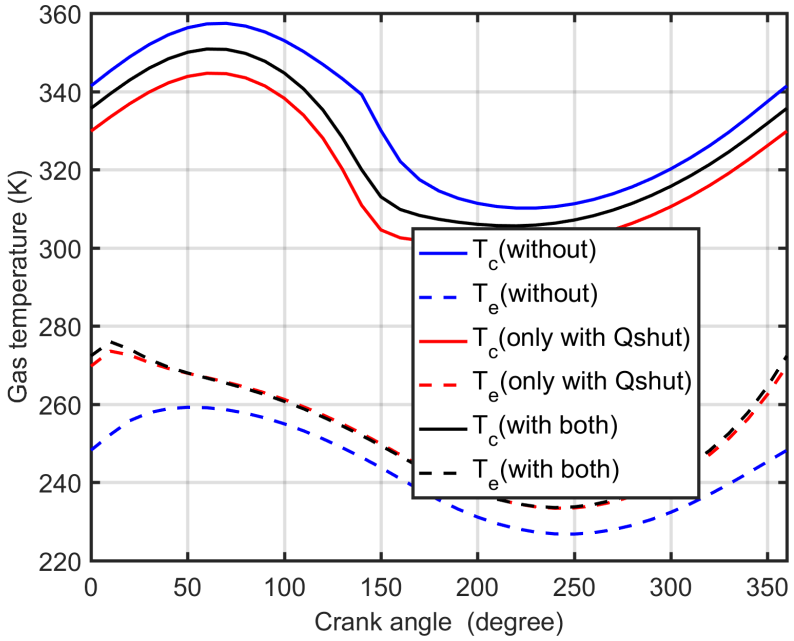

Figure 4.1: Effect of shuttle heat and mass leakage losses on the temperature of the gas in expansion and compression spaces at (T_{cr} = 270 K, T_h = 300 K, P = 17.5 bar and f = 7.5 Hz).

the P-V diagram at T_h=300 K, T_{cr} =270 K, charging pressure of 17.5 bar, and an operating frequency of 7.5 Hz when the analysis is performed first without including shuttle heat losses and then including it in the differential equations. It is noticeable that the P-V loop seems to become slenderer when shuttle heat losses are incorporated in the differential equation. This is because when heat is shuttled from compression space to expansion space, the pressure difference between the two spaces decreases. This resulted in a lower area enclosed in the P-V diagram, and therefore a lower cooling production.

4.2/ EFFECT OF WORKING FLUID ON COOLING PERFORMANCE

It is well known that the type of working fluid has an impact on performance of the Stirling machine. For Stirling engine with high temperature difference, helium has better working characteristics. However, for low lower temperature difference applications, air and nitrogen could also have comparable performance with helium as presented in [83].

The impact of different working fluids on the cooling power of a Stirling refrigerator with respect to operating frequency is presented in Fig. 4.3 at particular operating conditions of $T_h = 300K$, $T_{cr} = 270K$, and a charging pressure of 17.5 bar. It can be observed that the cooling production increases with the operating frequency for all working fluids types. Furthermore, it can be seen that air and nitrogen can produce more cooling power than helium and hydrogen gases. The potential reason for the lesser cooling performance of helium or hydrogen is due to the fact that the amount of working fluids are much lower as they have very high gas constant compared with that of air or nitrogen. Hence a lower heat removal rate take place in case of helium and hydrogen gases that can result in

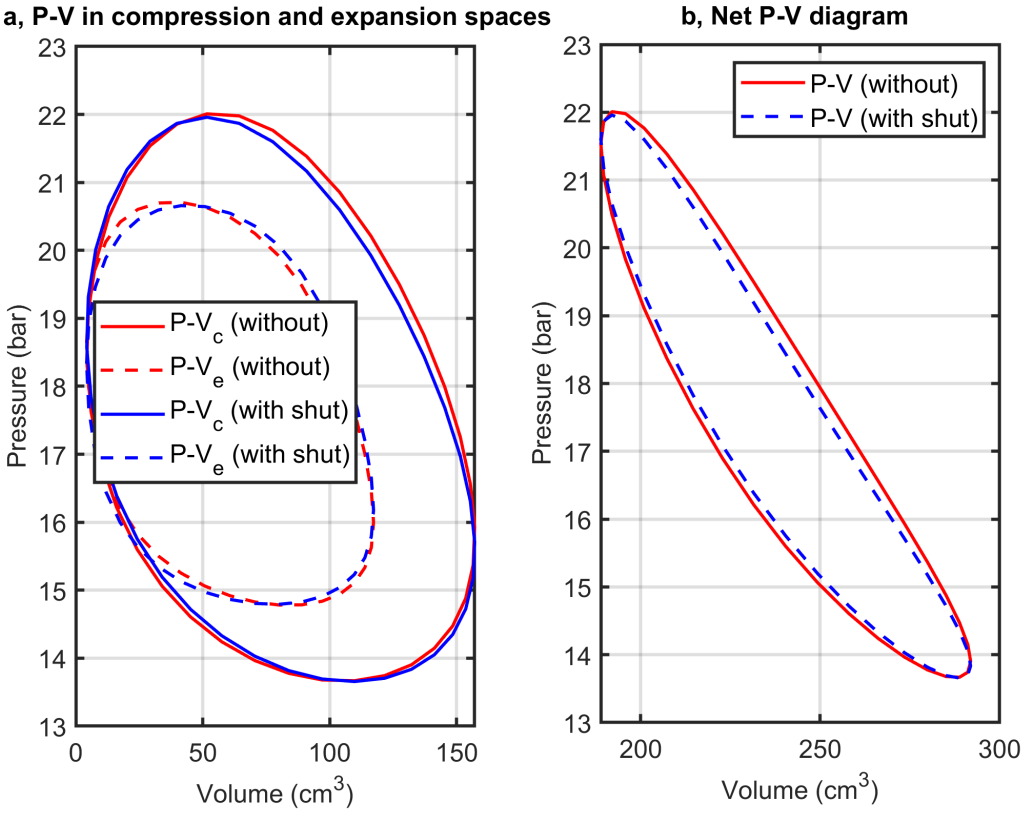

Figure 4.2: Effect of shuttle heat losses on the P-V diagram at ($T_{cr} = 270$ K, $T_h = 300$ K, P = 17.5 bar and $f = 7.5$ Hz).

lower cooling production. On the other hand, the cooling production for air and nitrogen is almost the same. This is because the fluid mass flux is almost the same.

Fig. 4.4 demonstrates the effect of different working fluids on the COP of a cooling machine with respect to operating frequency at $T_h = 300K$, $T_{cr} = 270K$, and charging pressure of 17.5 bar. It can be seen that air and nitrogen have better COP than helium and hydrogen within the range of operating frequency. Even though, both input power requirement and cooling power increase with operating frequency, COP decreases as a result of a higher rate of increase of fluid flow friction and mechanical friction losses. The COP for air and nitrogen decreases radically with operating frequency and this trend shows that at very high operating frequency, the COP for helium may be higher than the COP of air and nitrogen.

Fig. 4.5 displays the influence of working fluids (air, nitrogen, helium, and hydrogen) on cooling power with respect to charging pressure at $T_h = 300K$, $T_{cr} = 270K$, and a operating frequency of 7.5 Hz. It can be observed that the cooling power increases with charging pressure for all working fluids. Furthermore, it could be observed that the cooling power for air and nitrogen is greater than the cooling power of helium and hydrogen due to the higher mass flow rate in the case of air and nitrogen which leads to a higher heat removal rate.

Fig. 4.6 displays the influence of different types of working fluids on the COP of the re-

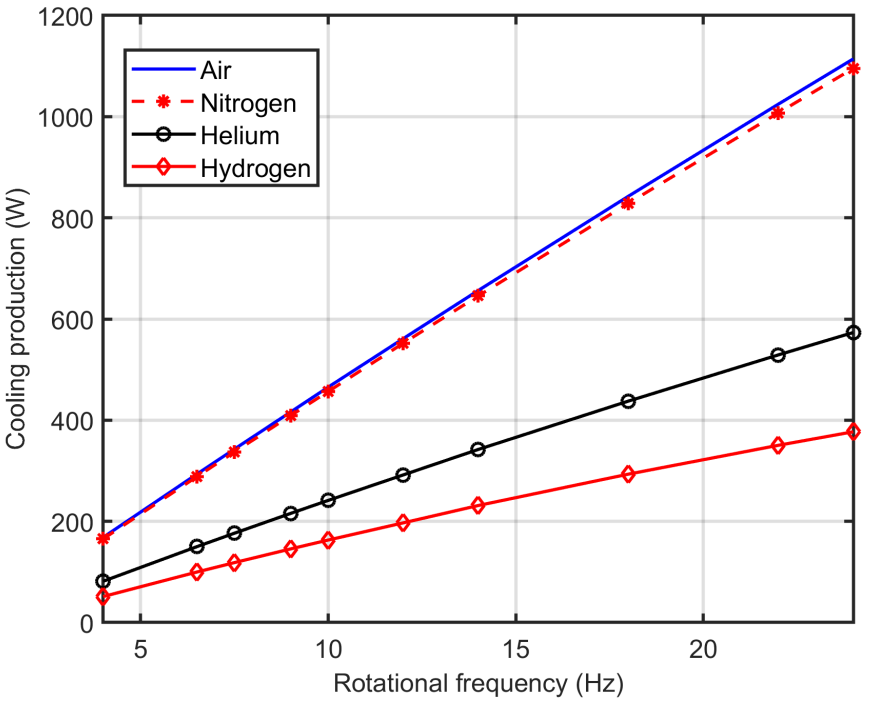

Figure 4.3: Cooling power versus operating frequency for different types of working fluid at (T_{cr} = 270 K, T_h = 300 K, P = 17.5 bar and f = 7.5 Hz).

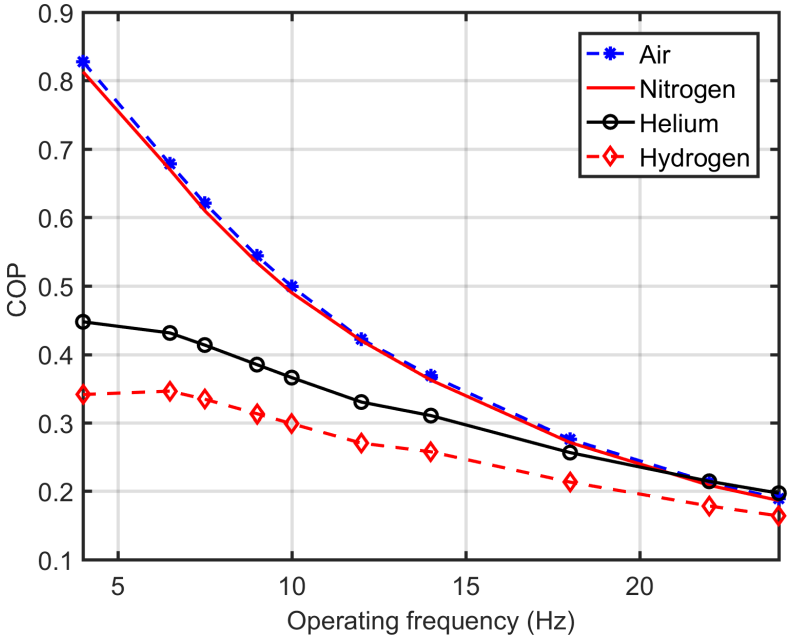

Figure 4.4: COP vs operating frequency for different types of working fluid at (T_{cr} = 270 K, T_h = 300 K, P = 17.5 bar and f = 7.5 Hz).

frigerating machine with charging pressure at T_h = 300 K, T_{cr} = 270 K, and an operating frequency of 7.5 Hz. Air and nitrogen demonstrates by far better COP than helium and

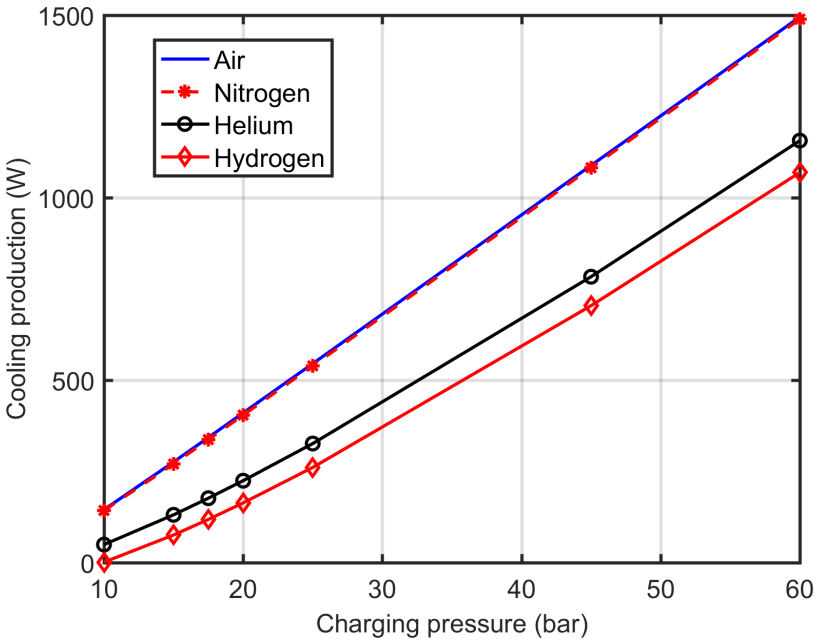

Figure 4.5: Effect different working fluid types on cooling power of Stirling cycle refrigerator with pressure at ($T_{cr} = 270$ K, $T_h = 300$ K, P = 17.5 bar and $f = 7.5$ Hz).

hydrogen at lower average pressure especially for pressure less than 30 bar. COP for almost all types of fluids show a wider dome shaped trend as a function of pressure. The COP for nitrogen increases from 0.35 to 1.06 as the charging pressure increases from 10 bar to 25 bar. The COPs for helium and hydrogen increase radically with charging pressure due to the lower rate of increase in flow friction losses and increased mass flux. At higher pressure the difference in mass flux between different working fluids decreases.

4.3/ EFFECT OF OPERATING PARAMETERS ON COOLING PERFORMANCE

In this part of the analysis, the effects of operating parameters such as charging pressure, operating frequency, and temperature (cold and hot ends) of the cooling machine on the refrigerator performance are investigated. The analysis is conducted with the variation of operating parameters keeping constant the design parameters. The effect of operational parameters on the PV-diagram as well as on the pressure drop in heat exchangers have been investigated. The input power requirement, cooling power, and coefficient of performance are evaluated at different operating parameters. Then, the trends and the optimum performance values of the refrigerator are identified in each case within the range of analysis.

Even though the operating frequency and average operating pressure of Stirling refrigerating machine are known to have a significant influence on machine in terms of its power demand and cooling production, the exact operating effect of these parameters are not well known. The variation of PV diagram as functions of operating frequency and charging pressure have been investigated in order to predict the operating condition of

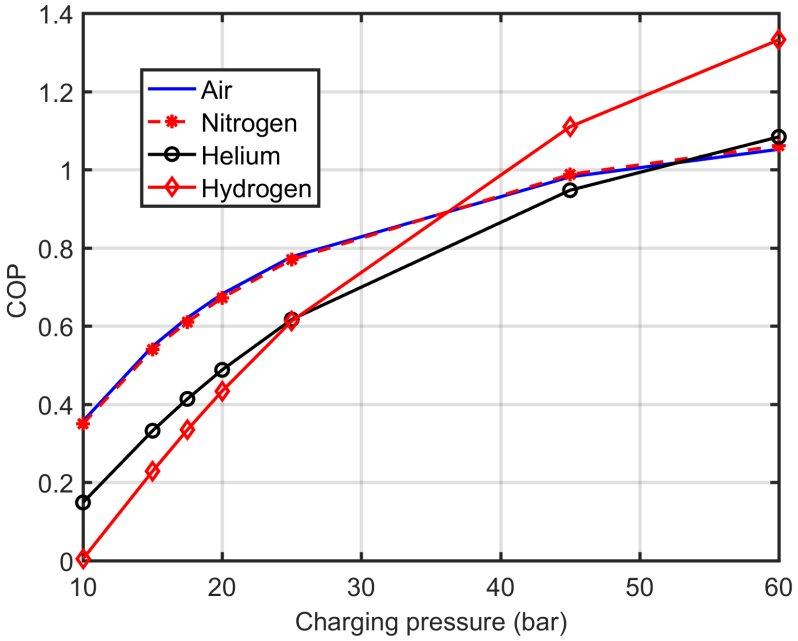

Figure 4.6: Effect different working fluid types on COP of Stirling cycle refrigerator with pressure at (T_{cr} = 270 K, T_h = 300 K, P = 17.5 bar and f = 7.5 Hz).

the machine.

Fig. 4.7a and b demonstrate the effect of operating frequency on the PV diagram at 6 Hz and 12 Hz respectively. The compression volume pressure range remains almost constant and the expansion volume pressure variations are highly reduced as operating frequency increases from 6 to 12 Hz. The PV curve area of expansion space is quite different for low and high machine frequencies. The reduction of the PV diagram area for the expansion space shows that as frequency increases the amount of heat transfer from the working fluid decreases as the working fluid spends lesser time in the heat exchangers including the regenerator. The working fluid also spends less time in the cold heat exchanger (chiller) as frequency increases. However, the PV diagram in compression spaces remains almost constant. Even though, it is expected to decrease on the other hand as frequency increases the amount of input power increases due to the increase of fluid friction losses, finite speed losses, and mechanical friction losses. Furthermore, the network input will increase as operating frequency increases and this network input is represented by the net area of compression and expansion space. The hollow curve in expansion volume pressure curve of Fig. 4.7b, shows that the higher pressure drop is around $40^o - 60^o$ crank angle and is more critical as the operating frequency increases. This results from a higher mass flow rate in heat exchangers including the regenerator achieved at a maximum value near 50^o as demonstrated in Fig. 3.10 and causes a higher pressure drop. This is also confirmed in section 4.4 of this research work.

Similarly, the effect of charging pressure on the PV diagram has been investigated as shown in Fig. 4.8, where PV curves of the two chambers of the Stirling refrigerator are compared for the cases of 15 bar and 25 bar. The lowest and highest pressures inside the compression space were about 11.7 bar and 18.9 bar and the lowest and highest pressures in expansion spaces were about 13.9 bar and 16.6 bar when the charging

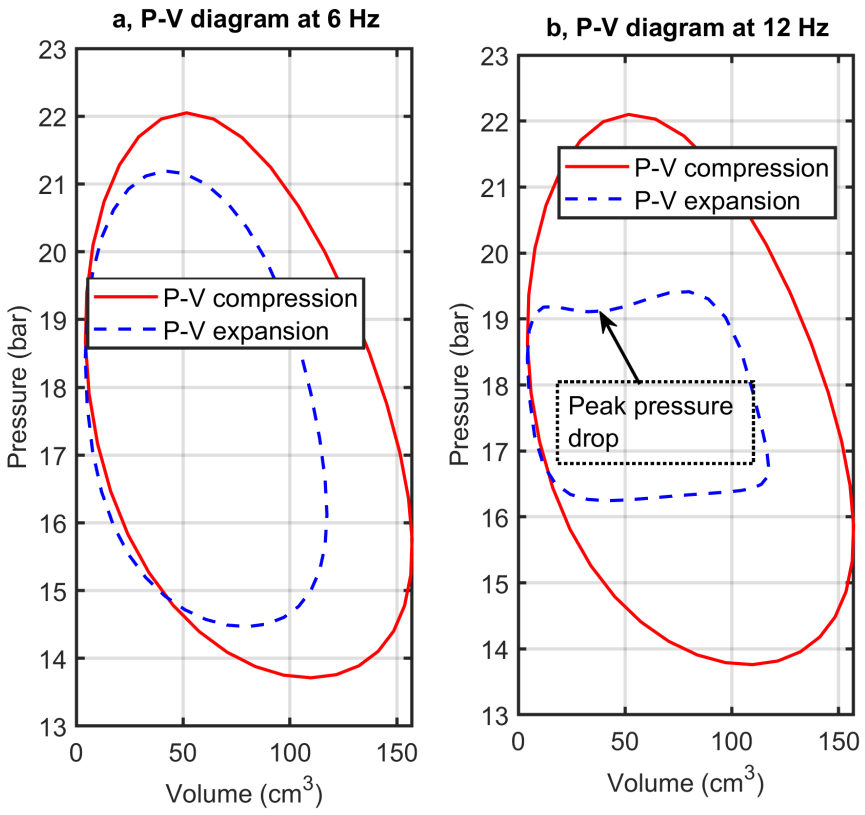

Figure 4.7: Effect of machine operating frequency on the P-V diagram of compression and expansion space at (T_{cr} = 270 K, T_h = 300 K, and P = 17.5 bar).

pressure is 15 bar. At a charging pressure of 25 bar, the lowest and highest pressures inside the compression space were about 19.6 bar and 31.5 bar and the lowest and highest pressures in expansion spaces were about 23 bar and 27.7 bar. As shown in the figure, the area for both PV diagrams of compression and expansion spaces increases as pressure increased from 15 bar to 25 bar. The net increase in area compression space is higher than the net increase in the area of expansion space as pressure increases. This confirms that the net power demand per cycle increases with charging pressure.

The variation of power demand, as a function of the operating frequency of the Stirling machine predicted by the developed modified simple numerical model for the Stirling refrigerator is studied and presented in Fig. 4.9. At this particular figure, the Stirling refrigerator was simulated at an ambient temperature of 300 K, chiller temperature of 270 K, and air as a working fluid. The analysis is conducted with operating frequency ranging from 1-12 Hz and charging pressure from 5-25 bar. The higher the pressure, the higher the input power requirement. This is because the increase in pressure of the Stirling refrigerator leads to an increase of the work done on the fluid and an increase in the mass of working fluid that would result in higher fluid friction (pressure) losses which require more power to drive the refrigerator.

The input power initially increases nearly linear and increases at a higher rate with an increase in operating frequency and in a good agreement with [132]. This indicates that the fluid friction and mechanical friction power losses increase more at higher rotation

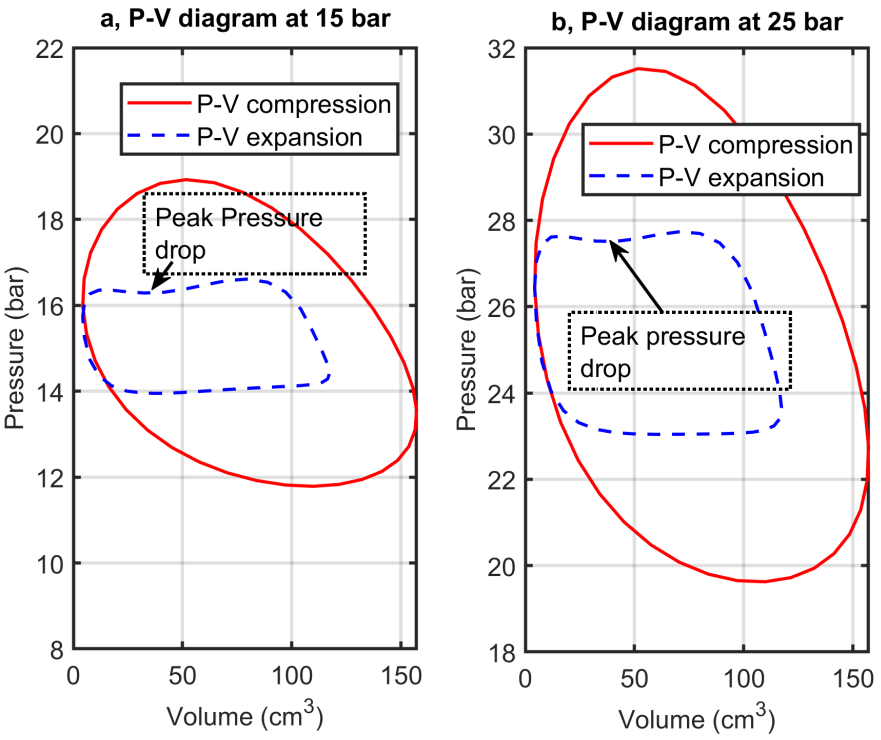

Figure 4.8: Effect of charging pressure on the P-V diagram of compression and expansion space at ($T_{cr} = 270$ K, $T_h = 300$ K, and $f = 7.5$ Hz).

frequencies. On the other hand, as operating frequency increases, the number of cycles per time increases which demands higher power. Hence, the power demand increases with charging pressure as well as with operating frequency.

Fig. 4.10 illustrates the effect of operating frequency on the cooling power of the Stirling refrigerator when the charging pressure is ranging from 5-25 bar, at an ambient temperature of 300 K, chiller temperature of 270 K, and air as a working fluid. The cooling power increases with charging pressure. This is because as the cooling machine charging pressure increases, the mass of working fluid increases that results in a higher heat removal rate and hence higher cooling power. Furthermore, it could be seen from this figure that cooling power increases linearly with an increase in operating frequency. In other words, increasing the operating frequency of the Stirling refrigerator will result in higher cooling power at the fixed cooling temperature. This is because as operating frequency increases, the thermodynamic cycle accompanied per unit time also increases, which results in higher cooling production at the chiller end. Therefore, a particular cooling power with a specific frequency and charging pressure could be found either at a lower frequency with increased charging pressure or at a higher frequency with decreased charging pressure. Hence, the choices of operating frequency and charging pressure are dependent on the cooling temperature requirement and the choice of a better COP of the machine.

In Fig. 4.11, the trend of COP as a function of operating frequency at different charging pressure is demonstrated. As COP is the ratio of cooling power and input power requirement, it can easily be determined from Fig. 4.9 and Fig. 4.10. As can be seen in Fig.4.9 and Fig. 4.10, the cooling power increases nearly linearly and the input power initially

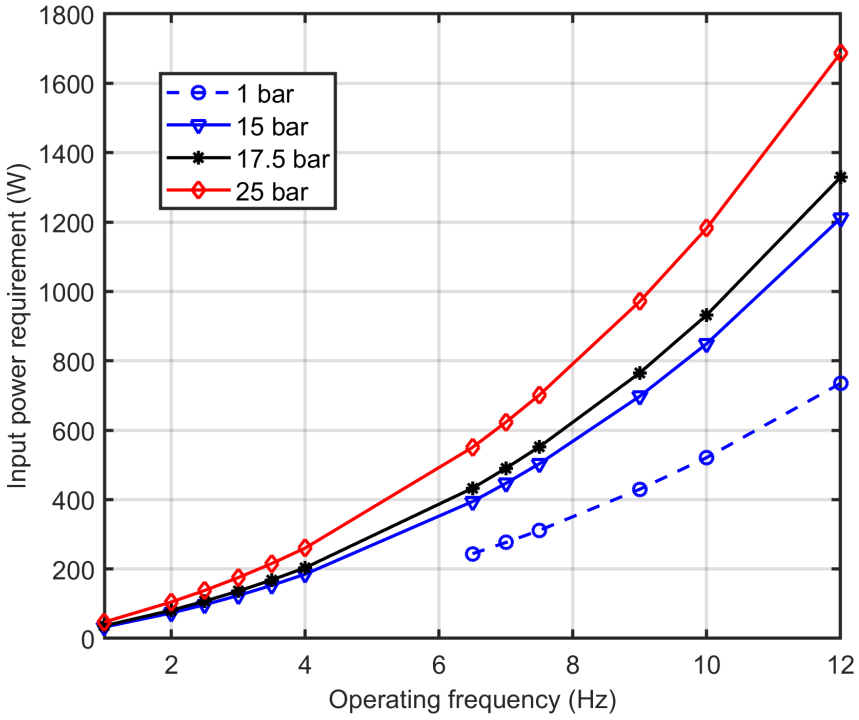

Figure 4.9: Trend of power demand for refrigerating machine with respect to operating frequency at different charging pressure.

increases nearly linearly and increases at a higher rate with an increase in operating frequency (also confirmed by [132]). On the other hand, even though both cooling power and power demand increase with operating frequency, the increase in power demand is higher than the increase in cooling power. This results in a reduction in COP of the cooling machine with an increase in frequency. COP shows a maximum value with respect to operating frequency and this was also described in [130]. The optimum point of COP varies with the charging pressure. The higher the charging pressure, the lower the frequency in which the optimum COP found. This may be due to the fact that at higher pressure, fluid friction increases the overall power demand at higher rate with increase in operating frequency and hence the COP will tend to reach its optimum value at relatively lower frequency.

On the other hand, the COP increases with charging pressure, this is because the effect of an increase of mass of working fluid with charge pressure on heat removal rate is higher than the increase of fluid friction. Furthermore, the higher the pressure the lower the operating frequency in which the optimum COP is found. This is because the rate of increase of fluid friction losses is higher at higher pressure.

4.4/ EFFECT OF OPERATING PARAMETERS ON LOSSES

The effects of operating parameters on different losses have been evaluated for the present modified simple model using the geometrical parameters of the FEMTO−ST machine model. The major power and heat losses have been identified and their effects on

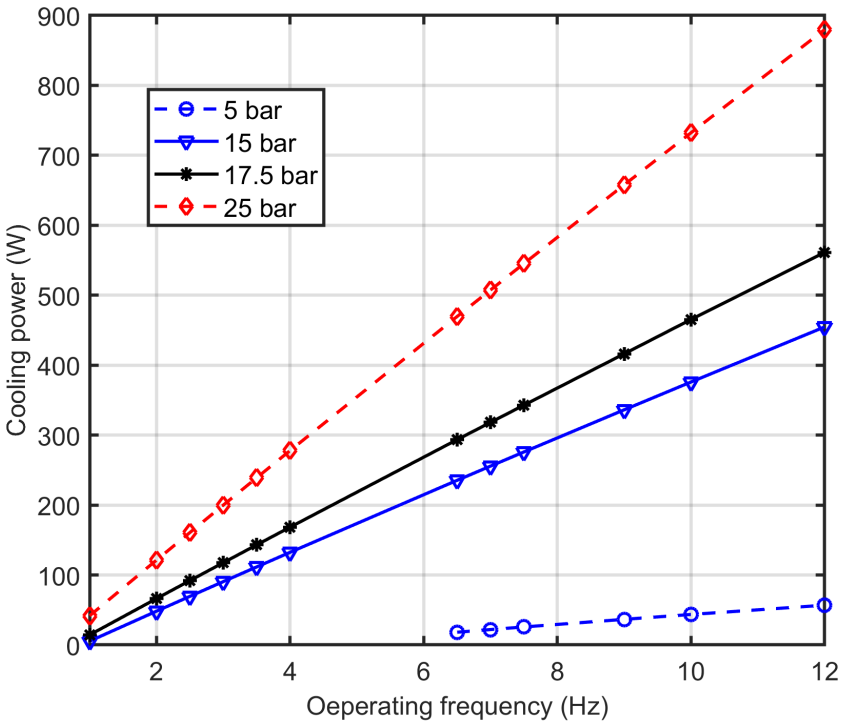

Figure 4.10: Trend of cooling power of refrigerating machine with respect to operating frequency at different charging pressure.

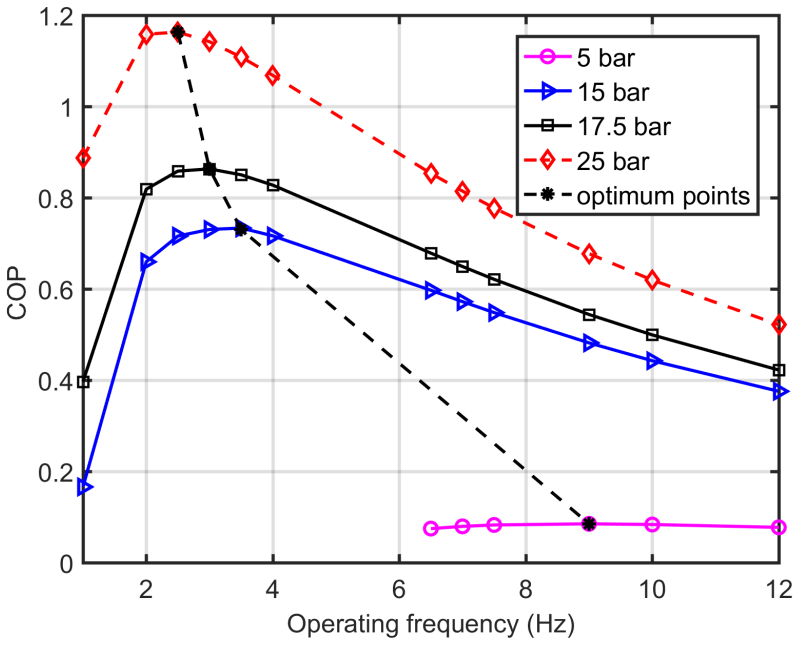

Figure 4.11: Trend of COP of refrigerating machine with respect to operating frequency at different charging pressure.

the performance of the cooling machine have been discussed. Furthermore, the effect of

pressure, frequency, and cold end temperature on different losses have been analyzed.

The variation of pressure drops across the regenerator and heat exchangers have been investigated as functions of operating frequency and charging pressure in order to predict the extent of fluid friction losses. Fig. 4.12a and b demonstrates the effect of operating frequency on pressure drop in the regenerator and two heat exchangers respectively for operating frequencys of 6 Hz and 12 Hz. It can be confirmed that the pressure drop increases with frequency. This is due to the fact that as frequency increases friction between flowing working fluid and heat exchanger solid surface increases as also described by [66]. For instance, the maximum pressure drop in regenerator increases from 0.81 bar to 2.83 bar which is 252% increase as frequency increases from 6 Hz to 12 Hz. Furthermore, the pressure drops in chiller and hot heat exchanger (HHX) increase by 230% and 233% respectively as operating frequency increases from 6 Hz to 12 Hz. Generally, operating frequency has critical impact on the overall pressure drop across heat exchangers. Most importantly, the pressure drop especially in regenerator has a large share on the total pressure drop and it also increases at higher rate with frequency.

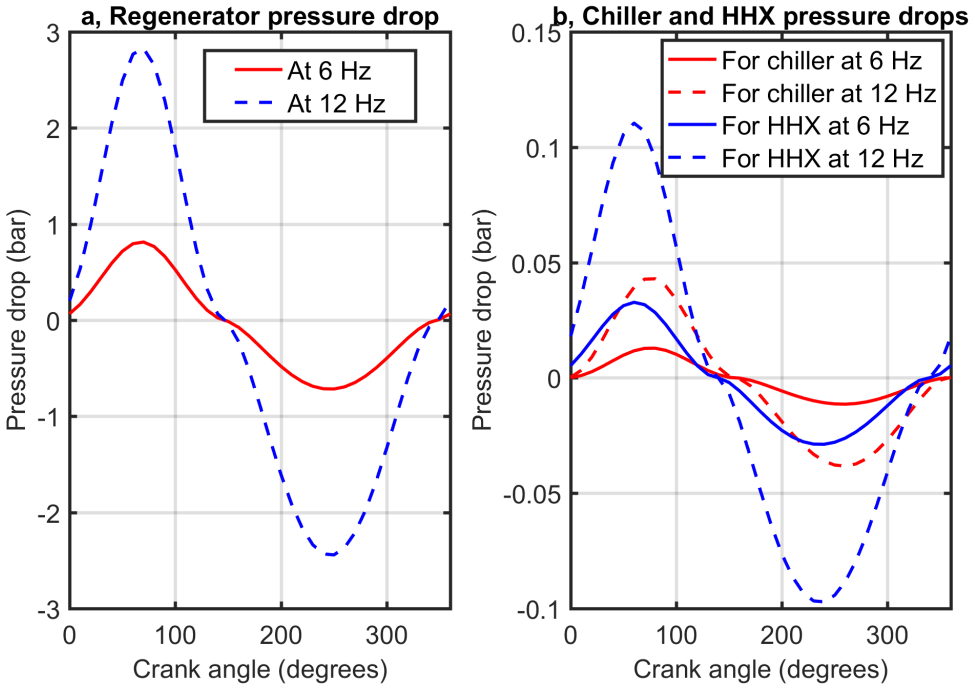

Figure 4.12: Effect of machine operating frequency on the pressure drop in heat exchangers.

The effect of charging pressure on the pressure drop across regenerator and heat exchangers have been also investigated as shown in Fig. 4.13, where the pressure drops of regenerator as well as other heat exchanges of a Stirling refrigerator are compared for the cases of 15 bar and 25 bar. From Fig. 4.13a, it could be observed that the pressure drop in the regenerator increases by 53% as pressure increase from 15 bar to 25 bar. Similarly, Fig. 4.13b demonstrates the pressure drops in chiller and hot heat exchanger (HHX) increases by 46.5% and 47.3% respectively as charging pressure increase from 15 bar to 25 bar. Hence, the pressure drop in regenerator has a large share on overall pressure drop and it also increases at higher rate with pressure. It means the fluid friction power loss increases with increase in charging especially due to pressure drop in

regenerator.

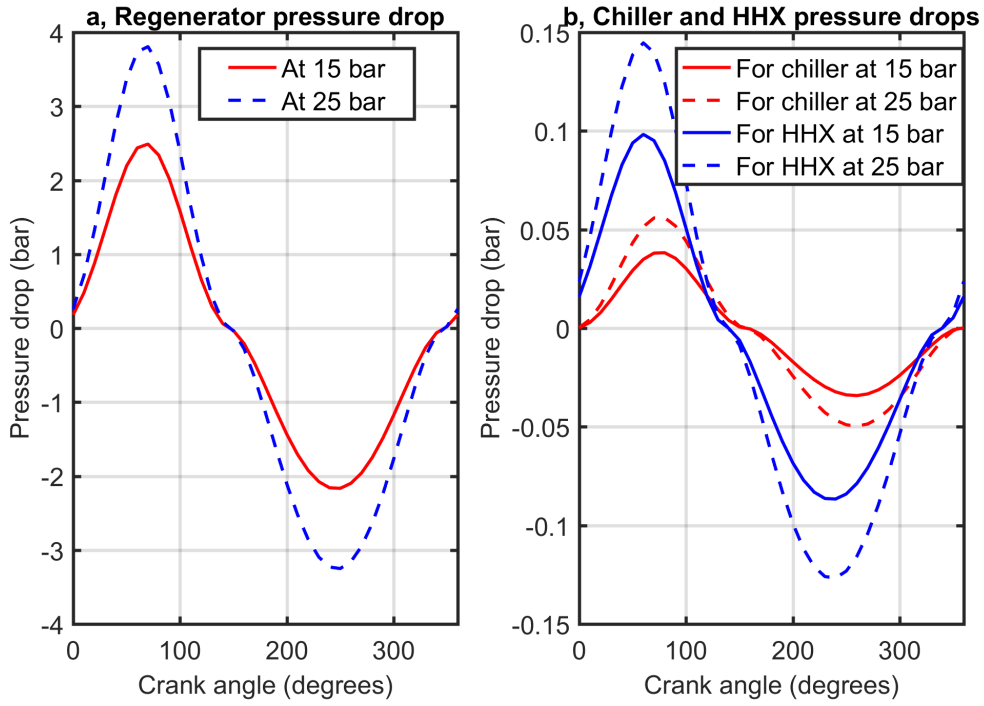

Figure 4.13: Effect of charging pressure on the pressure drop in heat exchangers.

Fig. 4.14a, b, c, and d illustrate the effect of operating frequency on the major power losses, major heat power losses, cooling power, and COP respectively at an ambient temperature of 300 K, chiller temperature of 270 K, and charging pressure of 17.5 bar. As demonstrated in Fig. 4.14a, except for gas hysteresis power losses, all power losses are majorly affected by operating frequency. Fluid friction losses increase strongly at a higher frequency. As it is shown in Fig. 4.14b regenerator imperfection loss linearly increases as it depends on mass flow rate of fluid based on Eq. 3.3.2 which is affected by frequency and all other heat power losses relatively remain unchanged with the operating frequency. From Fig. 4.14c, it can be seen that cooling power increases with an increase in operating frequency. This is mainly due to the increase in the thermodynamic cycle per unit time. Lastly, as it is seen in Fig. 4.14d, COP decreases with an increase in operating frequency. This is expected as demonstrated in Fig. 4.14a and 4.14b, both power and heat power losses increase which resulted in lower COP at a higher frequency.

Fig. 4.15a,b, c, and d illustrate the percentage share of different power and heat power losses as a function of charging pressure and operating frequency at an ambient temperature of 300 K and chiller temperature of 270 K. In Fig. 4.15a, the effect of charging pressure on the share of different power losses at an operating frequency of 7.5 Hz has been presented. It is clear from the figure that the share of fluid friction loss and loss due to finite speed increase and the share of mechanical friction loss decreases with an increase in the average pressure of the cooling machine. Furthermore, the major share is accounted for mechanical friction loss varies from 60% to 41.6% and fluid friction loss varies from 31.3% to 44% as the average pressure varies from 10 bar to 25 bar. Fig. 4.15b, illustrate the effect of average pressure on the share of different heat power losses at an operating frequency of 7.5 Hz. As it can be seen from this Fig. 4.15b, the

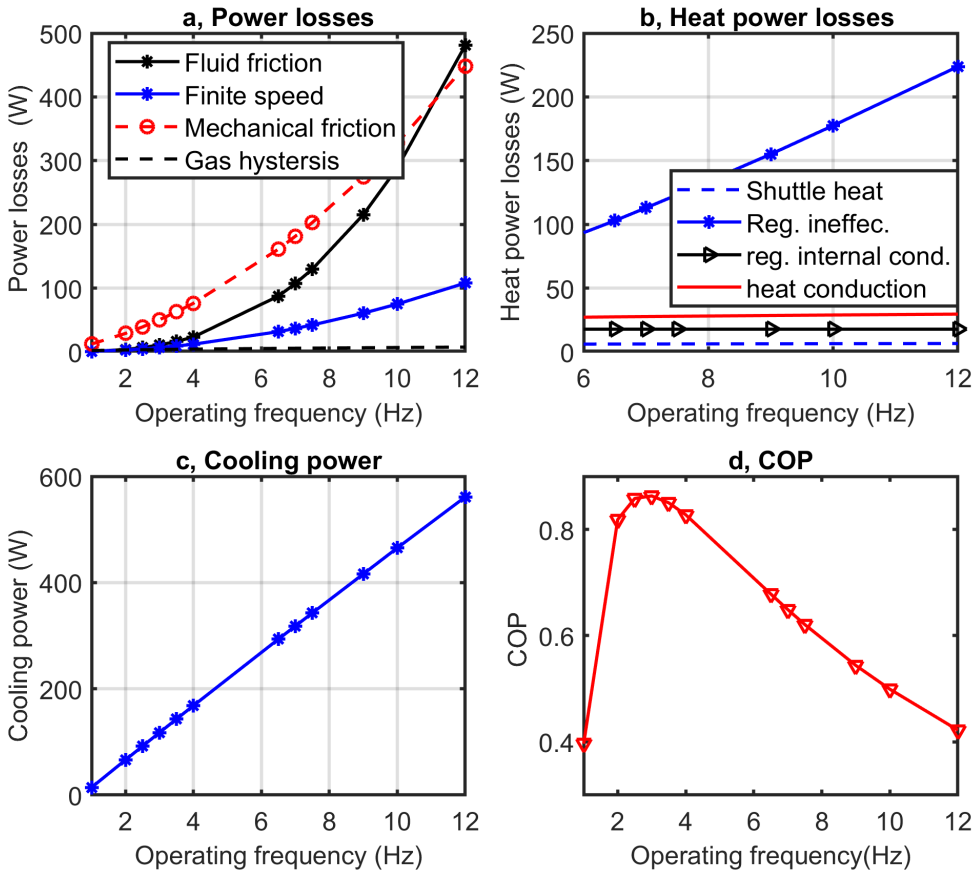

Figure 4.14: Trend of major losses and refrigeration performance with respect to the operating frequency.

share of regenerator imperfection loss increases and the shares of all other heat power losses decrease with an increase in the average pressure of the cooling machine.

The effects of operating frequency on the share of different power and heat power losses have been presented in Fig. 4.15c and 4.15d respectively. It is clear from Fig. 4.15c that, even though all power losses increase with operating frequency (as described in Fig. 4.14a), the share of fluid friction losses increases and the share of mechanical friction loss decreases with an increase in the operating frequency of the cooling machine. Furthermore, the shares of the major power losses (mechanical friction and fluid flow friction losses) vary from 54.4% to 37% and from 31.8% to 51.9%, respectively, as the operating frequency increases from 6.5 to 14 Hz. The shares of other power losses are less affected by the change in the frequency of the machine. As shown in Fig. 4.15d and similar to Fig. 4.15b the share of regenerator imperfection loss increases and the shares of all other heat power losses decrease with an increase in the average pressure of the cooling machine.

To evaluate the share of percentage of different losses at different pressures, the numerical model is simulated with different operating frequency for a fixed charging pressure and the average share of losses have been computed. The variation of shares of different losses on overall losses of respective category at charging pressures of 17.5 bar and

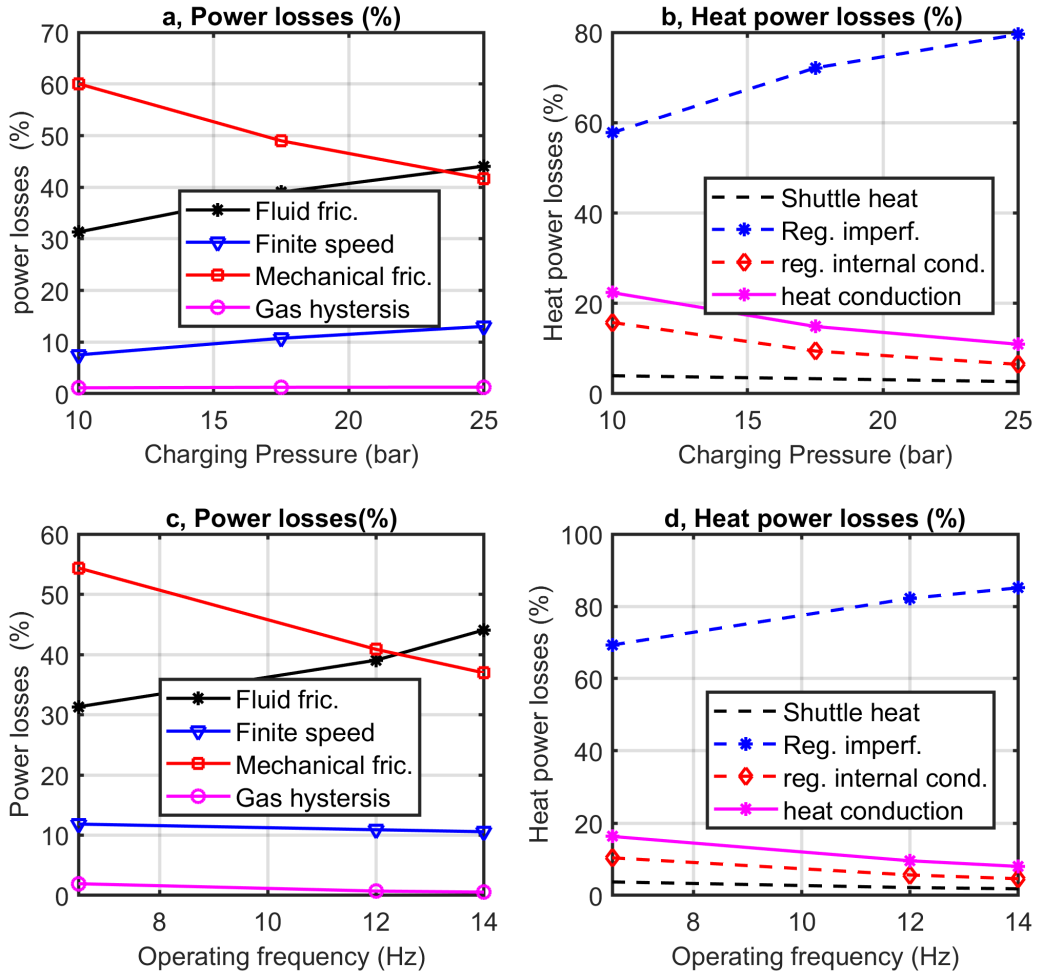

Figure 4.15: Average percentage of power and heat power losses with respect to pressure and operating frequency.

25 bar are presented Fig. 4.16. In Fig. 4.16 a and c, the average share of different power losses are presented at charging pressures of 17.5 bar and 25 respectively. As it is clearly shown in Fig. 4.16a, at a pressure of 17.5 bar from the total power loss of 3296 W, the major loss is mechanical friction loss (48%), followed by fluid friction loss due to pressure drop (40%). Others cover only 12% of the total power loss. Whereas, at a pressure of 25 bar as shown in Fig. 4.16c, from the total power loss of 3888 W, the major loss is fluid friction losses (45%) and followed by mechanical friction losses (41%). This is because as pressure increases fluid friction in a forced fluid flow increases.

Similarly, the variation of shares of different heat power losses at charging pressures of 17.5 bar and 25 bar are presented Fig. 4.16b, and d respectively. As it is clearly shown in Fig. 4.16b, at a pressure of 17.5 bar from the total power loss of 1210 W, the major loss is regenerator imperfection loss (74%). Other losses cover only 26% of the total heat power loss. At a pressure of 25 bar as shown in Fig. 4.16d, from the total power loss of 1771 W, the major loss is still regenerator imperfection (81%) and which shows that the share of this loss increases with charging pressure.

Generally, as pressure increases the shares of fluid friction power losses, regenerator imperfection loss, and loss due to finite speed of piston increase and the shares of other

losses decrease. Hence, when designing Stirling refrigerator with higher pressure, the fluid friction, regenerator imperfection and finite speed losses shall get great concern. Most importantly, the impact of losses associated with regenerator (fluid friction and regenerator imperfection losses) on the Stirling refrigerator performance will increase.

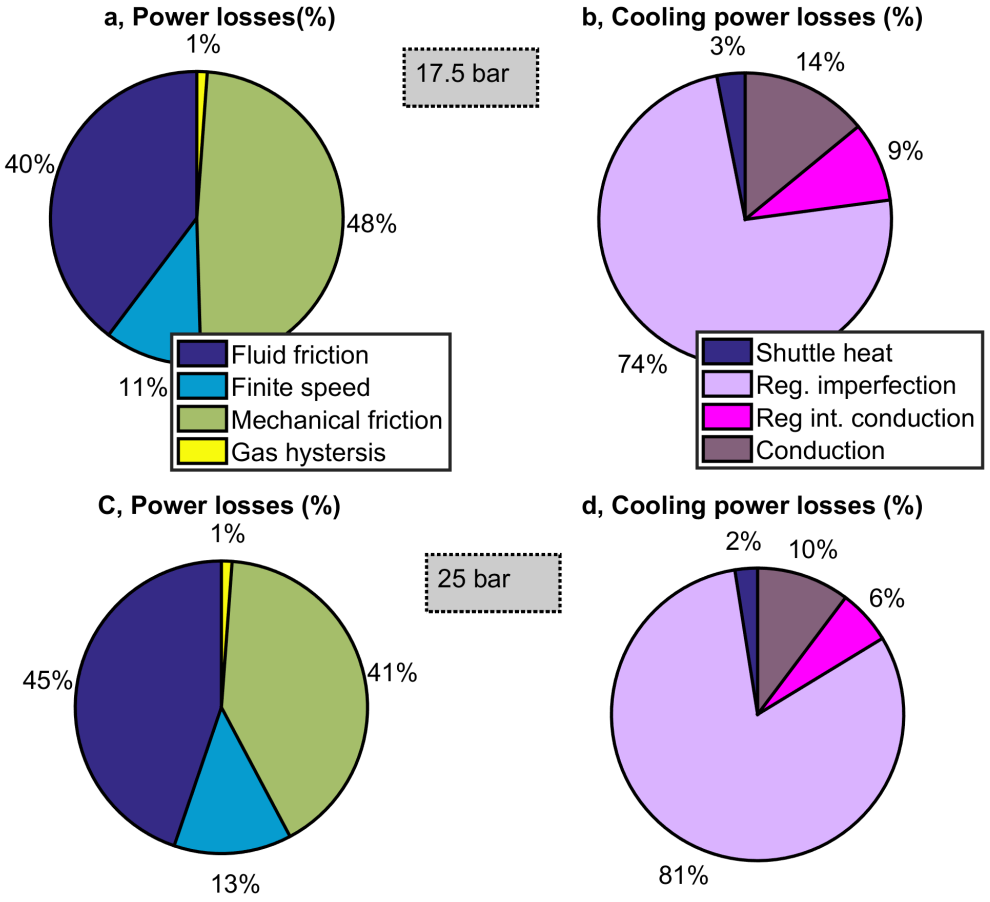

Figure 4.16: Percentage share of average power losses at charging pressures of 17.5 and 25 bar.

Fig. 4.17a, b, c and d illustrate the effect of cold end temperature on the major power losses, major heat power losses, cooling power, and COP respectively at an ambient temperature of 300 K, charging pressure of 17.5 bar, and an operating frequency of 7.5 Hz. As demonstrated in Fig. 4.17a, almost all power losses are not majorly affected by the cold end temperature. On the other hand, Fig. 4.17b shows the effect of cold side temperature on different heat power losses. As it can be seen from Fig. 4.17b, all heat power losses decrease with an increase in cold end temperature. This is because as the temperature difference lowers, the heat transfer losses due to temperature gap will also decrease. Especially, regenerator imperfection loss decreases remarkably with an increase in cold end temperature. Fig. 4.17c, investigates the effect of cold end temperature on the cooling power of the refrigerating machine. It is seen that due to the decrease of heat power losses, cooling power increases with an increase in cold temperature and it is confirmed by [132]. Lastly, Fig. 4.17d, demonstrates the relation between cold end temperature and COP of the cooling machine. As seen in Fig. 4.17a and 4.17b the power losses relatively remain constant and the decreasing of heat power losses respectively resulted in increasing in COP with an increase in cold end temperature.

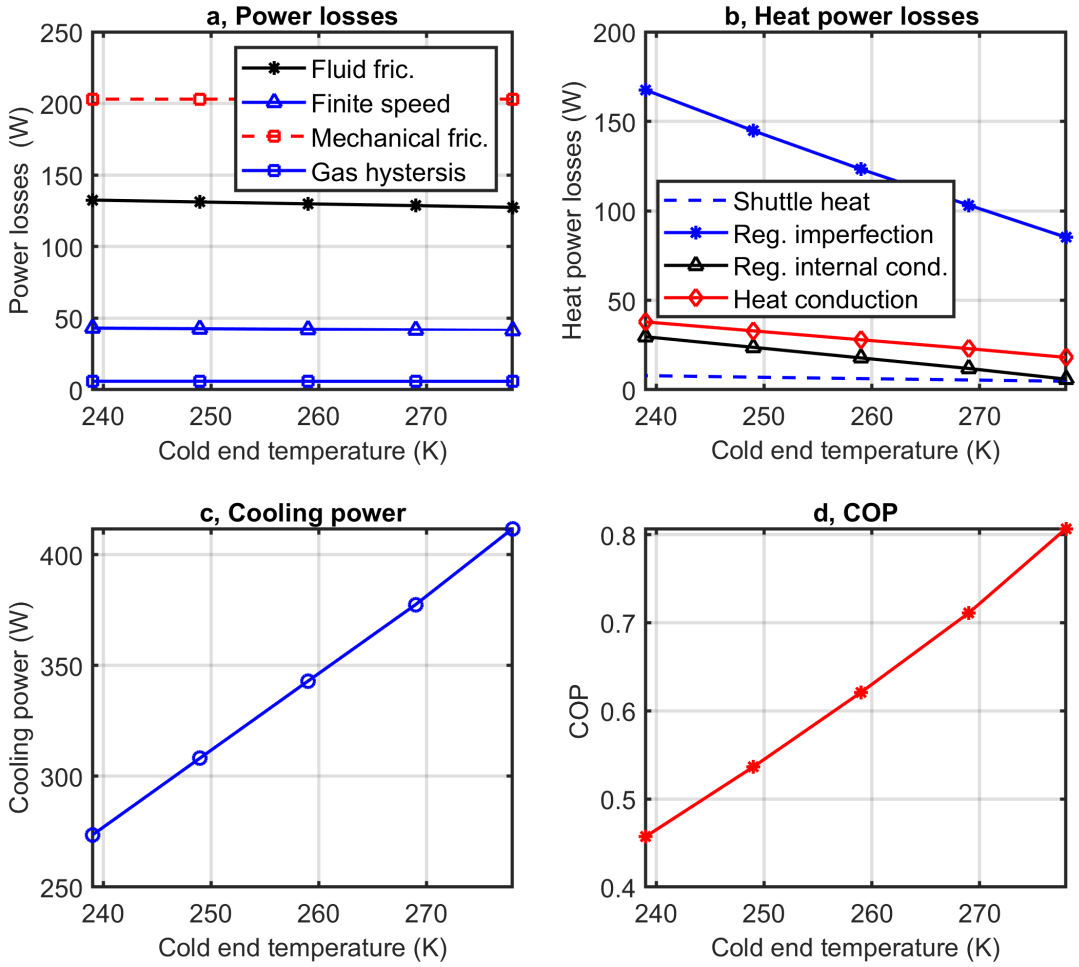

Figure 4.17: Trend of major losses and refrigeration performance with respect to cold end temperature.

Fig. 4.18a, b, c, and d represent the effect of hot/ambient temperature on the major power losses, major heat power losses, cooling power, and COP respectively at a cold temperature of 270 K, charging pressure of 17.5 bar, and an operating frequency of 7.5 bar. As demonstrated in Fig. 4.18a, almost all power losses are not majorly affected by the hot end temperature. On the other hand, Fig. 4.18b shows the effect of hot side temperature on different heat power losses. It could be seen from Fig. 4.18b, all heat power losses increase with an increase in hot end temperature because the temperature gap is increased. Especially, regenerator imperfection loss increases remarkably with an increase in hot-end temperature. Fig. 4.18c, illustrates the effect of hot-end temperature on the cooling power of the refrigerating machine. It is seen that due to the increase of heat power losses, cooling power decreases with an increase in ambient temperature. Fig. 4.18d, demonstrates the relationship between ambient temperature and COP of the cooling machine. As seen in Fig. 4.18a, 4.18b, and 4.18c, due to the decreasing of cooling power without much variation on input power, the COP shows a similar trend as that of cooling power and it decreases with increasing of hot−end temperature.

As the COP of a refrigerator is a function of temperature, so it is convenient to adopt percent of Carnot COP to evaluate the performance of the Stirling refrigerator. The latest survey of cryocooler performance with different cooling capacities has been presented [63].

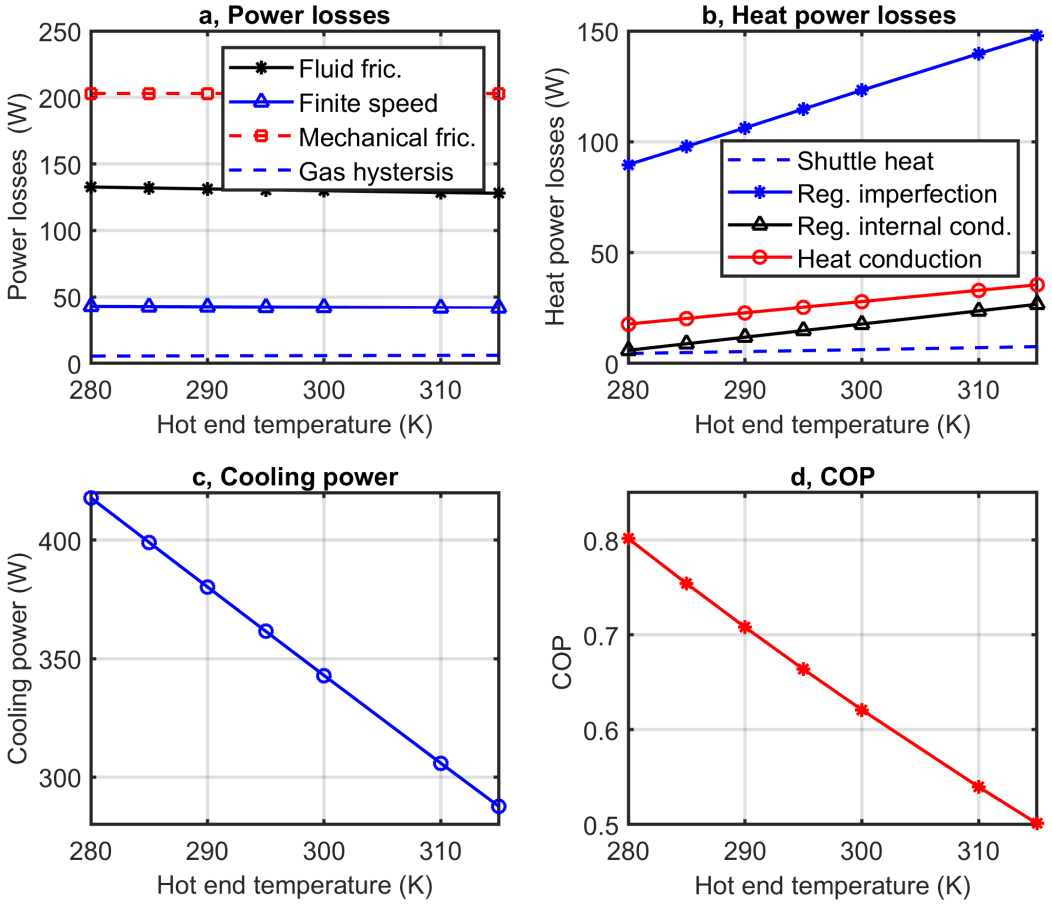

Figure 4.18: Trend of major losses and refrigeration performance with respect to hot end temperature.

The survey result shows that the percentage of Carnot COP significantly increases with the cooling capacity. Fig.4.19 depicts the percentage of actual COP to the Carnot COP, (COP/COP_c) at different cooling temperatures for domestic Stirling refrigerators at operating frequencies of 7.5 and 10 Hz. As it is seen in the figure, the percent of Carnot COP monotonously decreases and actual COP monotonously increases with an increase in cooling temperature. Accordingly, Fig. 4.19, the percentage of Carnot COP (COP/COP_c) is higher at 7.5 Hz than at 10 Hz in all temperature ranges analyzed. The differential of temperature is very low in our case which results in a very high Carnot COP. This resulted in relatively lower percentage Carnot COP as compared with other research findings (for instance as compared with [149]). This is because at very low temperature differential adiabatic nature of heat exchangers will limit heat transfer rate and then rate of increase of cooling will be limited.

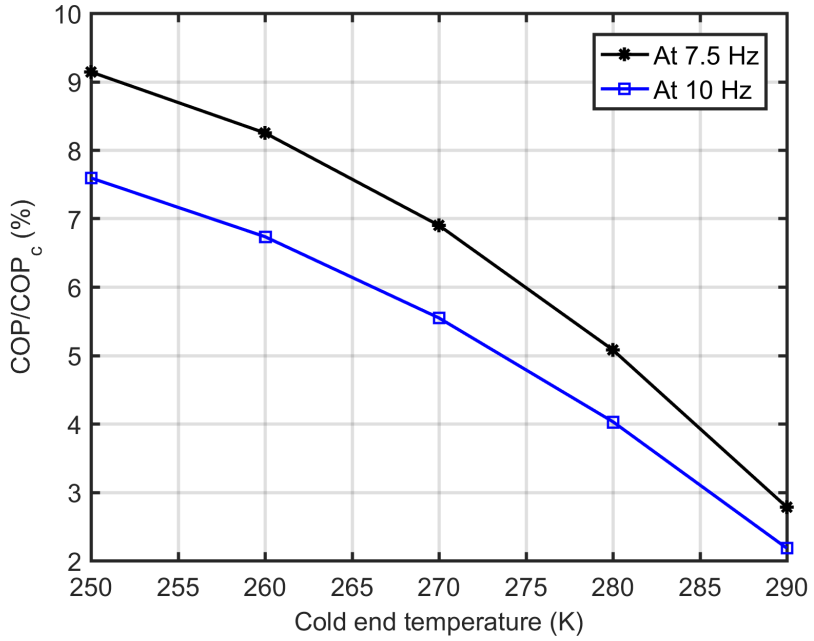

Figure 4.19: Trend of COP/COP_c with respect to cold end temperature.

4.5/ EFFECT OF DESIGN PARAMETERS ON COOLING PERFORMANCE

4.5.1/ EFFECT OF PHASE ANGLE

The phase advance of expansion space volume variations with respect to compression space variations is represented by phase angle. The phase angle determines the dynamics of piston–displacer movements and thus the volume variation during the cycle which is directly related to the work input and output. The effect of phase angle on cooling power and coefficient of performance have been indicated in Figs. 4.20 and 4.21.

Fig. 4.20 has presented that there is a single optimum angle (considering cooling power) for a single type of working fluid investigated at different operating frequencies using FEMTO 60 machine model. It should be noted that the optimum phase angle has been found as 90^o and 95^o for air and helium respectively. These obtained phase angles agree closely with the result provided for the engine by [146]. It could be stated that the optimum phase angle for gases like air with lower thermal capacity is lower.

Fig. 4.21 has demonstrated the COP of a Stirling refrigerator as a function of the phase angle. It has shown that the optimum phase angle for peak COP is different from the optimum phase angle for cooling capacity. Furthermore, the optimum phase angle for the peak COP varies with respect to the operating frequency, and the optimum phase angle for COP is mostly higher than the optimum phase angle for cooling power. The higher the operating frequency, the lower the optimum angle. Generally, the optimum COP with respect of phase angle varies with operating frequency as fluid friction loss depends both on operating frequency and phase angle(as it affects swept volume).

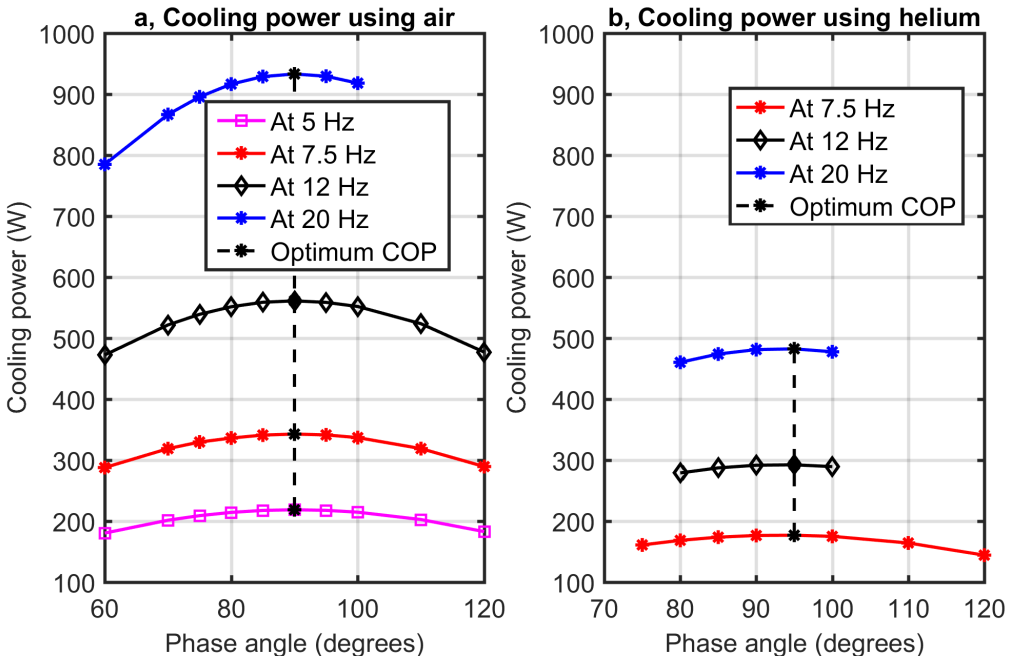

Figure 4.20: Cooling power versus phase angle at different operating frequency.

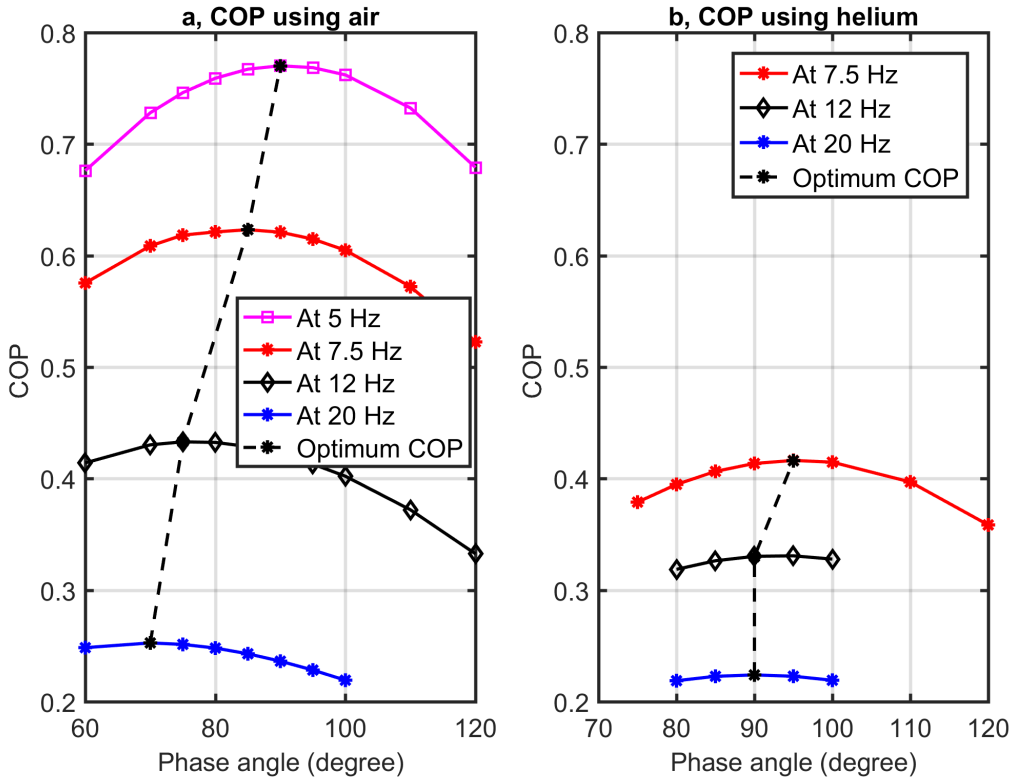

Figure 4.21: COP versus phase angle at different operating frequency.

4.5.2/ EFFECT OF LENGTH AND POROSITY OF REGENERATOR

The regenerator is an essential part of Stirling machines as it recovers a great part of the thermal energy of the working fluid. On the other hand, regenerator is typically the largest source of power loss in the system. Hence, the effects of regenerator parameters should be investigated based on the application of the Stirling machine. In this research, the effect of the most important parameters of the regenerator that are length and porosity of regenerator have been investigated as shown in Figs. 4.22 and 4.24, respectively. For optimization of the regenerator parameters, while keeping other parameters constant and one parameter subsequently has been made to vary.

Fig. 4.22 has shown that the performance of a Stirling refrigerator is higher at a relatively smaller length of the regenerator. The figure shows that both cooling power and COP demonstrate parabolic evolution with nearly the same optimum value at 25 mm of the regenerator length. It could be stated that both cooling power and COP show a decreasing trend as the regenerator length increases after the optimum value. This phenomenon results from decreasing of most of the heat losses and increasing of fluid friction loss with regenerator length as demonstrated in Fig.4.23. From Fig. 4.23, it could be understood that regenerator imperfection loss decreases and fluid friction loss increases at higher rate than other losses. Hence, the main reason for the decreasing of cooling performance is due to the fact that increasing fluid friction loss and the decreasing of regenerator imperfection loss with increase in regenerator length. As the length of the regenerator increases, fluid friction loss will increase which will result in lower performance of the Stirling refrigerator. The optimum design point for the case of regenerator length is therefore at a smaller length as much as possible for both cooling power and COP for the choosen porosity of 0.64.

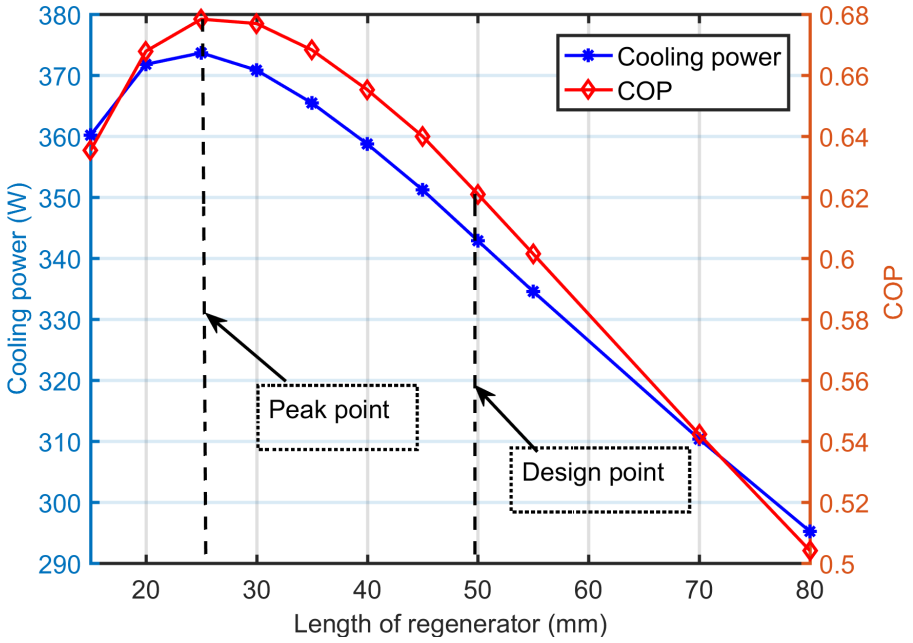

Figure 4.22: Cooling power and COP versus length of regenerator.

Pressure drop and heat regeneration in the regenerator are largely dependent on porosity. Fig. 4.24 shows the impact of regenerator porosity on the cooling performance of the

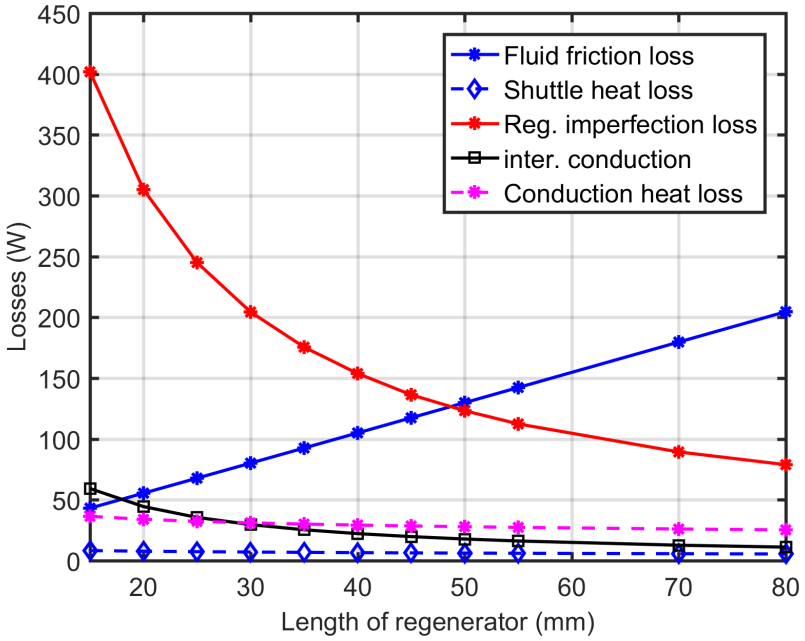

Figure 4.23: Variation of different losses versus length of regenerator.

Stirling refrigerator. It has shown that, within the range of the analysis, cooling power decreases with an increase in regenerator porosity and COP has the maximum value at relatively higher porosity. While the porosity of the regenerator increases, the heat transfer area of the matrix and the amount the heat transfer decreases. The working gas goes into the heater at a higher temperature. Thus the cooling production of the refrigerator decreases with an increase in porosity. On the other hand, due to a higher pressure drop, a low porosity regenerator requires higher input power to get the same pressure ratio to compress the working fluid compared to that of the high porosity regenerator. Thus the COP decreases at lower porosity. The curve shows that the optimum COP value is found at a porosity of 0.75 which is similar to the research conducted by [89]. The decreasing of cooling power with increase in porosity is due to the increasing of regenerator imperfection loss as demonstrated in Fig 4.25. Fig 4.25 also demonstrates the decreasing of fluid friction with increase inregenerator porosity which will tend to increase COP. On the other hand, regenerator imperfection loss increases at higher rate than the decreasing rate of fluid friction loss just after a porosity value of 0.75 that results in an optimum COP. Hence, the optimum design point in case of regenerator porosity could be at a compromise between maximum cooling power and maximum COP.

4.5.3/ Effect of gap between piston and cylinder

Fig. 4.26 demonstrates the effect of seal clearance between piston and cylinder on cooling performance (cooling production and COP). Both cooling power and COP decrease with a wider dome shape as a function of piston seal clearance. This is because as the piston seal clearance increases mass leakage to the buffer space increases as confirmed by [157]. It could be seen from Fig. 4.26 that the slope of decreasing of cooling production and COP increases more steeply at larger clearance gap as large quantity of mass

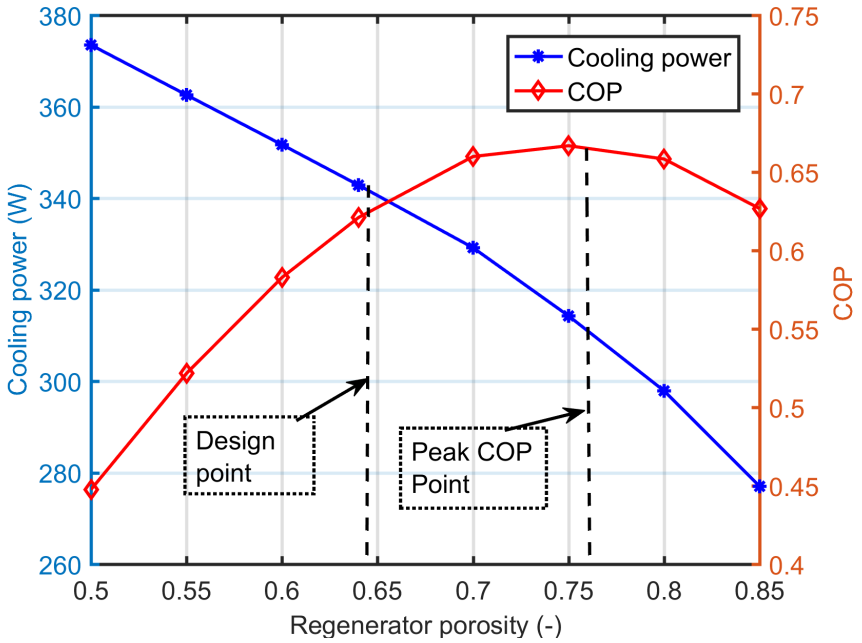

Figure 4.24: Cooling power and COP versus regenerator porosity.

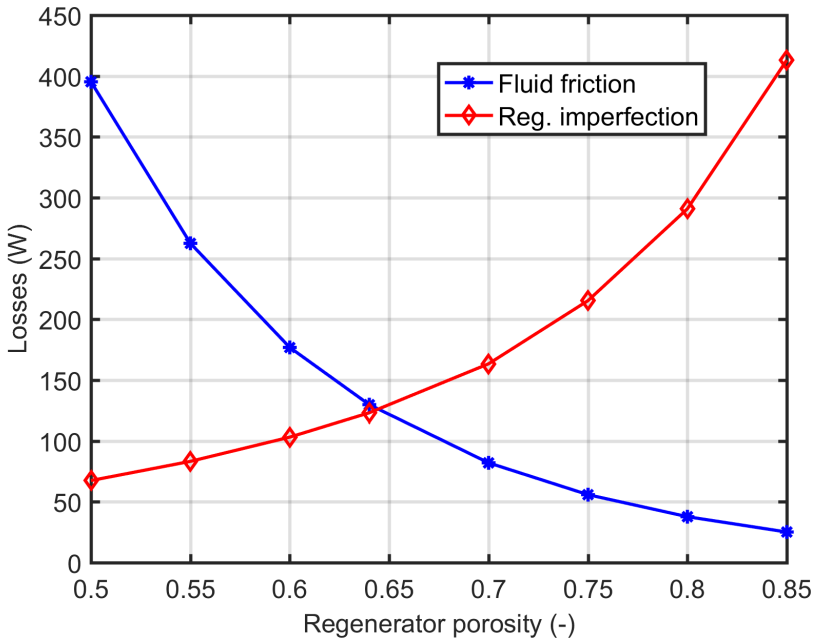

Figure 4.25: Variation of fluid friction and regenerator imperfection losses versus regenerator porosity.

leaks.

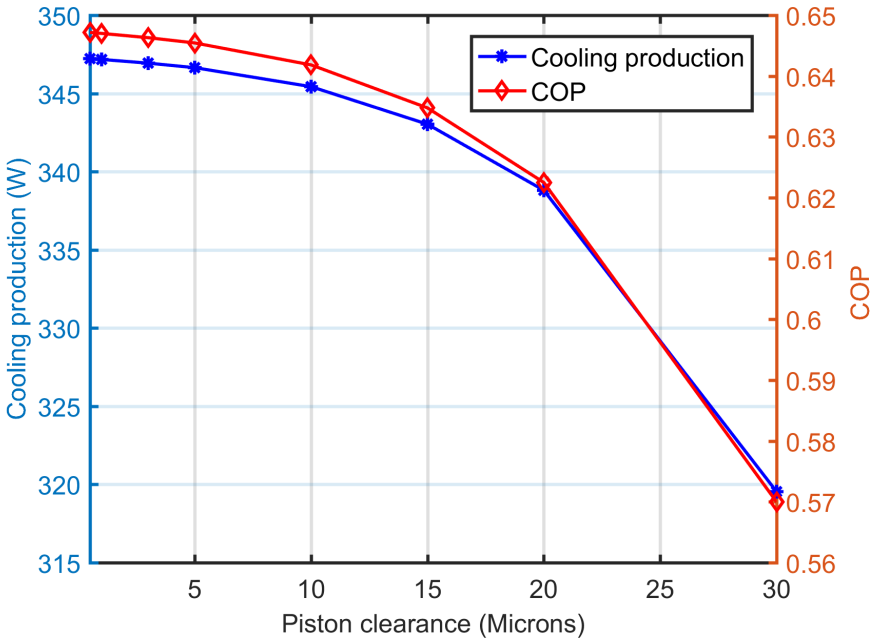

Figure 4.26: Cooling production and COP versus seal clearance between piston and cylinder.

4.5.4/ Effect of displacer height and displacer gap

Stirling refrigerator designs utilize displacers as a means of transferring the working fluid between the cold and hot regions of the device. In this research, the effects of displacer height and displacer clearance on cooling power and COP have been investigated. The height of the displacer affects the performance of the Stirling machine by changing the compression ratio as the swept volume of compression space varies with displacer height [158].

In this analysis, the height of the displacer is allowed to vary, still keeping the total length (height and length displacer rod) of the displacer fixed. As displacer height increases, keeping the total length fixed, the compression volume decreases, that results in a lower swept volume compression ratio. Fig. 4.27 has presented the impact of displacer height on cooling performance (cooling production and COP) using air as a working fluid at a charging pressure of 17.5 bar, operating frequency of 7.5 Hz, the hot−side temperature of 300 K, and chiller temperature of 270 K.

It has been noticed from the Fig. 4.27, that cooling power decreases monotonously with displacer height and there exists a peak value of COP. The peak COP value is found 0.72 at a displacer height of 10 cm with the associated cooling production of 544.4 W and a swept volume compression ratio of 1.58. Hence, with the same operating condition and keeping all other parameters constant, we could increase the peak cold production and COP by 61.6% and 13.3%, respectively only through displacer height optimization and associated compression space swept volume variation. The main reason for such improvement in cooling performance is the increase of mass of working fluid with the increase in compression space swept volume and increasing of swept volume compression ratio. Generally, the analysis confirms that shorter displacers with relatively higher swept

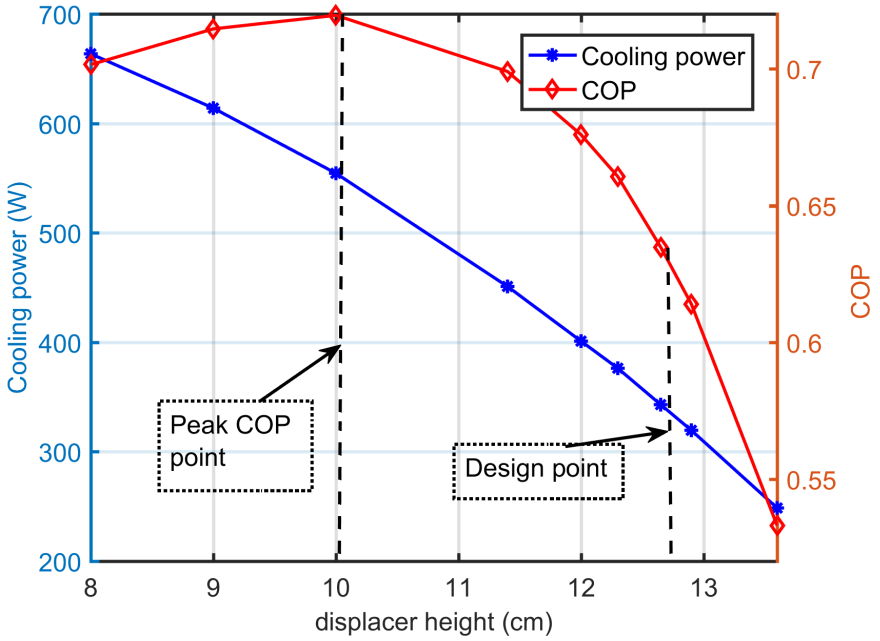

Figure 4.27: Cooling power and COP versus displacer height.

volume compression ratios show better performance for such types of domestic Stirling refrigerators.

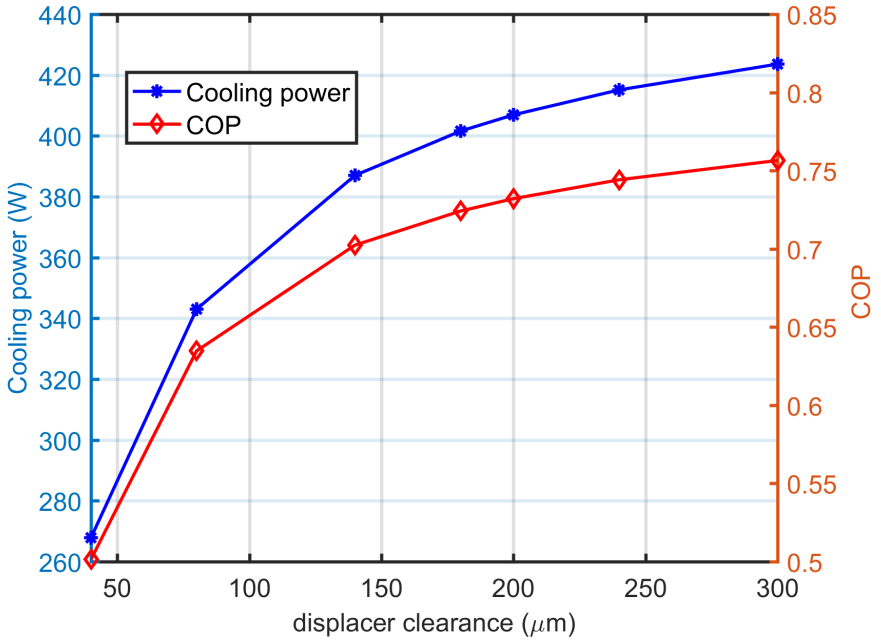

Figure 4.28: Cooling production and COP versus displacer clearance size.

Displacer clearance is another parameter that affects the cooling performance of the Stirling refrigerator. Fig. 4.28 demonstrates the effect of displacer clearance on cooling performance (cooling production and COP). Both cooling power and COP increase with a wider dome shape as a function of displacer clearance and the finding is similar to the re-

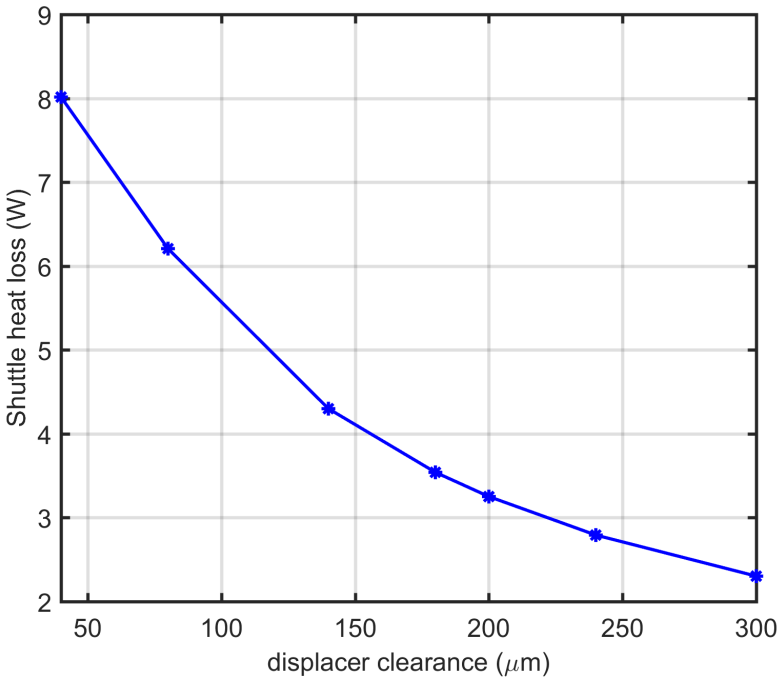

Figure 4.29: Shuttle heat losses versus displacer clearance size.

search work conducted on Stirling cryocooler by [132]. For an increase in displacer clearance from 80μm (design point) to 300μm, the cooling power increase by about 23.5% and the COP increases by about 19.2%. This effect is mainly due to the shuttle heat losses. As shown in Fig.4.29, shuttle heat losses decreases with an increase in clearance between displacer and cylinder. However, there will be a peak value of COP as regenerator effectiveness loss increases and fluid friction loss decreases due to decreased mass flow through the regenerator. Furthermore, the optimum COP and cooling power will exist at relatively lower clearance gap, if we incorporate the enthalpy loss in the differential equation. This is because as displacer clearance increases, shuttle heat loss decreases and enthalpy loss increases and there will be optimum point of clearance gap. Still at such low speed and low temperature differential machine the effect of enthalpy loss is relatively small.

4.5.5/ EFFECT OF SWEPT VOLUME RATIO

The swept volume ratio also greatly affects the performance of the Stirling machine. When we assume that the working fluid is an ideal gas, and the refrigerator is an ideal refrigerator in which the pressure loss can be ignored, then the swept volume ratio for the optimum performance of the machine equals to the ratio of the working fluid temperature in the compression space to that in the expansion space. However, in an actual refrigerator, the optimal value may be shifted due to its configuration and other factors. In this study, the effects of the volume ratio on the performance of the Stirling refrigerator have been examined numerically. Fig. 4.30 demonstrates the effect of the ratio of swept volume on cooling production and COP of the Stirling refrigerator at T_h=300 K, T_{cr} =270 K, charging pressure of 17.5 bar, and an operating frequency of 7.5 Hz using air as a working fluid. It can be seen from Fig. 4.30 that cooling production and COP of the Stirling

refrigerator as a function of volume ratio are not monotonic and there exist peak values. The peaks for cooling production and COP values are found to be 383.6 W and 0.7, respectively at a swept volume ratio of 1.7. Hence, with the same operating condition and keeping all other parameters constant, we could increase the peak cold production and COP by 11.8% and 10.9%, respectively only through swept volume ratio optimization. The analysis is conducted by keeping the total volume constant and still varying the two swept volumes vary through changing strokes of the displacer and power piston.

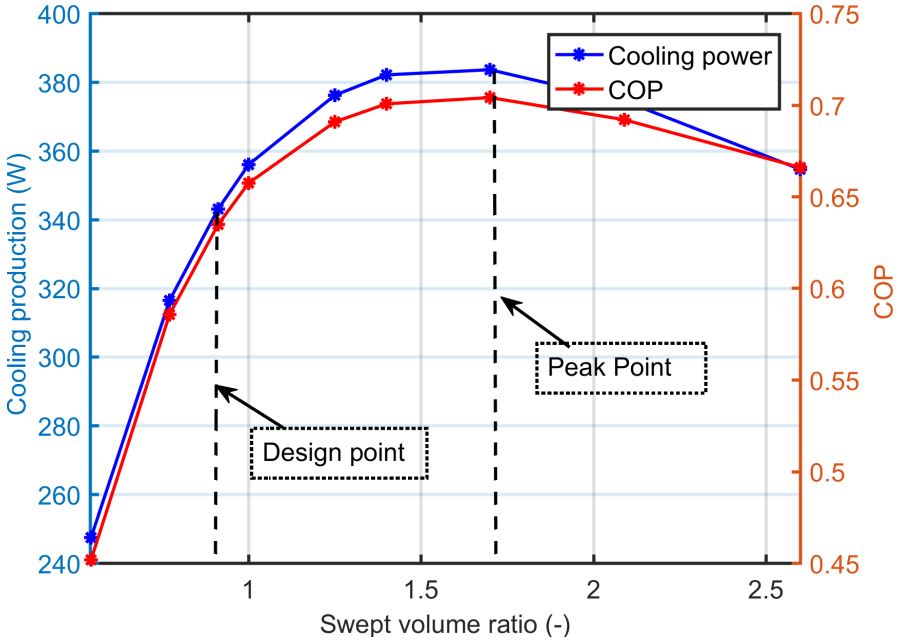

Figure 4.30: Cooling production and COP versus swept volume ratio.

Both Fig. 4.27 and Fig. 4.30 show the effect of volume ratio on the performance of the Stirling refrigerator keeping the overall cylinder volume fixed. However, in Fig. 4.27, due to the variation of displacer height, the swept volume of compression space varies keeping the swept volume of expansion space fixed. Whereas, in Fig. 4.30, both compression and expansion spaces vary keeping the summation of the two swept volumes still fixed. Hence, Fig. 4.31, illustrates the COP of the Stirling refrigerator as a function of swept volume ratio for the comparison of these two cases. It is seen in Fig. 4.31 that a better COP could be achieved when the volume ratio variation is due to the variation of compression space swept volume with displacer height and still keeping the total cylinder volume fixed. Furthermore, it could also be concluded from this figure that the optimum cooling performance for the domestic Stirling refrigerator can be found for the swept volume ratio ranging from 1.4 to 1.8.

4.5.6/ EFFECT OF RATIO OF DIAMETER TO STROKE OF PISTON

Fig. 4.32 shows the cooling production and COP variation versus the ratio of diameter to stroke of the piston keeping the piston swept volume constant (presented inTable 3.5). It can be seen that both cooling power and COP increase in a wide dome-shaped trend with an increase in diameter to piston stroke. This phenomenon is mainly due to the variation

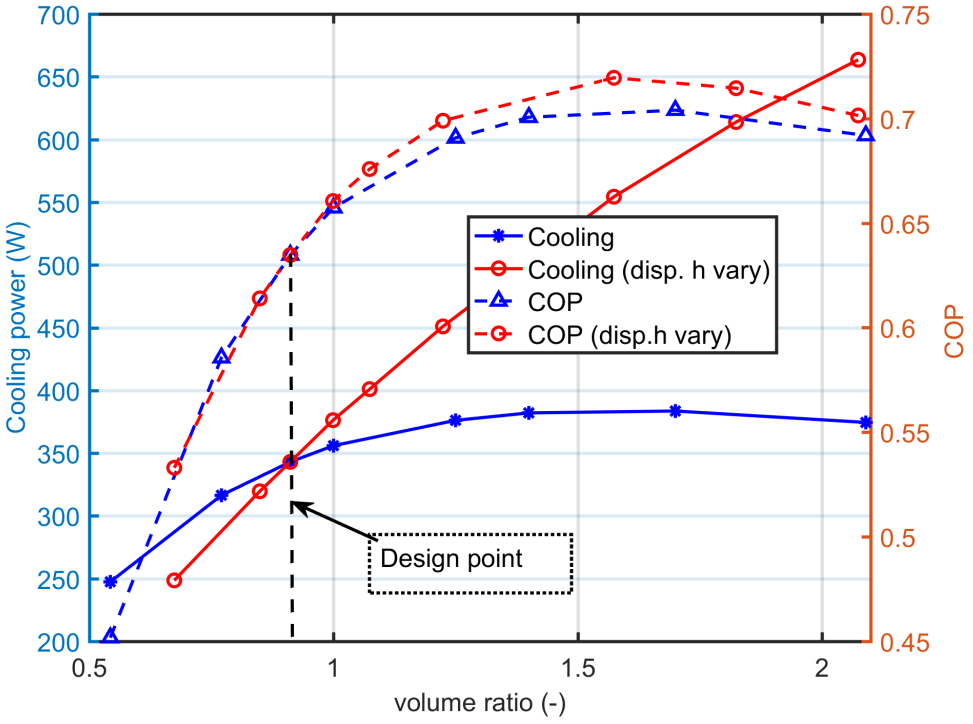

Figure 4.31: COP Comparison versus swept volume ratio for different cases of volume ratio.

of different power losses with the ratio as can be seen in Fig. 4.33. The effect of ratio of diameter to stroke of piston has been also investigated by [131]. It can be seen from Fig. 4.33a that the total power loss decreases mainly due to the decreasing of mechanical friction and piston finite speed losses as the stroke of piston decreases with an increase in ratio (d_P/s). On other hand, even though conduction heat loss increases, since shuttle heat losses decreases (see Fig. 4.33b) cooling production increases in a wider dome shape as the ratio (d_P/s) increases. Generally, the cooling production and COP increase by 17.3% and 32 % as the ratio (d_P/s) increases from 1.2 to 2.6.

4.6/ EFFECT OF COMBINED OPTIMIZED PARAMETERS

In the previous sections of this chapter, we use uni-variant analysis in which only one parameter is investigated while all other parameters are retained to pre-fixed values. This approach is simplistic and allows us to assess the most influential parameters. However, in only uni-variant optimization, it would be difficult to find the best combination of parameters for optimum machine performance. Hence, for the second-order numerical model, after investigating single parameter optimization, a trade-off between multiple conflicting parameters is indispensable.

Therefore, in this section, we try to investigate parameters with better performance as presented in sections 4.3 and 4.5, then combine them to find an optimized combination. Number of different combination of parameters which have positive impact on cooling performance have been first selected. These different combinations were simulated and lastly, a better combination of parameters has been proposed as presented in Table 4.2.

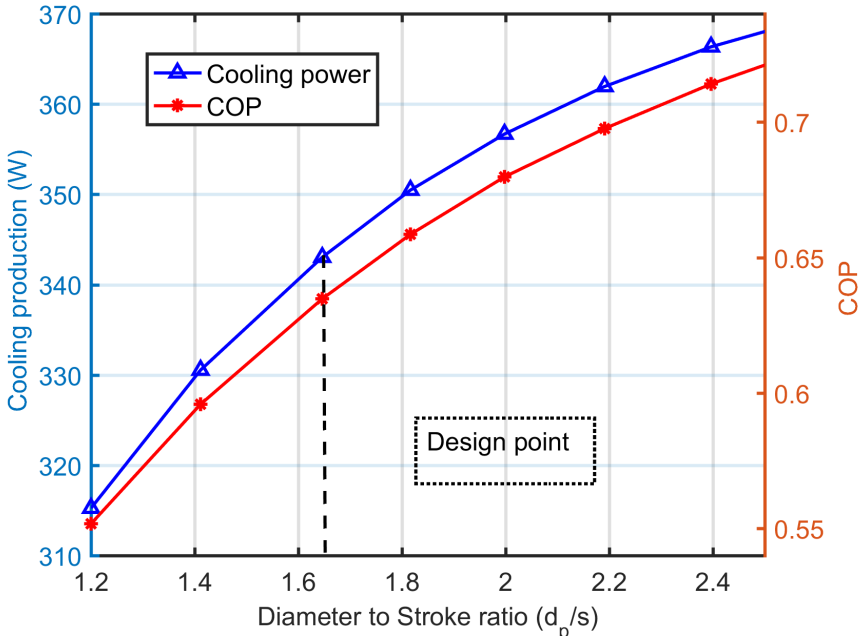

Figure 4.32: Cooling power and COP variation with ratio between diameter and stroke of piston.

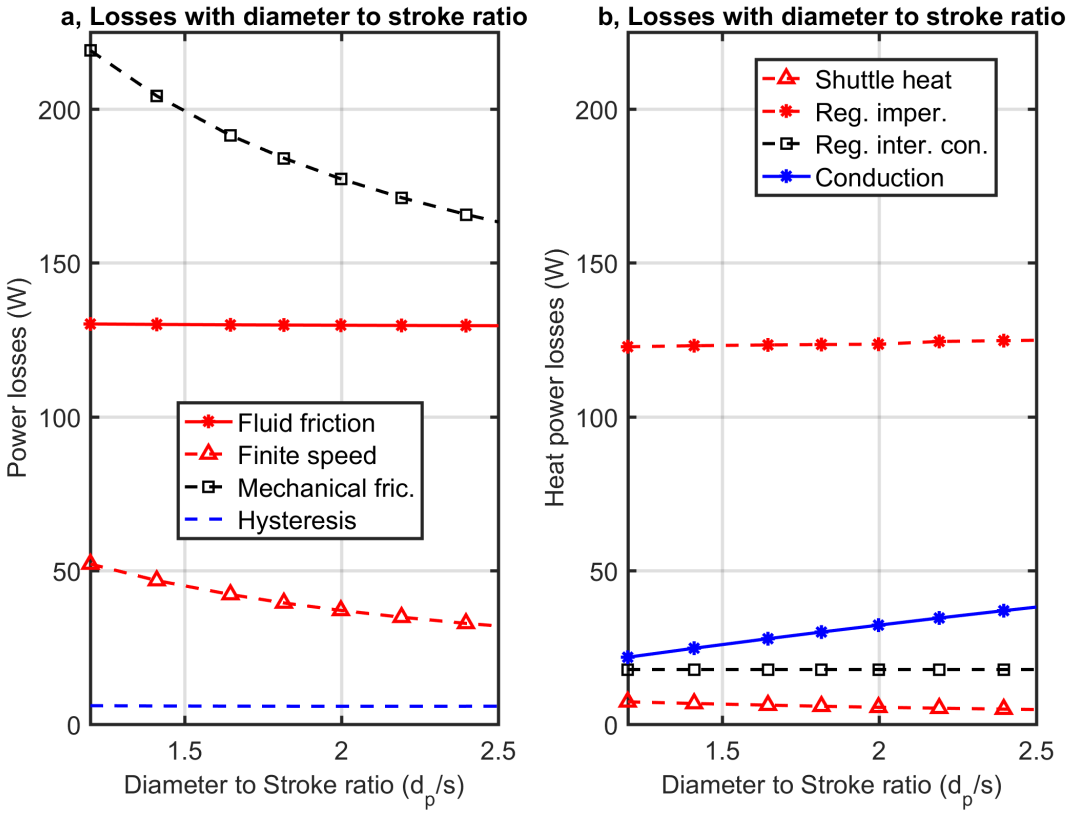

Figure 4.33: Power losses variation with the ratio between diameter and stroke of piston.

The differences in the combined optimized results as compared with the results of the existing design parameters have been demonstrated in Fig. 4.34. It could be seen that the performance of the Stirling refrigerator has been improved significantly with optimized parameters.

Specifications of Stirling machine for optimized analysis.			
No	*Parameters*	*Existing value*	*Optimized value*
1	Hot heat temperature (K)	305	
2	Cooling temperature (K)	270	
3	Piston diameter (mm)	60	62
4	Displacer diameter (mm)	59	61
5	Piston stroke (mm)	40	37
6	Regenerator length (mm)	50	40
7	Diameter of regenerator (mm)	82	
8	Regenerator wire made of	Stainless steel	
9	Wire diameter (μm)	112	
10	Porosity (%)	64	72
11	Compression space swept volume (cm^3)	103	140
12	Expansion space swept volume (cm^3)	113	
13	Compression dead volume (cm^3)	4.24	
14	Expansion dead volume (cm^3)	4.24	
15	Working gas	Nitrogen	
16	Frequency (Hz)	5-13	3-8
17	Charging pressure (bar)	15-20	20-25

Table 4.2: Specifications of Stirling machine for optimized analysis.

Regarding, operating parameter optimization, it can be seen from the optimized results presented in section 4.3 that relatively the lower operating frequency (3 to 8 Hz) at higher charging pressure are found to be the optimum operating parameters. But, due to the restricted operating conditions of the machine for safe working conditions and to minimize manufacturing cost, the average proposed operating frequency and charging pressure are set as 6 Hz and 22.5 bar, respectively.

The major design parameters considered for the analysis of combined parameters are regenerator length, porosity, displacer gap, swept volume ratio, and diameter to stroke ratio of the piston. It is found that all five optimized design parameters that are quite influential as individual parameters could enhance the COP of the refrigerator from 7% to 19% from the existing design value. Collectively, the optimized parameters (operating and specified design parameters) could deliver from 48% to 60 % more cold production and from 30% to 40% more COP than the existing design in a safe working condition.

At a proposed average pressure of 22.5 bar and average frequency of 6 Hz, using the optimized parameters it is possible to achieve COP of 1.3, cold production of 625 W at a temperature of -4^oC.

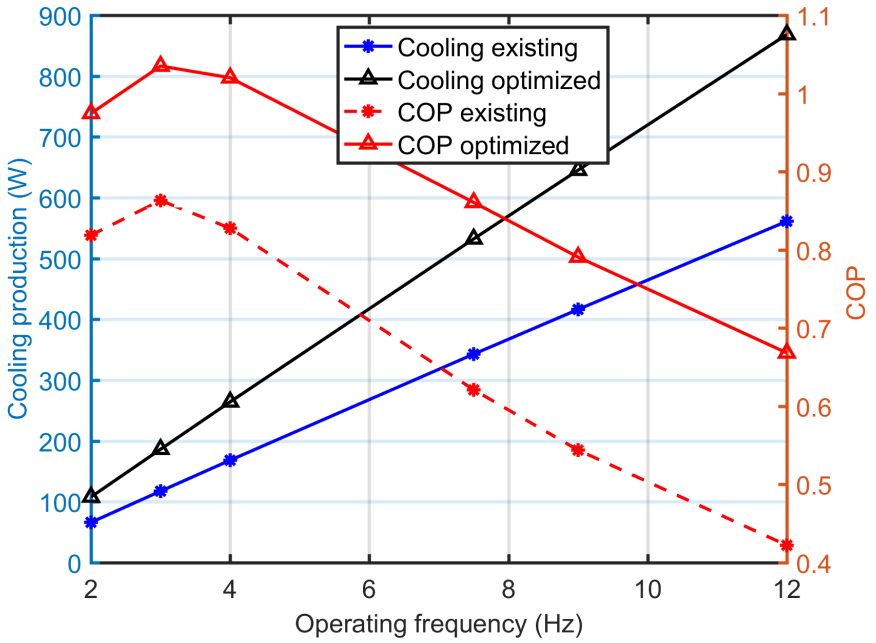

Figure 4.34: Comparison of results of existing and optimized cooling performance versus operating frequency.

4.7/ CONCLUSIONS

In this chapter, univariate analysis and optimization have been conducted to investigate the effect of parameters on the cooling performance of the Stirling refrigerator. The effects of different working fluids, shuttle heat losses, mass leakage, operating parameters (operating frequency, charging pressure, cold and hot temperature) and design parameters (phase angle between the oscillations of piston and displacer, length of the regenerator, porosity of regenerator, displacer height, displacer gap, piston-cylinder clearance gap, swept volume ratio, and piston diameter to stroke ratio) have been investigated. The effects of the inclusion of shuttle heat losses and mass leakage loss directly in the differential equations have been computed. The cold production and COP of the Stirling refrigerator have been computed for different working fluids. Input power requirement, cold production, COP, and the trends of major losses have been studied as a function of operating parameters. Moreover, the effects of operating frequency and charging pressure on the PV diagram of working spaces (compression and expansion) and pressure drops in heat exchangers have been investigated. The trend of cold production as well as COP of a refrigerating machine, are investigated as a function of design parameters. The analysis is conducted with the variation of a single parameter, keeping constant the other parameters at the design condition. Then, sets of analysis have been conducted using combination of optimized parameters. Finally, optimized parameters have been proposed. Some of the main results of this study are summarized below.

- To design Stirling machines, losses that a have direct effect on working condition of working fluid shall be directly incorporated with the differential equations. This is demonstrated with the analysis results of shuttle heat losses and mass leakages as independent losses as well as through direct incorporation in differential equations.

The result shows large variation in cooling performance.

- Air and nitrogen have resulted in better cooling performance as compared with helium and hydrogen for such domestic refrigeration within the range of analysis.
- The pressures in the compression volume remains unchanged and it reduced in expansion volume with an increase in operating frequency. These results in a decrease in cold production per cycle with an increase in operating frequency. However, as frequency increases the cycle per unit time increases and the total cold production increases.
- The cold production and input power requirement increase with the operating frequency. However, the increase in input power requirement accelerates at a higher rate at higher frequencies due to the increase in power losses especially fluid friction power losses, and hence COP decreases after some particular operating frequency. Then, COP has a maximum value as a function of operating frequency. On the other hand, COP increases with charging pressure. Furthermore, the higher the pressure, the lower the operating frequency in which the peak COP is found. This is because the rate of the increase of power losses especially fluid friction losses is higher at higher pressure.
- Cooling production has peak values at a single phase angle as a function of operating frequency. Whereas, the phase angle for the optimum COP increases slightly with an operating frequency. The point of optimum cooling performance as a function of phase angle is independent with type of working fluids.
- In optimizing the regenerator parameter, a relatively shorter regenerator gives an optimum cooling performance. The optimum regenerator length with the existing arrangement is found to be 25 mm as the peak values for both cold production and COP co-exist at this point. Cold production decreases and there exists a peak value of COP as porosity increases.
- Shorter displacers with relatively higher compression ratios show better performance for such types of domestic Stirling refrigerators as the swept volume compression volume increases.
- Cooling performance drops rapidly with an increase in clearance gap between piston and cylinder due to the increase in mass leakage loss.
- It could be seen from the optimized results presented in section 4.3 that relatively the lower operating frequency (3 to 8 Hz) at higher charging pressure are found to be the optimum operating parameters.
- Using combined parametric optimization, a higher performance Stirling refrigerator could bee designed. In this research, optimized design parameters that could enhance the overall performance of the existing machine from 30% to 60% are proposed. The optimized design for such domestic Stirling refrigeration could have a COP of 1.3 and cooling power of 625 W at a cooling temperature of -4^{o}C.

5

CONCLUSION AND PERSPECTIVES

5.1/ CONCLUSION

In recent decades, the demand for cooling systems has been increased for different applications including in domestic buildings, commercial halls, public spaces, transportation systems, manufacturing processes, and military affairs. This is due to the continuous increase in population and global warming mostly resulted from expansion of industrialization. Hence, alternative technologies with lower environmental impact have been demanded. Stirling cycle refrigerator for domestic cooling application is found to be a potential candidate to the current technology.

This study set out first to describe the overview of the Stirling refrigerating machine and its associated researches carried out in the area so far. A detailed review of literature has been conducted including configuration and drive mechanisms of the technology, thermodynamic modeling techniques developed so far, reviews of lower temperature cryocoolers as well as domestic Stirling refrigerators. The research gaps and potentials of development have been identified. From the review, it has been pointed out that Stirling refrigerator for domestic application is not well researched, it is still a potential area of further study as well as a promising technology. In the review, second order numerical model could be used for the design and optimization of Stirling machine with reasonable accuracy as well as with very less computational time. Furthermore, it could be easy to identify the type and effect of different losses so that further optimization will be easy through minimizing such major losses.

A key issue in the optimal designing of a Stirling machine is to develop a precise thermodynamic numerical model that could predict the performances and provide means for further optimization. In this paper, a non-ideal second-order numerical model called modified simple analysis model has been developed for the Stirling cycle refrigerating machine. The modified simple model constructed by directly incorporating the shuttle heat losses by displacer movement and mass leakage to the crankcase in the differential equations and treating other losses (imperfect regeneration loss, internal heat conduction loss in the regenerator, losses due to pressure drop in heat exchangers, heat conduction losses, gas spring hysteresis loss, mechanical friction loss, loss due to piston finite speed, and pumping loss) as independent losses. The classical fourth-order Runge Kutta method is applied to solve the system of the differential equations by taking the geometrical parameters and initial operating conditions of the machine as input parameters. Then, a MATLAB code is adapted to solve the system of these differential equations over consecutive cycles.

The results of numerical investigation have been compared in two ways to validate the model. First, it is validated with engine models by reversing the numerical model to the engine model and the parameters of the 3kW GPU-3 Stirling engine are used for validation. The simulation results of the reversed numerical model are compared with the previous theoretical research results as well as experimental results. Second, the simulation results of the numerical model (refrigeration) are compared with experimental results (refrigeration) conducted in the FEMTO-ST laboratory using the FEMTO-60 engine model in a cooling mode.

Finally, parametric optimizations have been conducted after validating the model to find the optimum combination of parameters. The study on parametric optimization contributes to the understanding of the effect of different operating and design parameters on power demand, cooling power, and COP as well as on the trend of major losses associated with the cooling machine. In this part, the effect of shuttle heat losses and mass leakage loss as well as effect of working fluid have been investigated with respect to operating parameters. The major optimized parameters were operating (operating frequency, charging pressure, hot and cold temperatures) and design (phase angle, regenerator porosity, regenerator length, displacer gap, displacer height, swept volume ratio, and diameter to stroke ratio of piston) parameters. Some of the main findings are summarized below

- The developed numerical model is for Beta type configuration. However the cooling capacity is related to compression ratio which is dependent on mechanical configuration. Then, the model could be extended to other mechanical drives by modifying the volume variation law, considering two cylinders instead of one for the mass leakage, shuttle heat losses, finite speed of piston, and gas spring hysteresis losses.

- The validation of the model confirm that the model could predict Stirling refrigeration machine with very good accuracy. Hence, the numerical model could be used for the design and optimization of such a machine.

- For low temperature differential with relatively lower charge pressure applications like domestic Stirling refrigerator, nitrogen or air could give better performance as compared with helium or hydrogen.

- As compared with other major losses (fluid friction losses, mechanical friction loss, regenerator imperfection loss), the amount of shuttle heat losses is very low. However, since shuttle heat losses have direct effect on the working condition of the working fluid, its effect on overall performance of the Stirling machine is very comparable with the effect of major losses. At a pressure of 17.5 bar and operating frequency of 7.5 Hz, shuttle heat decreases the cooling performance (cold production by more than 23% and COP by more than 19%). Hence, in designing the Stirling machine due attention shall be given for the reduction of shuttle heat losses.

- Fluid friction power losses and regenerator imperfection losses are the two major losses that are mostly affected by charging pressure and operating frequency. The shares of these two losses over their respective total losses increase with an increase in operating frequency as well as with charging pressure. Hence, exceptional attention shall be given to these types of losses particularly in designing higher operating frequency and higher charging pressure Stirling refrigerator.

- Even though, all power and heat losses have their own effect on cooling performance of the Stirling refrigerator, losses that have large share will have major impact. More importantly, the share of different power and heat losses depend on the operating conditions (operating frequency, charging pressure and temperature difference between heat source and heat sink) of the machine. Hence, designing Stirling machine shall consider the operating condition of the machine so as to give prior attention for the major losses.
- A cold production of 625 W and a COP of 1.3 have been found at a temperature of -4^{o}C using optimized parameters of Stirling refrigerator at a charging pressure of 22.5 bar and an operating frequency of 6 Hz. From such operating condition, the manufacturing cost of such machine could be reduced considerably as the operating condition do not need materials as that of the Stirling engine. Hence, it could be confirmed that domestic Stirling refrigerators can be a reliable alternative for the VCR in both cooling performance as well as cost of machine.
- Through the optimization of combined parameters, it is possible to enhance cold production from 48% to 60% and COP from 30% to 40% more from the existing design. This suggests that designing and optimization of Stirling machine for a particular application could increase the performance of the machine considerably.

5.2/ PERSPECTIVES

From the aforementioned discussions, it should be apparent that the performance of the Stirling refrigerator could be optimized through appropriate design consideration and optimization of parameters. This research has thrown up many questions in need of further investigation. To improve upon the operational performance of the Stirling refrigerator, the following recommendations are made for further research:

- Even though the choice of heat exchangers design and working volumes for Stirling machine depends on the application area, most researches that have done so far including this study particularly on moderate temperature Stirling cycle refrigerator are directly simulated and experimented by reversing the existing Stirling engine. In the Stirling engine, all the components are designed and manufactured to produce the maximum power output or efficiency. Such reversing a machine configuration may not produce the optimum cooling or COP. Furthermore, Stirling engines are designed for high temperature and high-pressure applications which demands high pressure and temperature resistant material for manufacturing. This increases the manufacturing cost of the machine. Whereas Stirling refrigerator relative demand ambient temperature and lesser operating pressure in which it may demand lesser manufacturing cost. Hence, future researches shall start with the design, production, and testing of the new Stirling cycle refrigerator.
- The regenerator is known to have a large share of fluid friction loss and regenerator imperfection loss. It has a higher impact on the cooling performance of the machine. Optimizing regenerator design will have a higher impact on improving the performance of the refrigerating machine. Hence, a wider variety of regenerator materials and configurations shall be tested and modeled for optimum refrigeration performance.

- The effect of variation of bounce space volume and other non optimized design parameters should be investigated.
- The effect of gas hysteresis loss on temperature and pressure of the working fluid as well as on the overall performance of the cooling machine has to be investigated through the inclusion of this loss directly in differential equations.
- The effect of drive mechanisms including Rhombic drive shall be studied and compared with the existing crank drive mechanism for cooling machine.

PUBLICATIONS

- **Journals (3)**

  1. **M. Z. Getie**, F. Lanzetta, S. Bégot, B. T. Admassu, A. A. Hassen. “Reversed regenerative Stirling cycle machine for refrigeration application: A review”. International Journal of Refrigeration. 118 (2020) 173–187.https://doi.org/10.1016/j.ijrefrig.2020.06.007.
  2. **M. Z. Getie**, F. Lanzetta, S. Bégot, B. T. Admassu, S. Djetel-Gothe. “A non-ideal second order thermal model with effects of losses for simulating Beta-type Stirling refrigerating machine”. International journal of refrigeration (2021).https://doi.org/10.1016/j.ijrefrig.2021.05.018.
  3. **M. Z. Getie**, F. Lanzetta, S. Bégot, B. T. Admassu. “Loss effect Analysis of irreversible Stirling cycle Refrigerator”. Submitted to Entropie (under review).

- **Conferences (4)**

  1. **M. Getie**, F. Lanzetta, S. Bégot, B. Admassu, S. Djetel-Gothe. “Optimization of a regenerative Stirling machine for moderate refrigeration”. 27th Congrès Français de Thermique (France, Nantes, 3 – 6 June 2019. work in progress).
  2. **M. Z. Getie**, F. Lanzetta, S. Bégot, B. T. Admassu, S. Djetel-Gothe. “Simulation and parametric study on a Beta-type Stirling refrigerating machine”. 28th Congrès Français de Thermique (France, Belfort, 9-12 June 2020). https://doi.org/10.25855/SFT2020-070.
  3. **M. Z. Getie**, F. Lanzetta, S. Bégot, B. T. Admassu, S. Djetel-Gothe. “Performance analysis of Beta-type Stirling cycle refrigerator for different working fluids”. 8th EAI International Conference on Advancements of Science and Technology (Ethiopia, Bahir Dar, 02-04 October, 2020).
  4. **M.Z. Getie**, F. Lanzetta, S. Bégot, B. T. Admassu. “Loss effect Analysis of irreversible Stirling cycle Refrigerator”. 29th Congrès Français de Thermique (France, Belfort, 1-3 June ,2021). https://doi.org/10.25855/SFT2021-035.

BIBLIOGRAPHY

[1] KIRK, A. C. **On the mechanical production of cold.(includes plates and appendix).** 244–282.

[2] KÖHLER, J., AND JONKERS, C. **Fundamentals of the gas refrigeration machine**. *Philips Tech. Rev 16*, 3 (1954), 69–78.

[3] FINKELSTEIN, T. **Generalized thermodynamic analysis of Stirling engines**. Tech. rep., SAE Technical Paper, 1960.

[4] KIRKLEY, D. **Determination of the optimum configuration for a Stirling engine**. *Journal of Mechanical Engineering Science 4*, 3 (1962), 204–212.

[5] GIFFORD, W. E., AND LONGSWORTH, R. **Pulse-tube refrigeration**. *Journal of Engineering for Industry 86*, 3 (1964), 264–268.

[6] KOHLER, J. W. **The Stirling refrigeration cycle in cryogenic technology**. *The Advancement of Science 25* (1968), 261.

[7] BEALE, W. T. **Free piston Stirling engines-some model tests and simulations**. Tech. rep., SAE Technical Paper 690230, 1969.

[8] BEALE, W. T. **Stirling cycle type thermal device**, Jan. 5 1971. US Patent 3,552,120.

[9] HORN, S., AND WALTERS, B. **Split cycle cryogenic cooler with rotary compressor**, Dec. 10 1974. US Patent 3,853,437.

[10] HAARHUIS, G. **The mc 80-a magnetically driven Stirling refrigerator**. *Cryogenics 18*, 12 (1978), 656–658.

[11] MARTINI, W. R. **Stirling engine design manual**. US Department of Energy, Office of Conservation and Solar Applications, Division of Transportation Energy Conservation, 1978.

[12] THIEME, L. G. **Low-power baseline test results for the GPU 3 Stirling engine**. NASA TM-79103, 1979.

[13] WALKER, G. **Stirling engines**. Oxford University Press, New York, NY, 1980.

[14] ACKERMANN, R. **Dynamic analysis of a small free-piston resonant cryorefrigerator**. In *Refrigeration for Cryogenic Sensors and Electronic Systems: Proceedings of a Conference Held at the National Bureau of Standards, Boulder CO, October 6-7, 1980* (1981), vol. 607, US Department of Commerce, National Bureau of Standards, p. 57.

[15] GOSNEY, W. B. **Principles of refrigeration**. Tech. rep., Cambridge (UK) Cambridge Univ. Press, 1982.

[16] CHEN, N., AND GRIFFIN, F. **Review of Stirling-engine mathematical models**. Tech. rep., Oak Ridge National Lab., TN (USA), 1983.

[17] MARTINI, W. **Stirling engine design manual second edition**. *Technical report, NASA CR 168088* (1983).

[18] READER, G. T., AND HOOPER, C. **Stirling engines**. E. and F. Spon, New York, NY, USA, 1983.

[19] MIKULIN, E., TARASOV, A., AND SHKREBYONOCK, M. **Low-temperature expansion pulse tubes**. In *Advances in cryogenic engineering*. Springer, 1984, pp. 629–637.

[20] URIELI, I., AND BERCHOWITZ, D. M. **Stirling cycle engine analysis**. A. Hilger Bristol, 1984.

[21] RADEBAUGH, R., ZIMMERMAN, J., SMITH, D. R., AND LOUIE, B. **A comparison of three types of pulse tube refrigerators: new methods for reaching 60k**. In *Advances in Cryogenic Engineering*. Springer, 1986, pp. 779–789.

[22] WALKER, G., WEISS, M., FAUVEL, R., AND READER, G. **Microcomputer simulation of Stirling cryocoolers**. *Cryogenics 29*, 8 (1989), 846–849.

[23] ATREY, M., BAPAT, S., AND NARAYANKHEDKAR, K. **Cyclic simulation of Stirling cryocoolers**. *Cryogenics 30*, 4 (1990), 341–347.

[24] SHAOWEI, Z., PEIYI, W., AND ZHONGQI, C. **Double inlet pulse tube refrigerators: an important improvement**. *Cryogenics 30*, 6 (1990), 514–520.

[25] FABIEN, M. **Evaluation of the free-piston Stirling cycle for domestic cooling applications**. *Int. Congr. of Refrig. Montreal, Quebec, Canada* (1991).

[26] BERCHOWITZ, D. **Free-piston Stirling coolers**. In *International Refrigeration and Air Conditioning Conference* (1992), Purdue University Purdue e-Pubs, pp. 326–336.

[27] TOMINAGA, A. **Phase controls for pulse-tube refrigerator of the third generation**. *TEION KOGAKU (Journal of Cryogenics and Superconductivity Society of Japan) 27*, 2 (1992), 146–151.

[28] BERCHOWITZ, D. M. **Free-piston Rankine compression and Stirling cycle machines for domestic refrigeration**. In *Greenpeace Ozon Safe Conference, Washington, DC* (1993).

[29] GAUGER, D. C. **Alternative technologies for refrigeration and air conditioning applications**. PhD thesis, Digital Repository @ Iowa State University, http://lib.dr.iastate.edu/rtd/10818, 1993.

[30] J., M. R., AND C., M. E. **Stm4-120rf as refrigerator for supermarket**. In *Refrigeration and air conditioning technology workshop* (1993).

[31] BAUWENS, L. **Adiabatic losses in Stirling cryocoolers: a stratified flow model**. *Cryogenics 34*, 8 (1994), 627–633.

[32] SWIFT, G. W. **Thermoacoustic engines and refrigerators**. *Physics today 48*, 7 (1995).

[33] BERCHOWITZ, D. M. **Stirling coolers for solar refrigerators**. In *International Appliance Technical Conference, West Lafayette, US* (1996).

[34] CHEN, J., AND YAN, Z. **The general performance characteristics of a Stirling refrigerator with regenerative losses**. *Journal of Physics D: Applied Physics 29*, 4 (1996), 987.

[35] GEDEON, D., AND WOOD, J. **Oscillating-flow regenerator test rig: hardware and theory with derived correlations for screens and felts**. Tech. rep., NASA Contractor Report 198442, 1996.

[36] CHEN, J. **Minimum power input of irreversible Stirling refrigerator for given cooling rate**. *Energy Conversion and Management 39*, 12 (1998), 1255–1263.

[37] CHEN, L., WU, C., AND SUN, F. **Cooling load versus COP characteristics for an irreversible air refrigeration cycle**. *Energy Conversion and Management 39*, 1-2 (1998), 117–125.

[38] COSTEA, M., PETRESCU, S., AND HARMAN, C. **The effect of irreversibilities on solar Stirling engine cycle performance**. *Energy Conversion and Management 40*, 15-16 (1999), 1723–1731.

[39] OGUZ, E., AND OZKADI, F. **An experimental study on the refrigeration capacity and thermal performance of free piston Stirling coolers**. In *International Refrigeration and Air Conditioning Conference* (2000), Purdue University, West Lafayette, IN, USA, pp. 496–504.

[40] RADEBAUGH, R. **Development of the pulse tube refrigerator as an efficient and reliable cryocooler**. *Proc. institute of refrigeration, London* (2000).

[41] CUN-QUAN, Z., YI-NONG, W., GUO-LIN, J., DONG-YU, L., AND LIE, X. **Dynamic simulation of one-stage oxford split-Stirling cryocooler and comparison with experiment**. *Cryogenics 42*, 9 (2002), 577–585.

[42] HAYWOOD, D., RAINE, J., AND GSCHWENDTNER, M. **Stirling-cycle heat-pumps and refrigerators–a realistic alternative?** Tech. rep., Institute of Refrigeration, Heating & Air Conditioning Engineers (IRHACE), 2002.

[43] KIRKCONNELL, C. **Experimental investigation of a unique pulse tube expander design**. In *Cryocoolers 10*. Springer, 2002, pp. 239–247.

[44] OTAKA, T., OTA, M., MURAKAMI, K., AND SAKAMOTO, M. **Study of performance characteristics of a small Stirling refrigerator**. *Heat Transfer—Asian Research 31*, 5 (2002), 344–361.

[45] PARK, S., HONG, Y., KIM, H., KOH, D., KIM, J., YU, B., AND LEE, K. **The effect of operating parameters in the Stirling cryocooler**. *Cryogenics 42*, 6-7 (2002), 419–425.

[46] TYAGI, S., KAUSHIK, S., AND SINGHAL, M. **Parametric study of irreversible Stirling and Ericsson cryogenic refrigeration cycles**. *Energy Conversion and Management 43*, 17 (2002), 2297–2309.

[47] HONG, Y., PARK, S., KIM, H., AND KOH, D. **Dynamic analysis of a free piston Stirling refrigerator**. In *Cryocoolers 12*. Springer, 2003, pp. 103–108.

[48] PARK, S., HONG, Y., KIM, H., AND LEE, K. **An experimental study on the phase shift between piston and displacer in the Stirling cryocooler**. *Current Applied Physics 3*, 5 (2003), 449–455.

[49] DYSON, R., WILSON, S., AND TEW, R. **Review of computational Stirling analysis methods**. In *2nd International Energy Conversion Engineering Conference* (2004).

[50] GROMOLL, B. **Technical and economical demands on 25k–77Krefrigerators for future hts—series products in power engineering**. In *AIP Conference Proceedings* (2004), vol. 710, AIP, pp. 1797–1804.

[51] NARASAKI, K., TSUNEMATSU, S., OOTSUKA, K., KYOYA, M., MATSUMOTO, T., MURAKAMI, H., AND NAKAGAWA, T. **Development of two-stage Stirling cooler for astro-f**. In *AIP Conference Proceedings* (2004), vol. 710, AIP, pp. 1428–1435.

[52] TWARD, E., NGUYEN, T., GODDEN, J., AND TOMA, G. **Miniature pulse tube cooler**. In *AIP Conference Proceedings* (2004), vol. 710, AIP, pp. 1326–1329.

[53] TYAGI, S., LIN, G., KAUSHIK, S., AND CHEN, J. **Thermoeconomic optimization of an irreversible Stirling cryogenic refrigerator cycle**. *International journal of refrigeration 27*, 8 (2004), 924–931.

[54] ZHU, S., AND MATSUBARA, Y. **Numerical method of inertance tube pulse tube refrigerator**. *Cryogenics 44*, 9 (2004), 649–660.

[55] ATAER, Ö. E., AND KARABULUT, H. **Thermodynamic analysis of the V-type Stirling-cycle refrigerator**. *International Journal of Refrigeration 28*, 2 (2005), 183–189.

[56] YUAN, J., AND MAGUIRE, J. **Development of a single stage pulse tube refrigerator with linear compressor**. In *Cryocoolers 13*. Springer, 2005, pp. 157–163.

[57] ZIA, J. **A commercial pulse tube cryocooler with 200 Wrefrigeration at 80 k**. In *Cryocoolers 13*. Springer, 2005, pp. 165–171.

[58] ANDERSEN, S. K. **Numerical simulation of cyclic thermodynamic processes**. Technical University of Denmark, Department of Mechanical Engineering, 2006.

[59] POTRATZ, S., NELLIS, G., MADDOCKS, J., KASHANI, A., HELVENSTEIJN, B., RHOADS, G., AND FLAKE, B. **Development of a large-capacity, Stirling-type, pulse-tube refrigerator**. In *AIP Conference Proceedings* (2006), vol. 823, AIP, pp. 3–10.

[60] ROSS JR, R. G., AND BOYLE, R. F. **An overview of NASA space cryocooler programs**. In *International Cryocooler Conference, Inc., Boulder, CO* (2006).

[61] DIETRICH, M., YANG, L., AND THUMMES, G. **High-power Stirling-type pulse tube cryocooler: Observation and reduction of regenerator temperature-inhomogeneities**. *Cryogenics 47*, 5-6 (2007), 306–314.

[62] HUANG, T., CAUGHLEY, A., YOUNG, R., AND CHAMRITSKI, V. **CFD simulation and experimental validation of a diaphragm pressure wave generator**. In *International Cryocooler Conference, Inc., CO* (2008).

[63] LADNER, D. **Performance and mass vs. operating temperature for pulse tube and Stirling cryocoolers**. Georgia Institute of Technology.

[64] TIMOUMI, Y., TLILI, I., AND NASRALLAH, S. B. **Design and performance optimization of GPU-3 Stirling engines**. *Energy 33*, 7 (2008), 1100–1114.

[65] TLILI, I., TIMOUMI, Y., AND NASRALLAH, S. B. **Analysis and design consideration of mean temperature differential Stirling engine for solar application**. *Renewable Energy 33*, 8 (2008), 1911–1921.

[66] TLILI, I., TIMOUMI, Y., AND NASRALLAH, S. B. **Analysis and design consideration of mean temperature differential Stirling engine for solar application**. *Renewable Energy 33*, 8 (2008), 1911–1921.

[67] TLILI, I., TIMOUMI, Y., AND NASRALLAH, S. B. **Thermodynamic analysis of the Stirling heat engine with regenerative losses and internal irreversibilities**. *International Journal of Engine Research 9*, 1 (2008), 45–56.

[68] CHEN, X., WU, Y. N., ZHANG, H., AND CHEN, N. **Study on the phase shift characteristic of the pneumatic Stirling cryocooler**. *Cryogenics 49*, 3-4 (2009), 120–132.

[69] HIRAI, H., SUZUKI, Y., HIROKAWA, M., KOBAYASHI, H., KAMIOKA, Y., IWAKUMA, M., AND SHIOHARA, Y. **Development of a turbine cryocooler for high temperature superconductor applications**. *Physica C: Superconductivity 469*, 15-20 (2009), 1857–1861.

[70] LE'AN, S., YUANYANG, Z., LIANSHENG, L., AND PENGCHENG, S. **Performance of a prototype Stirling domestic refrigerator**. *Applied Thermal Engineering 29*, 2-3 (2009), 210–215.

[71] NIE, W., HE, J., AND DU, J. **Performance characteristic of a Stirling refrigeration cycle in micro/nano scale**. *Physica A: Statistical Mechanics and its Applications 388*, 4 (2009), 318–324.

[72] RADEBAUGH, R. **Cryocoolers: the state of the art and recent developments**. *Journal of Physics: Condensed Matter 21*, 16 (2009), 164219.

[73] FORMOSA, F., AND DESPESSE, G. **Analytical model for Stirling cycle machine design**. *Energy Conversion and Management 51*, 10 (2010), 1855–1863.

[74] RADEBAUGH, R., AND GULLY, W. **Foundation of cryocoolers short course**. In *International cryocooler conference* (2010), vol. 16.

[75] RAZANI, A., DODSON, C., AND ROBERTS, T. **A model for exergy analysis and thermodynamic bounds of Stirling refrigerators**. *Cryogenics 50*, 4 (2010), 231–238.

[76] STRAUSS, J. M., AND DOBSON, R. T. **Evaluation of a second order simulation for Stirling engine design and optimisation**. *Journal of Energy in Southern Africa 21*, 2 (2010), 17–29.

[77] TEKIN, Y., AND ATAER, O. E. **Performance of V-type Stirling-cycle refrigerator for different working fluids**. *International Journal of Refrigeration 33*, 1 (2010), 12–18.

[78] YANG, L., XUN, Y., THUMMES, G., AND LIANG, J. **Single-stage high frequency coaxial pulse tube cryocooler with base temperature below 30 K**. *Cryogenics 50*, 5 (2010), 342–346.

[79] ZHU, S., AND NOGAWA, M. **Pulse tube Stirling machine with warm gas-driven displacer**. *Cryogenics 50*, 5 (2010), 320–330.

[80] CHENG, C.-H., AND YU, Y.-J. **Dynamic simulation of a Beta-type Stirling engine with cam-drive mechanism via the combination of the thermodynamic and dynamic models**. *Renewable energy 36*, 2 (2011), 714–725.

[81] DE BOER, P. **Optimal performance of regenerative cryocoolers**. *Cryogenics 51*, 2 (2011), 105–113.

[82] PETRESCU, S., COSTEA, M., PETRESCU, V., MALANCIOIU, O., BORIARU, N., STANCIU, C., BANCHES, E., DOBRE, C., MARIS, V., AND LEONTIEV, C. **Development of thermodynamics with finite speed and direct method**. *AGIR Bucharest 362* (2011).

[83] ASNAGHI, A., LADJEVARDI, S., SALEH IZADKHAST, P., AND KASHANI, A. **Thermodynamics performance analysis of solar Stirling engines**. *International Scholarly Research Notices 2012* (2012).

[84] CHEN, L., JIN, H., WANG, J., ZHOU, Y., ZHU, W., AND ZHOU, Q. **18.6 K single-stage high frequency multi-bypass coaxial pulse tube cryocooler**. *Cryogenics 54* (2013), 54–58.

[85] CHEN, L., ZHOU, Q., JIN, H., ZHU, W., WANG, J., AND ZHOU, Y. **386 mw/20 K single-stage Stirling-type pulse tube cryocooler**. *Cryogenics 57* (2013), 195–199.

[86] JAFARI, S., MOHAMMADI, B., AND BOROUJERDI, A. **Multi-objective optimization of a Stirling-type pulse tube refrigerator**. *Cryogenics 55* (2013), 53–62.

[87] AHMADI, M. H., AHMADI, M. A., MOHAMMADI, A. H., FEIDT, M., AND POURKIAEI, S. M. **Multi-objective optimization of an irreversible Stirling cryogenic refrigerator cycle**. *Energy Conversion and Management 82* (2014), 351–360.

[88] AHMADI, M. H., AHMADI, M.-A., MOHAMMADI, A. H., MEHRPOOYA, M., AND FEIDT, M. **Thermodynamic optimization of Stirling heat pump based on multiple criteria**. *Energy Conversion and Management 80* (2014), 319–328.

[89] BABAELAHI, M., AND SAYYAADI, H. **Simple-II: a new numerical thermal model for predicting thermal performance of Stirling engines**. *Energy 69* (2014), 873–890.

[90] GRAZZINI, G., AND ROCCHETTI, A. **Thermodynamic optimization of irreversible refrigerators**. *Energy Conversion and Management 84* (2014), 583–588.

[91] He, Y.-L., Zhang, D.-W., Yang, W.-W., and Gao, F. **Numerical analysis on performance and contaminated failures of the miniature split Stirling cryocooler**. *Cryogenics 59* (2014), 12–22.

[92] Hu, J., Zhang, L., Zhu, J., Chen, S., Luo, E., Dai, W., and Li, H. **A high-efficiency coaxial pulse tube cryocooler with 500 w cooling capacity at 80 K**. *Cryogenics 62* (2014), 7–10.

[93] Mahmoodi, M., Pirkandi, J., and Alipour, A. **Numerical simulation of Beta type Stirling engine considering heat and power losses**. *Iranian Journal of Mechanical Engineering Vol 15*, 2 (2014), 5–27.

[94] McFarlane, P. K. **Mathematical model and experimental design of an air-filled Alpha Stirling refrigerator**.

[95] Penswick, L., Olan, R. W., Williford, I., Draney, S., and Buchholz, G. **High-capacity and efficiency Stirling cycle cryocooler**. *International Cryocooler Conference, Inc., Boulder, CO* (2014), 155–162.

[96] Toghyani, S., Kasaeian, A., and Ahmadi, M. H. **Multi-objective optimization of Stirling engine using non-ideal adiabatic method**. *Energy Conversion and Management 80* (2014), 54–62.

[97] Xiang, B., Patra, P. K., Montzka, S. A., Miller, S. M., Elkins, J. W., Moore, F. L., Atlas, E. L., Miller, B. R., Weiss, R. F., Prinn, R. G., and others. **Global emissions of refrigerants HCFC-22 and HFC-134a: Unforeseen seasonal contributions**. *Proceedings of the National Academy of Sciences 111*, 49 (2014), 17379–17384.

[98] Xu, Y., Cai, Y., Sun, D., Shen, Q., Zhao, X., Zhang, J., and Cheng, Z. **Study on a high-power Stirling cryocooler**. In *International Cryocooler Conference* (2014), vol. 18.

[99] Yu, G., Dai, W., Qiu, J., Zhang, L., Li, X., Liu, B., Wu, Z., Xu, J., Luo, E., and Li, H. **Initial test of a Stirling cryocooler with a high cooling capacity**. In *International Cryocooler Conference* (2014), vol. 18, pp. 169–175.

[100] Ahmadi, M. H., Ahmadi, M. A., Bayat, R., Ashouri, M., and Feidt, M. **Thermo-economic optimization of Stirling heat pump by using non-dominated sorting genetic algorithm**. *Energy Conversion and Management 91* (2015), 315–322.

[101] Babaelahi, M., and Sayyaadi, H. **Modified PSVL: a second order model for thermal simulation of Stirling engines based on convective–polytropic heat transfer of working spaces**. *Applied Thermal Engineering 85* (2015), 340–355.

[102] Babaelahi, M., and Sayyaadi, H. **A new thermal model based on polytropic numerical simulation of Stirling engines**. *Applied Energy 141* (2015), 143–159.

[103] Boroujerdi, A., and Esmaeili, M. **Characterization of the frictional losses and heat transfer of oscillatory viscous flow through wire-mesh regenerators**. *Alexandria Engineering Journal 54*, 4 (2015), 787–794.

[104] Duband, L. **Space cryocooler developments**. *Physics Procedia 67* (2015), 1–10.

[105] HACHEM, H., GHEITH, R., NASRALLAH, S. B., AND ALOUI, F. **Impact of operating parameters on Beta type regenerative Stirling machine performances**. In *ASME/JSME/KSME 2015 Joint Fluids Engineering Conference* (2015), American Society of Mechanical Engineers, pp. V001T22A002–V001T22A002.

[106] HOSSEINZADE, H., AND SAYYAADI, H. **CAFS: The Combined Adiabatic–Finite Speed thermal model for simulation and optimization of Stirling engines**. *Energy Conversion and Management 91* (2015), 32–53.

[107] HOSSEINZADE, H., SAYYAADI, H., AND BABAELAHI, M. **A new closed-form analytical thermal model for simulating Stirling engines based on polytropic-finite speed thermodynamics**. *Energy Conversion and Management 90* (2015), 395–408.

[108] MABROUK, M. T., KHEIRI, A., AND FEIDT, M. **Effect of leakage losses on the performance of a {*Beta* type Stirling engine**. *Energy 88* (2015), 111–117.

[109] RAMOS, J. A. A. **Thermodynamic Analysis of Stirling Engine Systems: Applications for Combined Heat and Power**. PhD thesis, KTH School of Industrial Engineering and Management,Stockholm, 2015.

[110] WANG, X., DAI, W., ZHU, J., CHEN, S., LI, H., AND LUO, E. **Design of a two-stage high-capacity Stirling cryocooler operating below 30k**. *Physics Procedia 67* (2015), 518–523.

[111] ZHOU, Q., CHEN, L., ZHU, X., ZHU, W., ZHOU, Y., AND WANG, J. **Development of a high-frequency coaxial multi-bypass pulse tube refrigerator below 14 K**. *Cryogenics 67* (2015), 28–30.

[112] BABAELAHI, M., AND SAYYAADI, H. **Analytical closed-form model for predicting the power and efficiency of Stirling engines based on a comprehensive numerical model and the genetic programming**. *Energy 98* (2016), 324–339.

[113] CAUGHLEY, A., SELLIER, M., GSCHWENDTNER, M., AND TUCKER, A. **CFD analysis of a diaphragm free-piston Stirling cryocooler**. *Cryogenics 79* (2016), 7–16.

[114] CAUGHLEY, A., SELLIER, M., GSCHWENDTNER, M., AND TUCKER, A. **A free-piston Stirling cryocooler using metal diaphragms**. *Cryogenics 80* (2016), 8–16.

[115] CHAUDHARI, P., D'SOUZA, D., BORKAR, S., HARIBHAKTA, V., AND TRIMBAKE, S. **Mathematical formulation of free piston Stirling cooler for domestic refrigeration using loss factor**. *International Journal of Scientific & Engineering Research 7* (2016), 1505–1510.

[116] DANG, H., ZHANG, L., AND TAN, J. **Dynamic and thermodynamic characteristics of the moving-coil linear compressor for the pulse tube cryocooler. part a: Theoretical analyses and modeling**. *International Journal of Refrigeration 69* (2016), 480–496.

[117] DANG, H., ZHANG, L., AND TAN, J. **Dynamic and thermodynamic characteristics of the moving-coil linear compressor for the pulse tube cryocooler: Part b–experimental verifications**. *International Journal of Refrigeration 69* (2016), 497–504.

[118] GOETZLER, W., GUERNSEY, M., YOUNG, J., FUJRMAN, J., AND ABDELAZIZ, A. **The future of air conditioning for buildings**. Tech. rep., Navigant Consulting, Burlington, MA (United States), 2016.

[119] HU, J., CHEN, S., ZHU, J., ZHANG, L., LUO, E., DAI, W., AND LI, H. **An efficient pulse tube cryocooler for boil-off gas reliquefaction in liquid natural gas tanks**. *Applied energy 164* (2016), 1012–1018.

[120] JAN, W., AND MAREK, P. **Mathematical modeling of the Stirling engine**. *Procedia Engineering 157* (2016), 349–356.

[121] KHIRZADA, H. **Optimisation et caractérisation d'un moteur Stirling de faible puissance pour la génération électrique**. PhD thesis, Université Bourgogne de Franche-Comté, 2016.

[122] UNEP. **Further amendment of the montreal protocol: Submitted by the contact group on hfcs, twenty-eighth meeting of the parties to the montreal protocol on substances that deplete the ozone layer**. Tech. rep., United Nations Environment Programme (UNEP), 10–14 October 2016, Kigali, Rwanda, UNEP/OzL.Pro.28/CRP/10, 2016.

[123] URIELI, I. **Stirling cycle machine analysis**, 2016.

[124] WANG, K., DUBEY, S., CHOO, F. H., AND DUAN, F. **Modelling of pulse tube refrigerators with inertance tube and mass-spring feedback mechanism**. *Applied energy 171* (2016), 172–183.

[125] WANG, K., SANDERS, S. R., DUBEY, S., CHOO, F. H., AND DUAN, F. **Stirling cycle engines for recovering low and moderate temperature heat: A review**. *Renewable and Sustainable Energy Reviews 62* (2016), 89–108.

[126] WANG, X., ZHU, J., CHEN, S., DAI, W., LI, K., PANG, X., YU, G., AND LUO, E. **Study on a high capacity two-stage free piston Stirling cryocooler working around 30 k**. *Cryogenics 80* (2016), 193–198.

[127] ZHAO, Y., AND DANG, H. **CFD simulation of a miniature coaxial Stirling-type pulse tube cryocooler operating at 128 Hz**. *Cryogenics 73* (2016), 53–59.

[128] AHMADI, M. H., AHMADI, M.-A., AND POURFAYAZ, F. **Thermal models for analysis of performance of Stirling engine: A review**. *Renewable and Sustainable Energy Reviews 68* (2017), 168–184.

[129] AHMED, H., ALMAJRI, A. K., MAHMOUD, S., AL-DADAH, R., AND AHMAD, A. **CFD modelling and parametric study of small scale Alpha type Stirling cryocooler**. *Energy Procedia 142* (2017), 1668–1673.

[130] HACHEM, H., GHEITH, R., ALOUI, F., AND NASRALLAH, S. B. **Optimization of an air-filled Beta type Stirling refrigerator**. *International Journal of Refrigeration 76* (2017), 296–312.

[131] LI, R. **Applications of Stirling engine in sustainable development: context-experimental and numerical study**. PhD thesis, Université Paris Nanterre 10, 2017.

[132] LI, R., AND GROSU, L. **Parameter effect analysis for a Stirling cryocooler**. *International Journal of Refrigeration 80* (2017), 92–105.

[133] MUNGAN, C. E. **Coefficient of performance of Stirling refrigerators**. *European Journal of Physics 38*, 5 (2017), 055101.

[134] NARENDRA N WADASKAR AND, D. S., AND R.D.ASKHEDKAR, D. **Analysis of coefficient of performance & heat transfer coefficient on Stirling cycle refrigeration system**. *Int. Journal of Engineering Research and Application www.ijera.com 7*, 8 (2017), 78–85.

[135] ROUT, S. K., BEHURA, A. K., DALAI, S., AND SAHOO, R. K. **Numerical analysis of a modified type pulse tube refrigerator**. *Energy Procedia 109* (2017), 456–462.

[136] SAUER, J., AND KUEHL, H.-D. **Numerical model for Stirling cycle machines including a differential simulation of the appendix gap**. *Applied Thermal Engineering 111* (2017), 819–833.

[137] SHENDAGE, D., KEDARE, S., AND BAPAT, S. **Cyclic analysis and optimization of design parameters for Beta-configuration Stirling engine using rhombic drive**. *Applied Thermal Engineering 124* (2017), 595–615.

[138] TANG, K., FENG, Y., JIN, T., JIN, S., AND YANG, R. **Impact of gedeon streaming on the efficiency of a double-inlet pulse tube refrigerator**. *Applied Thermal Engineering 111* (2017), 445–454.

[139] WILLS, J. A. **Exergy analysis of a Stirling cycle**. PhD thesis, University of Cape Town, 2017.

[140] XU, Y., SUN, D., QIAO, X., YAN, S., ZHANG, N., ZHANG, J., AND CAI, Y. **Operating characteristics of a single-stage Stirling cryocooler capable of providing 700 Wcooling power at 77 k**. *Cryogenics 83* (2017), 78–84.

[141] BATOOEI, A., AND KESHAVARZ, A. **A Gamma type Stirling refrigerator optimization: An experimental and analytical investigation**. *International Journal of Refrigeration* (2018).

[142] CHEN, L., WU, X., WANG, J., LIU, X., PAN, C., JIN, H., CUI, W., ZHOU, Y., AND WANG, J. **Study on a high frequency pulse tube cryocooler capable of achieving temperatures below 4 Kby helium-4**. *Cryogenics 94* (2018), 103–109.

[143] DING, G., CHEN, W., ZHENG, T., LI, Y., AND JI, Y. **Volume ratio optimization of Stirling engine by using an enhanced model**. *Applied Thermal Engineering 140* (2018), 615–621.

[144] EGAS, J., AND CLUCAS, D. M. **Stirling engine configuration selection**. *Energies 11*, 3 (2018), 584.

[145] HACHEM, H., GHEITH, R., ALOUI, F., AND NASRALLAH, S. B. **Technological challenges and optimization efforts of the Stirling machine: A review**. *Energy Conversion and Management 171* (2018), 1365–1387.

[146] UCHMAN, W., REMIORZ, L., GRZYWNOWICZ, K., AND KOTOWICZ, J. **Parametric analysis of a Beta Stirling engine – a prime mover for distributed generation**. *Applied Thermal Engineering 145* (2018), 693–703.

[147] AHMED, F., HULIN, H., AND KHAN, A. M. **Numerical modeling and optimization of Beta-type Stirling engine**. *Applied Thermal Engineering 149* (2019), 385–400.

[148] CHENG, C.-H., HUANG, C.-Y., AND YANG, H.-S. **Development of a 90-KBeta type Stirling cooler with rhombic drive mechanism**. *International Journal of Refrigeration 98* (2019), 388–398.

[149] EID, E. I., KHALAF-ALLAH, R. A., SOLIMAN, A. M., MANSOUR, T. M., AND MOHAMMED, A. A. **Performance of Gamma Stirling refrigerator having shell and tube condenser and evaporator**. *International Journal of Scientific Engineering Research 10* (2019), 57–66.

[150] GUO, Y., CHAO, Y., WANG, B., WANG, Y., AND GAN, Z. **A general model of Stirling refrigerators and its verification**. *Energy Conversion and Management 188* (2019), 54–65.

[151] KARABULUT, H., OKUR, M., HALIS, S., AND ALTIN, M. **Thermodynamic, dynamic and flow friction analysis of a stirling engine with scotch yoke piston driving mechanism**. *Energy 168* (2019), 169–181.

[152] SURANJAN, S., JOHN, J. S., MATHEW, A. J., JOSE, J., JOSHY, G., RAMESH, A., AND SACHIDANANDA, H. **Determination of coefficient of performance of Stirling refrigeration sm**. *International Journal of Innovative Technology and Exploring Engineering (IJITEE) 8* (2019), 2522–2529.

[153] DJETEL-GOTHE, S., BÉGOT, S., LANZETTA, F., AND GAVIGNET, E. **Design, manufacturing and testing of a beta Stirling machine for refrigeration applications**. *International Journal of Refrigeration 115* (2020), 96–106.

[154] GETIE, M. Z., LANZETTA, F., BÉGOT, S., ADMASSU, B. T., AND HASSEN, A. A. **Reversed regenerative Stirling cycle machine for refrigeration application: A review**. *International Journal of Refrigeration 118* (2020), 173–187.

[155] MOTA-BABILONI, A., BARBOSA JR, J. R., MAKHNATCH, P., AND LOZANO, J. A. **Assessment of the utilization of equivalent warming impact metrics in refrigeration, air conditioning and heat pump systems**. *Renewable and Sustainable Energy Reviews 129* (2020), 109929.

[156] MÜLLEROVÁ, M., KRTKOVÁ, E., AND ROŠKOVÁ, Z. **F-gases: Trends, applications and newly applied gases in the czech republic**. *Atmosphere 11*, 5 (2020), 455.

[157] MUNIR, U., KAMRAN, M. S., SHAH, A. N., FARHAN, M., AND ANWAR, Z. **CFD methodology for simulating pumping loss from displacer and piston seals of free piston Stirling engine**. *Thermal Science*, 00 (2020), 295–295.

[158] RAGHAVENDRA, H., RAJU, P. S., AND REDDY, K. H. **Effect of geometric and operational parameters on the performance of a Beta-type Stirling engine: A numerical study**. *Iranian Journal of Science and Technology, Transactions of Mechanical Engineering* (2020), 1–13.

[159] UDEH, G. T., MICHAILOS, S., INGHAM, D., HUGHES, K. J., MA, L., AND POURKASHANIAN, M. **A new non-ideal second order thermal model with additional loss effects for simulating Beta Stirling engines**. *Energy Conversion and Management 206* (2020), 112493.

[160] GETIE, M. Z., LANZETTA, F., BÉGOT, S., ADMASSU, B. T., AND DJETEL-GOTHE, S. **A non-ideal second order thermal model with effects of losses for simulating Beta-type Stirling refrigerating machine**. *International Journal of Refrigeration* (2021).

[161] WANG, H., ZHAO, L., CAO, R., AND ZENG, W. **Refrigerant alternative and optimization under the constraint of the greenhouse gas emissions reduction target**. *Journal of Cleaner Production 296* (2021), 126580.

III

APPENDIX

A

ISOTHERMAL SCHMIDT ANALYSIS EQUATION DERIVATIONS

The following derivations are for calculating the mass of working fluid from a specified mean pressure. The equations derived are used in the ideal adiabatic model as a means of quickly calculating the mass of working fluid that results in a specified mean machine pressure for the specific engine configuration. Here, the Schmidt engine analysis equations are adapted for cooling machine. The following derivations assume that the pistons are connected by a slider crank mechanism and that the resultant piston motion is sinusoidal.

A.1/ FLUID MASS FOR BETA CONFIGURATION

$$V_e = V_{cle} + \frac{1}{2}V_{swe}(1 + cos\theta) \tag{A.1}$$

$$V_c = V_{clc} + \frac{1}{2}V_{swc}(1 + cos(\theta - \alpha)) + \frac{1}{2}V_{swe}(1 - cos\theta) - V_b \tag{A.2}$$

where V_b is the overlap volume in compression space.

$$V_b = \frac{(V_{swc} + V_{swe})}{2} - \sqrt{\frac{(V_{swc})^2 + (V_{swe})^2}{4} - \frac{V_{swe}V_{swc}cos\alpha}{2}} \tag{A.3}$$

Overlap volume is the volume shared by both the displacer and piston movements. It is a unique characteristic of a Beta-type Stirling machine and needs consideration while estimating the actual performance of the machine.

$$DV_e = -\frac{1}{2}V_{swe}(1 + sin\theta) \tag{A.4}$$

$$DV_c = \frac{1}{2}V_{swc}cos(\theta - \alpha) + \frac{1}{2}V_{swe}sin\theta - V_b \tag{A.5}$$

$$P = \frac{mR}{\frac{V_c}{T_c} + \frac{V_h}{T_h} + \frac{V_r}{T_r} + \frac{V_{cr}}{T_{cr}} + \frac{V_e}{T_e}} \tag{A.6}$$

$$s = \frac{V_{swc}}{2T_h} + \frac{V_{swe}}{2T_h} + \frac{V_h}{T_h} + \frac{V_{clc}}{T_h} - \frac{V_b}{T_h} + \frac{V_r}{T_r} + \frac{V_{swe}}{2T_{cr}} + \frac{V_{cle}}{T_{cr}} + \frac{V_{cr}}{T_{cr}} \tag{A.7}$$

$$P = \frac{mR}{s + \frac{V_{swc}cos(\theta-\alpha)}{2T_h} - \frac{V_{swe}cos\theta}{2T_h} + \frac{V_{swe}cos\theta}{2T_{cr}}} \tag{A.8}$$

Expanding

$$P = \frac{mR}{s + \left(\frac{V_{swc}cos\alpha}{2T_h} - \frac{V_{swe}}{2T_h} + \frac{V_{swe}}{2Tcr}\right)cos\theta + \frac{V_{swe}sin\alpha}{2T_h}sin\theta} \tag{A.9}$$

To simlify

$$Csin\beta = \frac{V_{swe}sin\alpha}{2T_h} \tag{A.10}$$

$$Ccos\beta = \frac{V_{swc}cos\alpha}{2T_h} - \frac{V_{swe}}{2T_h} + \frac{V_{swe}}{2Tcr} \tag{A.11}$$

Defining A and β explicitly

$$C = \sqrt{\left(\frac{V_{swc}cos\alpha}{2T_h} - \frac{V_{swe}}{2T_h} + \frac{V_{swe}}{2T_{cr}}\right)^2 + \left(\frac{V_{swe}sin\alpha}{2T_h}\right)^2} \tag{A.12}$$

$$\beta = \arctan\left(\frac{\frac{V_{swe}sin\alpha}{2T_h}}{\frac{V_{swc}cos\alpha}{2T_h} - \frac{V_{swe}}{2T_h} + \frac{V_{swe}}{2T_{cr}}}\right) \tag{A.13}$$

Hence the expression for average pressure in the machine

$$P = \frac{mR}{s + Bcos\phi} \tag{A.14}$$

Where

$$B = \frac{C}{s}$$

and

$$\phi = \theta - \beta$$

Evaluating equation (A.18), it can be seen

$$P_{max} = \frac{mR}{s(1-B)} \tag{A.15}$$

$$P_{min} = \frac{mR}{s(1+B)} \tag{A.16}$$

In order to calculate the mean pressure, equation A.18 is integerated over a cycle, yielding:

$$P_{mean} = \frac{mR}{s} \int_0^{2\pi} \frac{1}{1 + Bcos\phi} d\phi = \frac{mR}{s\sqrt{1 - B^2}} \tag{A.17}$$

Rearranging equation A.17 to find the mass of working fluid, gives:

$$m = \frac{P_{mean} s \sqrt{1 - B^2}}{R} \tag{A.18}$$

B

REGENERATOR ANALYSIS

The regenerator geometric and thermal properties could be analyzed as follows. First, the area of the regenerator matrix is given by:

$$\text{Amat} = \frac{\pi \times (D_{ro}^2 - D_{ri}^2)}{4} \tag{B.1}$$

The wall area of the regenerator housing is then given as:

$$A_{wr} = \frac{\pi \times (D_{rho}^2 - D_{ro}^2)}{4} \tag{B.2}$$

The area of regenerator with no matrix is given by:

$$A_{wgr0} = \pi \times (D_{ri} + D_{ro}) \times L_r \tag{B.3}$$

$$Cqwr = k_{wr} \times \frac{A_{wr}}{L_r} \tag{B.4}$$

The free flow area of regenerator is given as:

$$A_r = Amat \times \phi \tag{B.5}$$

Then, the void volume of the regenerator could be found from the free flow area and the length of the regenerator as:

$$V_r = A_r \times L_r \tag{B.6}$$

$$d_r = d_w \frac{\phi}{(1-\phi)} \tag{B.7}$$

The total wetted area of the regenerator is then as the summation of internal and external wetted areas as:

$$A_{wg} = 4 \times \frac{V_r}{d_r} + A_{wgr0} \tag{B.8}$$

C

MATLAB FUNCTION SET

The MATLAB code is adapted from [20] engine model for cooling machine and some additional losses have been included.

The function sets of overall Stirling refrigerator analysis (sra), first calls all the main functions (define function, adiabatic function and modified simple function) as shown in Fig. C.1.

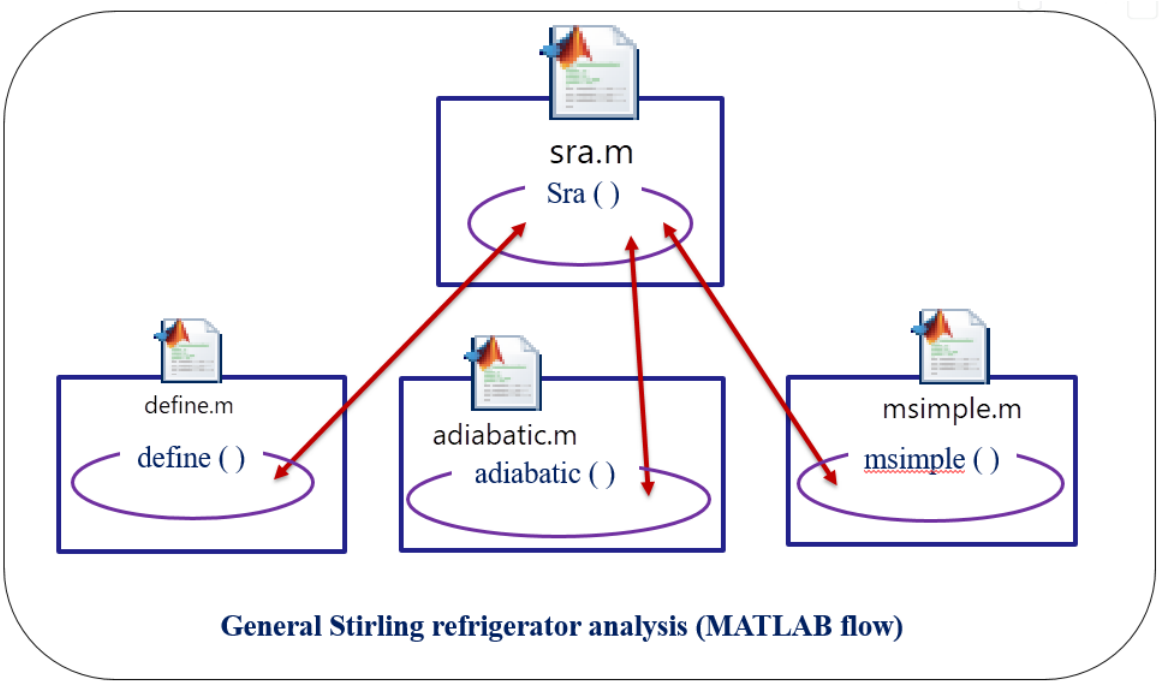

Figure C.1: General MATLAB flow function for Stirling refrigerator performances analysis.

Then, define function calls of all functions that define different design and operating parameters of machine as presented in Fig. C.2.

The MATLAB functions that take input parameters from define functions and simulate modified ideal differential equations are grouped as show in Fig. C.3.

Finally, all the losses are invoked by the modified simple function(msimple.m) as shown in Fig. C.4.

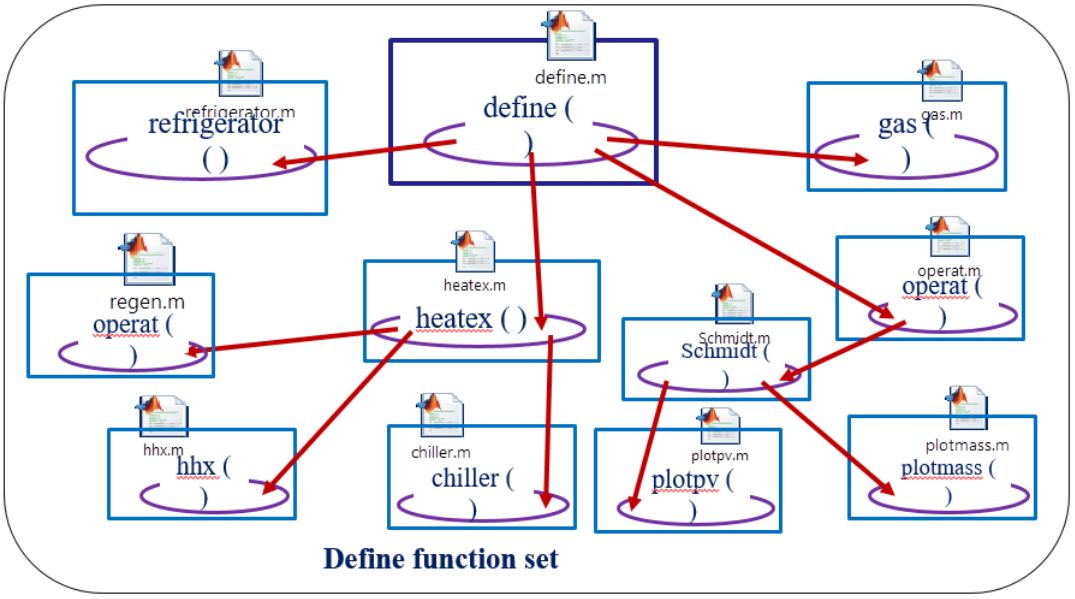

Figure C.2: MATLAB flow function for define function set.

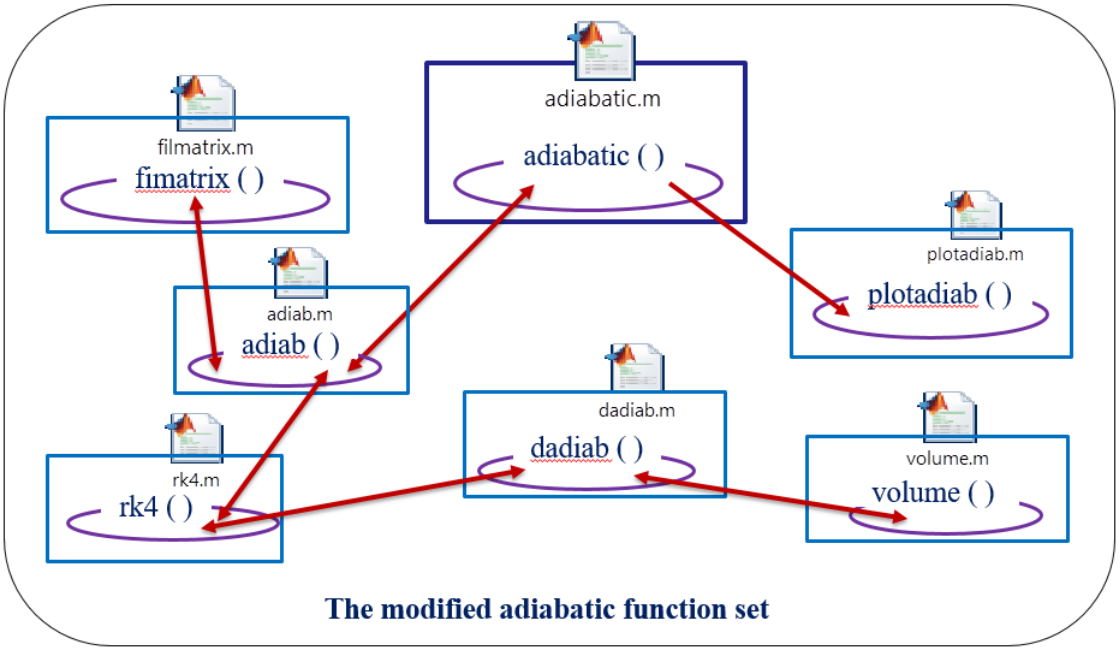

Figure C.3: MATLAB flow function for analysis of adiabatic function set.

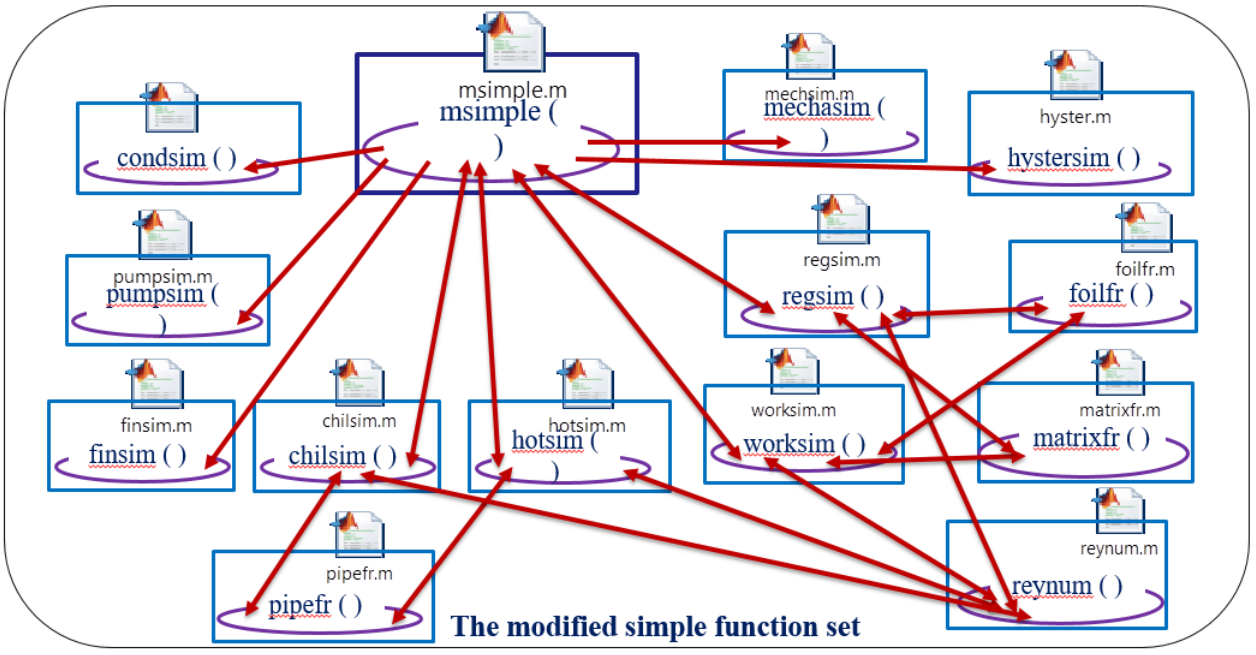

Figure C.4: MATLAB flow function for analysis of modified simple function set.

Document generated with LaTeX and:
the LaTeX style for PhD Thesis created by S. Galland — http://www.multiagent.fr/ThesisStyle
the tex-upmethodology package suite — http://www.arakhne.org/tex-upmethodology/